Photoperiod Affects the Phenotype of Mitochondrial Complex I Mutants[1][OPEN]

Pierre Pétriacq, Linda de Bont, Lucie Genestout[2], Jingfang Hao, Constance Laureau, Igor Florez-Sarasa[3], Touhami Rzigui[4], Guillaume Queval, Françoise Gilard, Caroline Mauve, Florence Guérard, Marlène Lamothe-Sibold, Jessica Marion, Chantal Fresneau, Spencer Brown, Antoine Danon[5], Anja Krieger-Liszkay, Richard Berthomé, Miquel Ribas-Carbo, Guillaume Tcherkez, Gabriel Cornic, Bernard Pineau[6], Bertrand Gakière*, and Rosine De Paepe

Institute of Plant Sciences Paris-Saclay, Centre National de la Recherche Scientifique, Institut National de la Recherche Agronomique, Université Paris-Sud, Université Evry, Université Paris-Diderot, Université Paris-Saclay, 91405 Orsay, France (P.P., L.d.B., L.G., J.H., G.Q., A.D., B.P., B.G., R.D.P.); Ecologie, Systématique et Evolution, Université Paris-Sud, Centre National de la Recherche Scientifique, Université Paris-Saclay, 91405 Orsay cedex, France (C.L., T.R., C.F., G.C.); Grup de Recerca en Biologia de les Plantes en Condicions Mediterranies, Departament de Biologia, Universitat de les Illes Balears, 7122 Palma de Mallorca, Spain (I.F.-S., M.R.-C.); Plateforme Métabolisme Métabolome, Institute of Plant Sciences Paris-Saclay, Centre National de la Recherche Scientifique, Institut National de la Recherche Agronomique, Université Paris-Sud, Université Evry, Université Paris-Diderot, Université Paris-Saclay, 91405 Orsay, France (F.Gi., C.M., F.Gu., M.L.-S., B.G.); Institute for Integrative Biology of the Cell, Centre National de la Recherche Scientifique, Commissariat à l'Energie Atomique, Université Paris-Sud, Université Paris-Saclay, Campus de Gif, Centre National de la Recherche Scientifique, 91190 Gif-sur-Yvette cedex, France (J.M., S.B.); Institute for Integrative Biology of the Cell, Centre National de la Recherche Scientifique, Commissariat à l'Energie Atomique, Université Paris-Sud, Université Paris-Saclay, Campus de Saclay, Commissariat à l'Energie Atomique Saclay, 91191 Gif-sur-Yvette cedex, France (A.K.-L.); Laboratoire des Interactions Plantes Microorganismes, Unité Mixte de Recherche Institut National de la Recherche Agronomique 441/Centre National de la Recherche Scientifique 2594, 31326 Castanet Tolosan cedex, France (R.B.); Research School of Biology, College of Medicine, Biology, and Environment, Australian National University, Canberra, Australian Capital Territory 2601, Australia (G.T.); and biOMICS Facility, Department of Animal and Plant Sciences, University of Sheffield, Sheffield, United Kingdom S10 2TN (P.P.)

ORCID IDs: 0000-0001-8151-7420 (P.P.); 0000-0002-7570-1528 (L.G.); 0000-0002-1862-7931 (I.F.-S.); 0000-0003-4512-9003 (S.B.); 0000-0001-6311-6076 (A.D.); 0000-0001-7141-4129 (A.K.-L.); 0000-0003-4781-6210 (R.B.); 0000-0002-7337-2089 (M.R.-C.); 0000-0003-4074-0583 (G.C.); 0000-0003-0285-5160 (B.G.).

Plant mutants for genes encoding subunits of mitochondrial complex I (CI; NADH:ubiquinone oxidoreductase), the first enzyme of the respiratory chain, display various phenotypes depending on growth conditions. Here, we examined the impact of photoperiod, a major environmental factor controlling plant development, on two Arabidopsis (*Arabidopsis thaliana*) CI mutants: a new insertion mutant interrupted in both *ndufs8.1* and *ndufs8.2* genes encoding the NDUFS8 subunit and the previously characterized *ndufs4* CI mutant. In the long day (LD) condition, both *ndufs8.1* and *ndufs8.2* single mutants were indistinguishable from Columbia-0 at phenotypic and biochemical levels, whereas the *ndufs8.1 ndufs8.2* double mutant was devoid of detectable holo-CI assembly/activity, showed higher alternative oxidase content/activity, and displayed a growth retardation phenotype similar to that of the *ndufs4* mutant. Although growth was more affected in *ndufs4* than in *ndufs8.1 ndufs8.2* under the short day (SD) condition, both mutants displayed a similar impairment of growth acceleration after transfer to LD compared with the wild type. Untargeted and targeted metabolomics showed that overall metabolism was less responsive to the SD-to-LD transition in mutants than in the wild type. The typical LD acclimation of carbon and nitrogen assimilation as well as redox-related parameters was not observed in *ndufs8.1 ndufs8*. Similarly, NAD(H) content, which was higher in the SD condition in both mutants than in Columbia-0, did not adjust under LD. We propose that altered redox homeostasis and NAD(H) content/redox state control the phenotype of CI mutants and photoperiod acclimation in Arabidopsis.

Complex I (CI; NADH:ubiquinone oxidoreductase; EC 1.6.5.3), the first enzyme of the respiratory chain of most eukaryotes, including plants, couples electron transfer to proton translocation through the inner mitochondrial membrane (Klodmann et al., 2010). CI is an L-shaped multimeric enzyme of around 1 MD in size composed of a matrix-faced peripheral arm carrying the NADH-oxidizing activity (N module), a connecting module (Q module transferring electrons to the quinone-binding site), and a hydrophobic intramembrane arm carrying the proton translocation activity (P module). Eukaryotic CI comprises more than 40 subunits,

of which 14 also are present in the ancestral bacterial enzyme (core subunits; Efremov et al., 2010). They are encoded by either mitochondrial genes (e.g. NAD) or by nuclear genes that might be present in multiple copies (see Table 1 in Meyer et al., 2011). Mutations in both mitochondrial and nuclear genes have been characterized in various plant species. Mutants devoid of NAD subunits were characterized in maize (*Zea mays*; *ncs2*, deleted for NAD4; Marienfeld and Newton, 1994) and in *Nicotiana sylvestris* (CMSI and CMSII, deleted for NAD7; Pla et al., 1995). Mutations in genes controlling NAD cis/trans-processing have been described in *N. sylvestris*, maize, and Arabidopsis (*Arabidopsis thaliana*; for review, see Colas des Francs-Small and Small, 2014), and insertion mutants lacking nucleus-encoded subunits have been characterized in Arabidopsis (Meyer et al., 2009; Kühn et al., 2015; Soto et al., 2015). Impaired holocomplex assembly/activity are common features of all plant mutants characterized so far, but putative intermediate assembly forms have been observed in several cases (Gutierres et al., 1997; Karpova and Newton, 1999; Perales et al., 2005; Pineau et al., 2008; Meyer et al., 2009, 2011; Kühn et al., 2015). A general respiratory impairment, measured as either oxygen consumption of leaf discs or CO_2 emission by attached leaves in the dark (dark respiration), has not been observed, and in organello experiments showed the induction of nonphosphorylating NAD(P)H dehydrogenases (Rasmusson et al., 2008) in all cases analyzed (Marienfeld and Newton, 1994; Sabar et al., 2000; Meyer et al., 2009; Keren et al., 2012). Furthermore, both the capacity of the alternative oxidase (AOX) pathway, which bypasses the cytochrome oxidase (COX) pathway, and the AOX protein content were increased in all mutants.

Plant CI mutants have various phenotypes, from mild to severe or even near lethal (Kühn et al., 2015); in addition to a slow-growing phenotype, morphological distortions and male sterility were reported in maize NCS2 (Karpova and Newton, 1999) and in *N. sylvestris* NMS1 and CMSII (De Paepe et al., 1990). Seedlings of Arabidopsis *nMat1/4* (Keren et al., 2012; Cohen et al., 2014) and *ndufv1* (Kühn et al., 2015) mutants barely survive unless grown in vitro with Suc supplementation. Differential impact of the mutations also was observed at the physiological and metabolic levels. Decreased photosynthetic activity is not a general effect and was reported in the *N. sylvestris* CMSII and NMS1 mutants (Sabar et al., 2000; Dutilleul et al., 2003a; Priault et al., 2007) and in the Arabidopsis *ca2 cal2* mutant only (Soto et al., 2015). In the *N. sylvestris* mutants, limited carbon supply resulting from higher photorespiration is likely to contribute to the slow-growth phenotype (Priault et al., 2006b). Although similar metabolic alterations were observed in *N. sylvestris* (Dutilleul et al., 2005; Szal et al., 2008; Djebbar et al., 2012) and Arabidopsis CI mutants (Meyer et al., 2009; Keren et al., 2012) as increased levels of amino acids, ATP, and NAD(H), noteworthy differences were reported recently between Arabidopsis mutants (Kühn et al., 2015). Moreover, an increase in total reactive oxygen species (ROS) content was reported for many Arabidopsis CI mutants (Meyer et al., 2009; Keren et al., 2012; Soto et al., 2015) but not in the CMSII mutant (Dutilleul et al., 2003b). The reasons for these inconsistencies are unknown at present. Complementation studies, performed for CMSII (Pineau et al., 2005), *opt43* (de Longevialle et al., 2007), *ndufs4* (Meyer et al., 2009), and mutants in CA2/CAL2 genes encoding CA/CAL γ-carbonic anhydrase subunits (Sunderhaus et al., 2006; Soto et al., 2015), indicated that additional mutations are not involved in the altered phenotype in these cases. It has been proposed that the presence of traces of holo-CI might attenuate mutant deficiencies (Kühn et al., 2015). Alternatively, it is possible that assembly intermediates might interfere with normal oxidative phosphorylation or have additional functions, as suggested by Keren et al. (2012).

The phenotype of several CI mutants is affected by growth conditions. CMSII plants showed altered responses to environmental conditions such as light (Priault et al., 2006a), nitrogen, and CO_2 (Pellny et al., 2008; Hager et al., 2010) and were fully male sterile under very low illumination only (De Paepe et al., 1990). They were differentially affected by drought stress (Galle et al., 2010; Djebbar et al., 2012). Also, the growth defect of the Arabidopsis *ca2 cal2* mutant was rescued under nonphotorespiratory conditions (Soto et al., 2015). However, despite its importance for plant development

[1] This work was supported by the Université Paris-Sud, the Centre National de la Recherche Scientifique, the Commissariat à l'Energie Atomique Saclay, the Institut Jean Pierre Bourgin, the Spanish Ministry of Science and Innovation, and the French Agence Nationale de la Recherche (Génoplante program grant no. GNP0508 and project Jeunes Chercheurs under contract no. 12–0001–01).

[2] Present address: Labogena, Domaine de Vilvert, 78352 Jouy-en-Josas cedex, France.

[3] Present address: Central Metabolism Group, Molecular Physiology Department, Max Planck Institute of Molecular Plant Physiology, Am Mühlenberg 1, 14476 Potsdam-Golm, Germany.

[4] Present address: Institut Sylvo-Pastorale, BP n 345, 8110 Tabarka, Tunisia.

[5] Present address: LBMCE, Unité Mixte de Recherche 8226, Sorbonne Université, UPMC Université Paris 06, Centre National de la Recherche Scientifique, Institut de Biologie Physico-Chimique, 75005 Paris, France.

[6] Deceased.

* Address correspondence to bertrand.gakiere@u-psud.fr.

The author responsible for distribution of materials integral to the findings presented in this article in accordance with the policy described in the Instructions for Authors (www.plantphysiol.org) is: Bertrand Gakière (bertrand.gakiere@u-psud.fr).

R.D.P. conceived the original screening and research plans; B.G., G.T., R.B., and G.C. supervised the experiments; P.P., B.G., L.G., P.B., F.Gu L.d.B., J.H., I.F.-S., C.L., G.Q., J.M., T.R., C.F., M.L.-S., S.B., A.D., B.P., and A.K.-L. performed most of the experiments; F.Gi. and C.M. provided technical assistance; M.R.-C. and G.T. designed the experiments and analyzed the data; R.D.P. conceived the project and wrote the article with contributions of all the authors; B.G., G.C., and G.T. supervised and complemented the writing.

[OPEN] Articles can be viewed without a subscription.
www.plantphysiol.org/cgi/doi/10.1104/pp.16.01484

and productivity, the photoperiod response in CI mutants has not been investigated yet. Plants can be classified into day neutral, short day (SD), and long day (LD) on the basis of the minimum duration of light per day necessary to trigger the transition from a vegetative growth phase to a reproductive state. Arabidopsis is a facultative LD species that blooms earlier in LD (12 h or greater daylength) than in SD, and photoperiod affects morphological (leaf thickness and thylakoid organization) and physiological (carbon assimilation-related parameters and stomatal conductance) parameters, redox state, and stress responses (Robbins and Pharr, 1987; Gibon et al., 2004, 2009; Becker et al., 2006; Lepistö and Rintamäki, 2012; Queval et al., 2012). Although it has been reported that daylength (16 h versus 12 h) impacts on the phenotype of the ABA overly-sensitive 5 mutant affected in *nad2* splicing (Liu et al., 2010) and that photoperiodic control was altered in *cal* mutants (Wang et al., 2012), Arabidopsis CI mutants have been fully characterized in LD only, and the link between CI and photoperiod remains to be studied.

Here, we examined the impact of different photoperiod regimes on two different Arabidopsis CI mutants: a new insertion mutant interrupted in both *ndufs8.1* and *ndufs8.2* genes encoding the NDUFS8 subunit belonging to the core CI (Efremov et al., 2010) and the previously characterized *ndufs4* mutant (Meyer et al., 2009; Kühn et al., 2015). Under greenhouse LD condition, both *ndufs8.1* and *ndufs8.2* single mutants were indistinguishable from Columbia-0 (Col-0) at both the biochemical and phenotypic levels. In contrast, the *ndufs8.1 ndufs8.2* double mutant was devoid of holo-CI assembly/activity and displayed a growth-retardation phenotype similar to that of *ndufs4*. Although growth was less affected in *ndufs8.1 ndufs8.2* than in *ndufs4* under SD conditions, both mutants had an impaired growth response when transferred from SD to LD. We further provide insights into metabolomics and biochemical alterations associated with the acclimation to LD and discuss how mitochondrial CI activity might interact with photoperiod acclimation in Arabidopsis.

RESULTS

Molecular and Biochemical Characterization of Single and Double Mutants of the NDUFS8 Subunit

Mutant lines carrying a T-DNA insertion in the *ndufs8.1* (*At1g16700*) and *ndufs8.2* (*At1g79010*) genes (Col-0 accessions) were obtained from the Salk Institute collection. Both genes are composed of six exons (Fig. 1A), and their proteins share 94% similarity. By sequencing T-DNA left border insertion PCR products, we localized the insertion sites in the first intron and in the third intron in *ndufs8.1* and *ndufs8.2*, respectively. Knockout mutations were confirmed by PCR and reverse transcription (RT)-PCR using *ndufs8.1* and *ndufs8.2* primer combinations: no *ndufs8.1* and *ndufs8.2* transcripts could be detected in the corresponding mutants

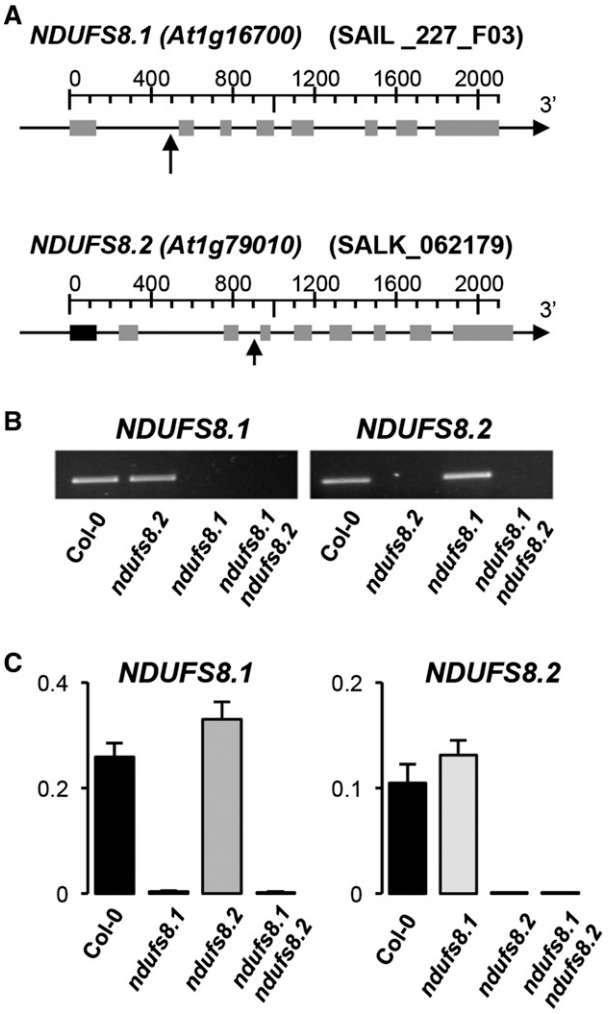

Figure 1. Molecular characterization of single and double insertion mutants affected in the two Arabidopsis genes encoding the NDUFS8 subunit of CI. A, Gene structures and sites of insertion of T-DNA in *ndufs8.1* (*At1g79010*) and *ndufs8.2* (*At1g16700*) genes (arrows). B, Electrophoresis of RT-PCR products using *NDUFS8.1*- and *NDUFS8.2*-specific primers in the wild type (Col-0), *ndufs8.1* and *ndufs8.2* single mutants, and the *ndufs8.1 ndufs8.2* double mutant. C, RT-quantitative PCR (qPCR) analysis of *NDUFS8.1* and *NDUFS8.1* genes in the wild type (Col-0), the *ndufs8.1* and *ndufs8.2* single mutants, and the *ndufs8.1 ndufs8.2* double mutant, using *ACTIN2* (*ACT2*) as a reference. Data are means + SE of three independent measurements.

(Fig. 1, B and C). In Col-0 seedlings and leaves, *NDUFS8.2* was found to be about 2.5 times more expressed than *NDUFS8.1* (Fig. 1C). No changes for *NDUFS8.2* transcripts were detected in the *ndufs8.1* mutant or for *NDUFS8.1* transcripts in the *ndufs8.2* mutant, indicating no adjustment at the gene expression level. The *ndufs8.1 ndufs8.2* double mutant, recovered from crossing single mutants with the *ndufs8.2* mutant used as the male donor, lacked both *NDUFS8.1* and *NDUFS8.2* transcripts (Fig. 1, B and C). In both single and double mutants, DNA and RNA patterns were stably maintained over five selfing generations; thus, all

biochemical and physiological analyses were performed on S3 to S5 offspring.

In order to see whether the expression of *ndufs8.1* and *ndufs8* genes was required for CI assembly and activity, leaf proteins were solubilized with digitonin, a detergent preserving the association of respiratory chain supercomplexes, in particular the I-III$_2$ supercomplex (Pineau et al., 2008), and subjected to blue native (BN)/PAGE. In-gel NADH dehydrogenase activity, revealed by NDH/nitroblue tetrazolium (NBT) staining, was observed around 1 MD (which corresponds to CI size) in the wild type and in *ndufs8.1* and *ndufs8.2* single mutants but was not detectable in the *ndufs8.1 ndufs8.2* double mutant (Fig. 2, left). Moreover, a signal around 1,500 kD corresponding to supercomplex I-III$_2$ (Pineau et al., 2008) was observed in single mutants as in the wild type but not in the double mutant. Similarly, the immunostaining obtained using antiserum directed against NAD9 (mitochondrion-encoded CI subunit located in the peripheral arm; Klodmann et al., 2010) was observed in the wild type and single mutants but not in the double mutant (Fig. 2, middle). By contrast, the antibody directed against the COX2 subunit of cytochrome oxidase (complex IV) gave a similar signal in all cases (Fig. 2, right). Two-dimensional BN/SDS-PAGE of total root membrane proteins solubilized with

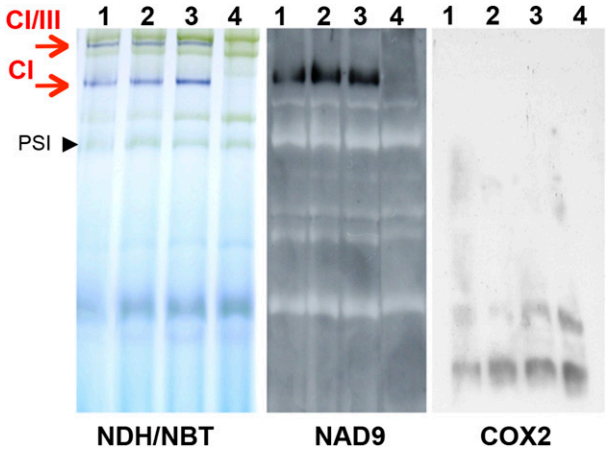

Figure 2. CI assembly/activity in Col-0 and single and double mutants for the NDUFS8 subunit. Membrane proteins extracted from leaves of Col-0 (lanes 1), single *ndufs8.1* (lanes 2) and *ndufs8.2* (lanes 3) mutants, and the *ndufs8.1 ndufs8.2* double mutant (lanes 4) were solubilized with digitonin that preserves the assembly of supercomplexes and resolved by BN/PAGE on 4%/13% gradient acrylamide gels. After migration, gels were stained for CI activity using NDH/NBT or blotted on polyvinylidene difluoride membranes for immunodetection studies. Left, In-gel NDH/NBT-stained leaf proteins. CI and the CI/III supercomplex (purple signals and red arrows), detected in Col-0 and in both *ndufs8.1* and *ndufs8.2* single mutants, are absent in the double mutant. The PSI complex that originated from thylakoid membranes is indicated by the arrowhead (Pineau et al., 2008). Middle, The anti-NAD9 immunosignal, revealed at the level of CI in the wild type and in both *ndufs8.1* and *ndufs8.2* single mutants, is not detected in the *ndufs8.1 ndufs8.2* double mutant. Right, The accumulation of complex IV using anti-COX2 antibody (bottom of the gel) is similar in all genotypes.

β-dodecylmaltoside, which dissociates respiratory supercomplexes, failed to reveal a clear CI pattern in the double mutant, despite the presence of trace amounts of CI subunits (Supplemental Fig. S1). For example, the 76-kD subunit, which is part of the NADH dehydrogenase module located on the peripheral arm, was hardly distinguishable in the mutant.

In spite of the impaired CI activity, leaf total oxygen consumption in the dark was similar in *ndufs8.1 ndufs8.2* and Col-0 (Fig. 3A). The cytochrome versus AOX partitioning, determined using oxygen isotope discrimination (Guy et al., 1989; Ribas-Carbo et al., 1995), showed a slight increase in the oxygen consumption rate by the AOX pathway in the mutant. This was associated with a marked increase in AOX capacity (Fig. 3B) and protein content (Fig. 3C). Although the anti-CA2 antibody is partly aspecific, a mitochondrion-specific CA signal was observed in comparable amounts in both mutants and the wild type (Fig. 3C). Similarly, the signal corresponding to the NAD9 subunit (synthesized inside mitochondria) was found in both genotypes.

Hence, these results indicate that, as expected from undetectable levels of *NDUFS8.1* and *NDUFS8.2* transcripts, the NDUFS8 subunit is not synthesized (or only in trace amounts) in the double mutant, resulting in CI misassembly. Despite marked disturbances in the composition of respiratory complexes, including the accumulation of AOX proteins, no abnormalities of mitochondrial (ultra)structure could be observed by electron microscopy in *ndufs8.1 ndufs8.2* (Supplemental Fig. S2), in contrast to what was observed in *nMat* mutants (Keren et al., 2012; Cohen et al., 2014).

Development of Single and Double Mutants for the NDUFS8 Subunit under LD Condition

Under greenhouse conditions (i.e. natural illumination, supplemented by 16 h of lighting with fluorescent tubes), seedling development, rosette morphology, and adult-stage size of *ndufs8.1* and *ndufs8.2* single mutants were similar to those of the wild type (Supplemental Fig. S3). That is, the lack of any of the two NDUFS8 proteins appeared to be fully compensated for at all developmental stages under greenhouse conditions. However, the development of in vitro germinated seedlings was delayed slightly in both single mutants (Supplemental Fig. S3D).

In contrast to single mutants, the growth of the *ndufs8.1 ndufs8.2* double mutant was delayed markedly under both greenhouse and growth chamber (16-h/8-h day/night at 100 μmol m^{-2} s^{-1} photosynthetically active radiation [PAR]) conditions. Reduced development of in vitro germinating seedlings could be partly alleviated by Suc supplementation, as reported previously for other Arabidopsis CI mutants (Keren et al., 2012; Kühn et al., 2015). Leaves were somewhat more round shaped in *ndufs8.1 ndufs8.2* than in Col-0, although not otherwise malformed. Bolting was delayed for about 2 weeks, whereas leaf size at the mature rosette stage,

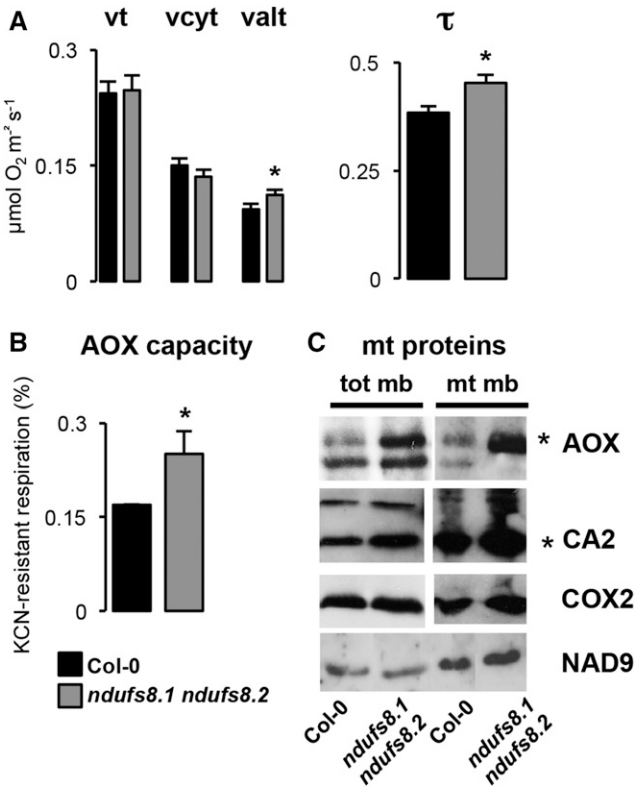

Figure 3. Respiratory pathways and mitochondrial proteins in Col-0 and the *ndufs8.1 ndufs8.2* mutant. A, Respiration rates of Col-0 and the *ndufs8.1 ndufs8.2* double mutant were determined by oxygen discrimination. Measurements were performed on plants grown in controlled chambers under 12-h/12-h day/night. vt, Total oxygen uptake; vcyt, COX activity; valt, AOX activity; τ, partition to the AOX pathway. Data are means + SE of measurements performed on at least three different plants. Asterisks indicate significant differences between the wild type and the mutant. B, AOX capacity. The percentage of cyanide (KCN)-resistant respiration in leaf tissues was determined as described by Florez-Sarasa et al. (2009). Data are means + SE of measurements performed on at least three different plants. The asterisk indicates a significant difference between Col-0 and the mutant. C, Immunodetection of mitochondrial proteins on total leaf membranes (tot mb; left) and mitochondrial membranes (mt mb; right); asterisks indicate mitochondrion-specific immunosignals. The experiment was performed at least three times with similar results.

height and leaf dimensions of adult plants, structure of the inflorescence, flower morphology, and number of siliques were unaffected (Supplemental Fig. S3B). Pollen was fully fertile, as tested by Alexander dye staining (Supplemental Fig. S3C). At both rosette and adult stages, dimensions and aspect of *ndufs4* plants were similar to those of *ndufs8.1 ndufs8.2*, despite a lower germination rate (Supplemental Fig. S3C) and a slightly lower growth rate of young plantlets (Supplemental Fig. S4B). Taken together, and considering the absence of phenotypic alterations in single mutants, these observations provide compelling evidence that the slow-growth phenotype of the *ndufs8.1 ndufs8.2* double mutant is caused by the high reduction in CI activity.

Growth Enhancement Associated with the Transfer from SD to LD Conditions Is Similarly Compromised in Both *ndufs8.1 ndufs8.2* and *ndufs4* Mutants

To determine how the photoperiod regime influenced the slow-growth phenotype when CI was deficient, *ndufs8.1 ndufs8.2* and *ndufs4* mutants were grown in controlled chambers (100 μmol m^{-2} s^{-1} PAR) in the SD condition (8-h/16-h day/night) up to the eight- to nine-leaf stage (stage referred to as SD0 hereafter) and then either transferred to LD (16-h/8-h day/night) or maintained in SD under the same light intensities. In what follows, LD plants and SD plants refer to plants that were transferred to LD or maintained under SD, respectively. The number of days after the transition is denoted as SD3 and LD3 (after 3 d), SD6 and LD6 (after 6 d), and so on.

Surprisingly (and in marked contrast to the LD condition; Supplemental Fig. S3), *ndufs4* plants grew less rapidly than *ndufs8.1 ndufs8.2* plants in the SD condition (Supplemental Fig. S4). Young rosette plants were more compact in *ndufs4* than in the two other genotypes, and necrotic points could be seen in some long-term SD-grown plants (inset in Supplemental Fig. S4A).

However, despite their developmental difference, the growth acceleration of *ndufs8.1 ndufs8.2* and *ndufs4* plants following their transfer to LD was similarly lower than in Col-0, for which enhanced growth under LD was already obvious at day 3 after transfer (Fig. 4A). The LD6-to-SD0 and LD6-to-SD6 ratios of shoot biomass were lower for both mutants compared with the wild type (Fig. 4B). In LD12 plants, the increase in all parameters of mature leaves (shoot biomass, leaf mass area and thickness, and dimensions of palisade cells) was lower in *ndufs8.1 ndufs8.2* than in Col-0 (Supplemental Fig. S5). Hence, despite the lower growth rate of *ndufs4* under the SD condition, the response of both mutants to their transfer to the LD condition was similarly impaired compared with the wild type. This suggests that the altered photoperiod response of growth is associated with reduced levels of CI activity but not with the absence of a specific CI subunit or another genetic alteration.

The Leaf Metabolome Responds Differently to Photoperiod in Wild-Type, *ndufs8.1 ndufs8.2*, and *ndufs4* Plants

Previous studies in *N. sylvestris* (Dutilleul et al., 2003b, 2005; Hager et al., 2010) and Arabidopsis CI mutants (Meyer et al., 2009; Keren et al., 2012; Cohen et al., 2014; Kühn et al., 2015) reported alterations in metabolic signature under standard LD conditions, with higher contents in tricarboxylic acid intermediates and amino acids. Here, we compared wild-type and mutant metabolic profiles during transfer from SD to LD by untargeted hydrophobic interaction liquid chromatography (HILIC)-quadrupole time of flight (qTOF)-mass spectrometry (MS) using leaves sampled at day 6 in the middle of the light cycle. This technique provides a signature of polar metabolites, in particular organic and amino acids,

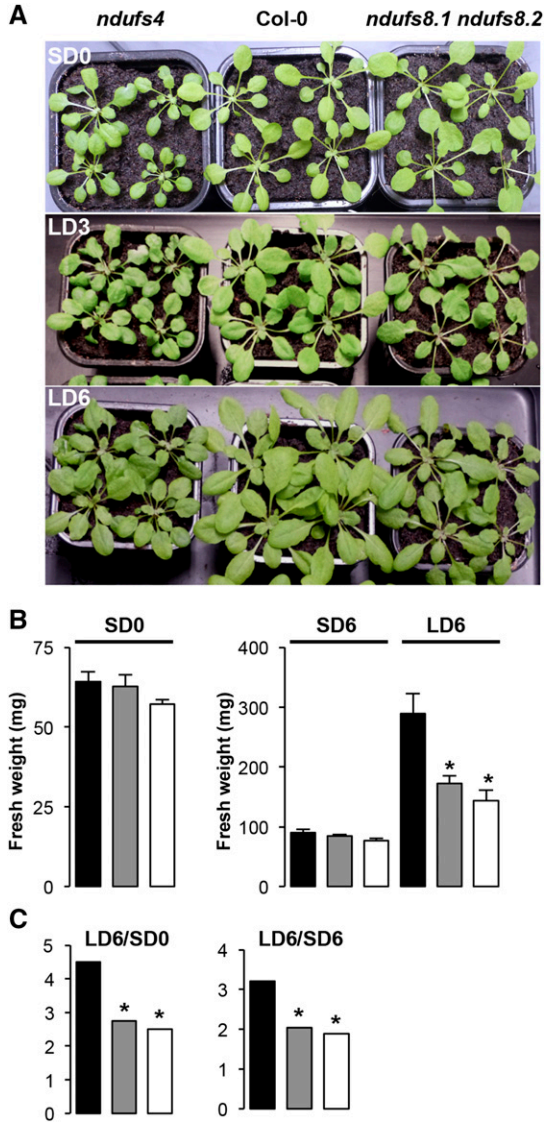

Figure 4. Growth comparisons of Col-0, *ndufs8.1 ndufs8.2*, and *ndufs4* plants in the SD-to-LD transfer experiment. A, Col-0 and mutant plants (*ndufs8.1 ndufs8.2* and *ndufs4*) were initially grown in controlled rooms under SD to achieve a similar development (eight- to nine-leaf stage; SD0), then transferred to LD for 3 d (LD3) or 6 d (LD6). B, Histograms of fresh weight (mg) of SD0, SD6, and LD6 plants in Col-0 (black bars), *ndufs8.1 ndufs8.2* (gray bars), and *ndufs4* (white bars). Data are means + SE of measurements on at least eight different plants in all genotypes. Differences between mutant and Col-0 values are much higher in the LD than in the SD condition. Asterisks indicate significant differences between mutants and Col-0 according to Student's *t* test. C, LD-SD ratios of plant biomass (fresh weight) in Col-0 (black bars), *ndufs8.1 ndufs8.2* (gray bars), and *ndufs4* (white bars) plants. Asterisks indicate significant differences between mutants and Col-0.

sugars, and other metabolites involved in central metabolism (Supplemental Methods S1; Paglia et al., 2012; Pétriacq et al., 2016). Accurately detected mass-to-charge features (error = 0.4 ppm) in negative (ESI^-; 17,326 ions) and positive (ESI^+; 18,341 ions) ionization modes were integrated using XCMS (Smith et al., 2006). The resulting ion intensities were subjected to unsupervised principal component analysis (Fig. 5A) to obtain a metabolic overview between genotypes and photoperiod regimes. Principal component analysis showed complete separation of both genotypes and photoperiods in ESI^- and ESI^+. In SD, all three genotypes were rather distinct, and *ndufs4* seemed to show the most distinct metabolic phenotype. In LD, while ESI^- analysis showed a close grouping of *ndufs8.1 ndufs8.2* with *ndufs4* compared with the wild type, ESI^+ analysis revealed overlapping profiles between the two CI-deficient mutants. Furthermore, untargeted HILIC profiles were poorly impacted by the SD-to-LD transfer in both mutants, especially for ESI^+ (Fig. 5A). Metabolic relationships between samples also were visualized by hierarchical clustering analysis in order to reveal metabolic similarities between genotypes and photoperiod (Fig. 5B). Clearly, both CI mutants were rather similar in LD, and *ndufs4* displayed the greater metabolic variation in SD. Hence, untargeted metabolomics support the outcome of growth analysis: both CI mutants are more similar in LD than in SD (Supplemental Figs. S4 and S5) and show limited response to SD-to-LD transfer (Fig. 4).

In order to identify metabolites driving the differences in LD acclimation between the wild type and mutants, we carried out targeted metabolomics by gas chromatography (GC)-MS at 6 d (SD6 and LD6). In SD, both mutants had elevated contents in tricarboxylic acid intermediates (citrate, succinate, fumarate, and malate), glycerol-3-phosphate (a redox shuttle metabolite), and most amino acids compared with the wild type (Fig. 6). In most cases, the increase was higher in *ndufs4* than in *ndufs8.1 ndufs8.2*, and 2-oxoglutarate was detected in *ndufs4* only. While the SD-to-LD transition was associated with a slight increase in succinate and malate and in some amino acids (Ala, Val, Arg, Pro, γ-aminobutyrate, and Lys) in *ndufs8.1 ndufs8.2*, it induced a decrease in these metabolites in *ndufs4*. As a result, metabolite pools of tricarboxylic acid intermediates and most amino acids were similar and higher than in the wild type in both *ndufs8.1 ndufs8.2* and *ndufs4* under LD. This is consistent with untargeted metabolomics, showing lower metabolic differences between the mutants under LD than under SD (Fig. 5), possibly reflecting their similar growth rates under the LD condition (Supplemental Fig. S4).

To get precise data on the timing and day/night effect of photoperiod-dependent metabolomics, GC-MS profiling was performed on wild-type and *ndufs8.1 ndufs8.2* plants at days 3 and 6 after transfer, both at the middle of the light period and at the end of the dark period at day 6. Forty metabolites were significantly (ANOVA, $P < 0.01$) affected by the genotype (Fig. 7). These included sugars (Glc and Fru), tricarboxylic acid intermediates (citrate, malate, succinate, and fumarate), and amino acids (Gly, Ser, Ala, Gln, Glu, and Gln), which were in larger amounts in the mutant regardless of the time point considered, the light condition, and the photoperiod (Supplemental Figs. S7–S9). Thirty-three analytes were significantly affected by the photoperiod, partly overlapping with genotype-significant

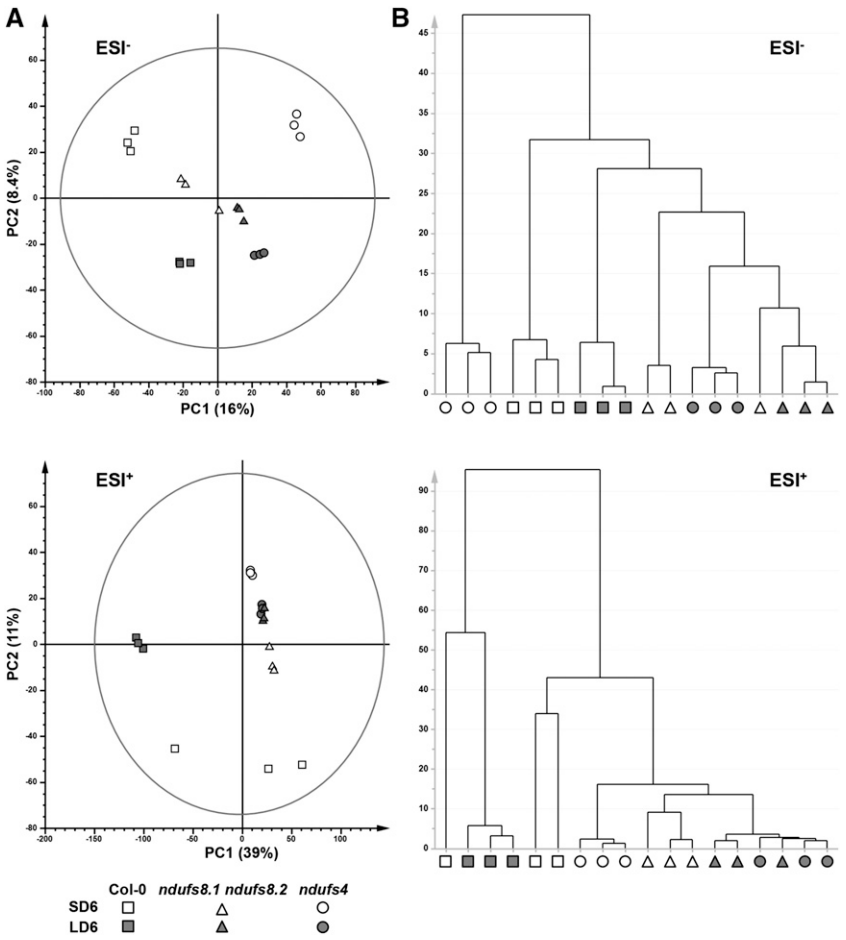

Figure 5. Untargeted metabolomics by HILIC-qTOF-MS. Multivariate analyses of the number of anions (ESI^-) and cations (ESI+) detected by HILIC-qTOF-MS from Col-0 (squares), *ndufs8.1 ndufs8.2* (triangles), and *ndufs4* (circles) plants grown in SD (white symbols) or LD (gray symbols; $n = 3$). A, Unsupervised principal component analysis displaying the overall metabolic trends between samples. Variances are given in parentheses. PC1 and PC2, Principal components 1 and 2. B, Hierarchical clustering analysis showing metabolic relationships between genotypes and photoperiods (single linkage, tree sorted by size).

ones (e.g. malate and succinate; Supplemental Fig. S10). From a supervised orthogonal partial least-squares-discriminant analysis ($r^2 = 0.99$ and $q^2 = 0.89$) in each genotype, the effect of each feature in explaining the discrimination was quantified using a Volcano plot representing the variable importance for the projection against the coefficient along axis 1 (loading score; Supplemental Fig. S11, A and B). Using ANOVA, 18 analytes were found to be significant for the genotype-photoperiod interaction (Supplemental Fig. S11C), including hexoses (Glc and Fru), tricarboxylic acid derivatives (succinate, malate, and citramalate), and amino acids (Ser, Asn, Glu, and Gln). HPLC quantitation of amino acids revealed larger overall differences between *ndufs8.1 ndufs8.2* and Col-0 under LD than under SD (Supplemental Fig. S12). There was a substantial effect of LD on amino acids derived from photorespiration and/or glycolysis (Ser, Gly, Ala, Val, Trp, and Leu) and 2-oxoglutarate (Glu, Gln, Arg, and Orn) in the mutant but a limited effect on oxaloacetate-derived amino acids (Asp, Asn, Thr, Lys, and Met).

Finally, we examined whether the marked differences in tricarboxylic acid derivatives between the wild type and *ndufs8.1 ndufs8.2* were associated with changes in transcripts associated with enzymes believed to be rate-limiting steps for the tricarboxylic acid pathway in the light (Tcherkez et al., 2009, and refs. therein; Araújo et al., 2012). Except for lower *2-OXOGLUTARATE DEHYDROGENASE2* (*OXO2*) and *ACONITASE3* transcripts under SD and *OXO2* and *FUMARASE* (*FUM*) transcripts under LD (Supplemental Fig. S13), few significant differences were observed between the wild type and mutants. Regarding the photoperiod effect, the accumulation of *FUM* transcripts in LD wild-type leaves was consistent with that of fumarate. Although a comprehensive study would require an analysis of all transcripts of tricarboxylic acid-related enzymes, these results suggest that the impact of photoperiod on tricarboxylic acid cycle gene expression is reduced in the *ndufs8.1 ndufs8.2* mutant.

In summary, our metabolomic analyses (both untargeted HILIC-qTOF-MS and targeted GC-MS) show that, as for growth phenotype (Fig. 4), *ndufs8.1 ndufs8.2* and *ndufs4* display a rather similar metabolic phenotype in LD compared with SD (Figs. 5 and 6). Also, despite differences in tricarboxylic acid derivatives and some amino acids upon transfer from SD to LD, there is limited metabolic adaptation to LD in both mutants, in agreement with their impaired growth response.

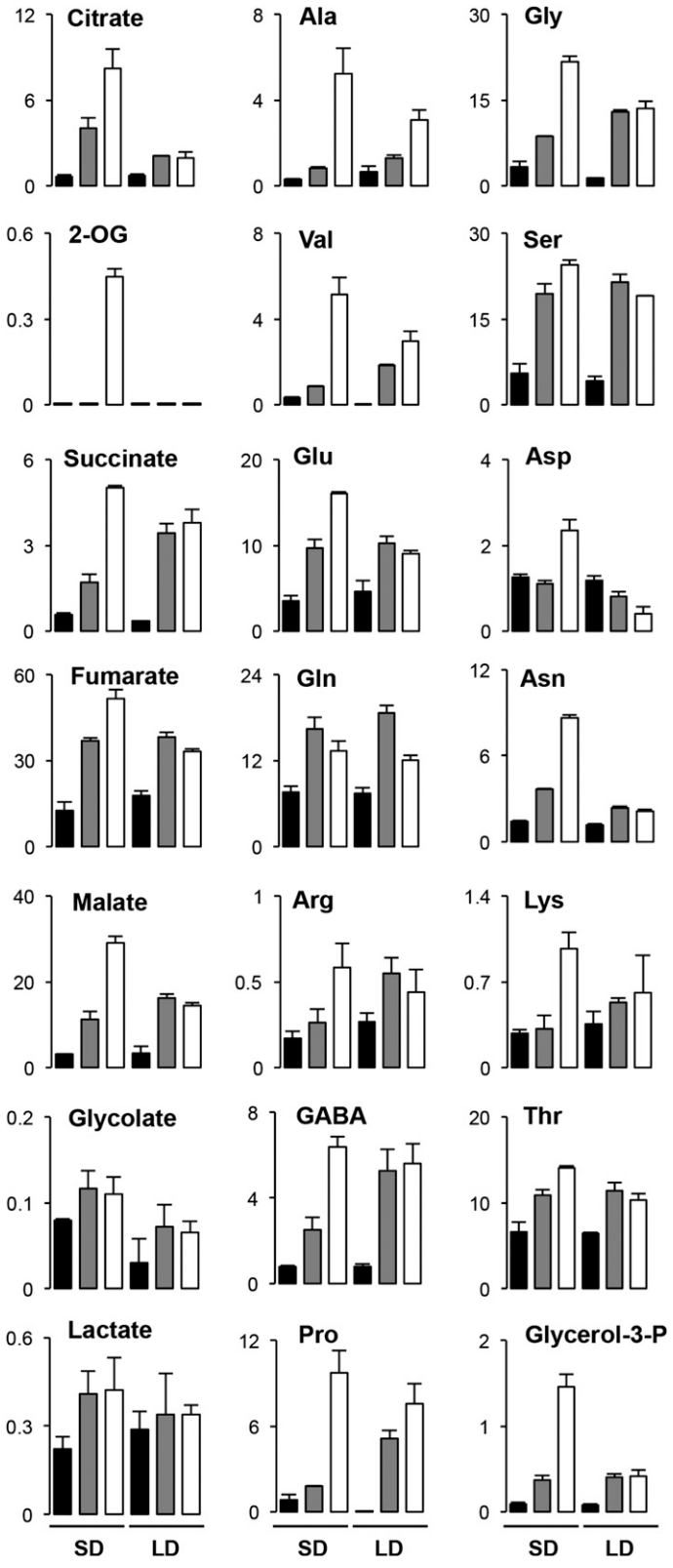

Figure 6. GC-MS determination of metabolites in Col-0, *ndufs8.1 ndufs8.2*, and *ndufs4* plants. Leaves were sampled from SD6/LD6 plants at the middle of the day period. Analyte contents are expressed in relative units. Black columns, Col-0; gray columns, *ndufs8.1 ndufs8.2*; white columns, *ndufs4*. GABA, γ-Aminobutyrate; 2-OG, 2-oxoglutarate.

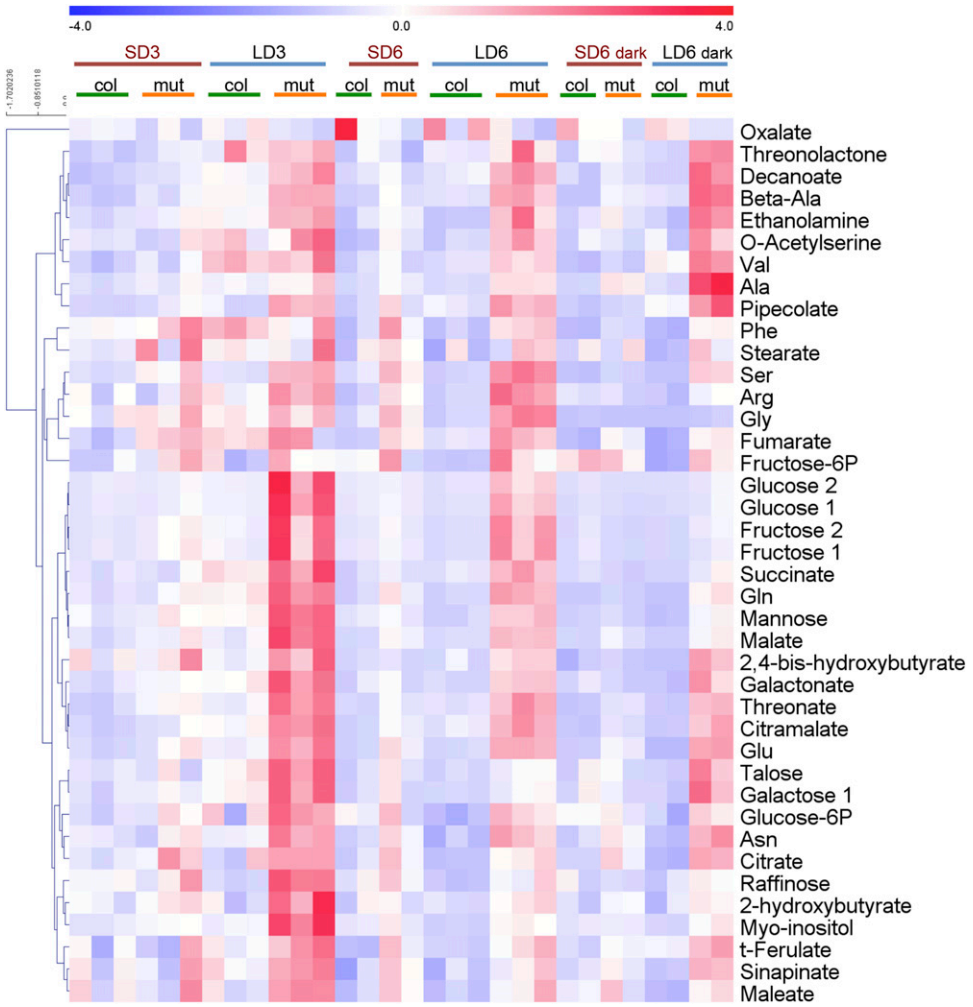

Figure 7. Heat map and hierarchical clustering (cosine correlation) of metabolites found to be significant with respect to genotype in a two-way ANOVA (GC-MS metabolomics). Col-0 (col) and *ndufs8.1 ndufs8.2* (mut) leaves were sampled from SD3/LD3 plants at the middle of the light period and from SD6/LD6 plants both at the middle of the light period and at the end of the night period (dark). Metabolomics analyses were carried out three times (i.e. three biological replicates). Relative metabolite contents are represented as mean-centered values with a color scale (blue, low content; red, high content). Numbers close to metabolite names refer to individual analytes associated with the metabolite of interest.

Photoperiod Modulates Alterations of Carbon and Nitrogen Assimilation-Related Parameters in the *ndufs8.1 ndufs8.2* Mutant

The remodeled metabolomes of CMSII (Sabar et al., 2000; Dutilleul et al., 2003a; Priault et al., 2006a, 2007) and *ndufs4* (Meyer et al., 2009) mutants were associated with alterations in carbon and nitrogen assimilation under the LD condition. Here, we found that although net CO_2 assimilation (A) was lower in the *ndufs8.1 ndufs8.2* mutant than in the wild type under elevated light and was stimulated by LD in both genotypes (light response curves shown in Supplemental Fig. S14A), it was similar in all cases at growth PAR (100 μmol m^{-2} s^{-1}; see inset). Likewise, the response of A to intercellular CO_2 mole fraction (C_i) at moderate light (300 μmol m^{-2} s^{-1} PAR) and its stimulation by the LD condition did not differ significantly between the two genotypes (Supplemental Fig. S14B). Interestingly, the relationship between intracellular CO_2 mole fraction at the carboxylation sites and C_i was the same in the two genotypes (Supplemental Fig. S14C), suggesting that internal conductance for CO_2 (dissolution-diffusion) was similar. Also, we did not detect differences in chloroplast number and thylakoid organization (distribution or ultrastructure) between the wild type and *ndufs8.1 ndufs8.2* (Supplemental Fig. S6) in either the LD or SD condition. Moreover, the electron flux to oxygenation and leaf glycolate oxidase activity did not differ significantly between genotypes and photoperiods (Supplemental Fig. S14D), indicating a similar photorespiration rate in all cases. Nevertheless, apparent carboxylation efficiency (the initial slope of the A/C_i relationship; inset in Supplemental Fig. S14A), Rubisco capacity, and total leaf ATP contents were higher in the mutant than in the wild type in SD but were not stimulated by LD (Fig. 8A). Also, chlorophyll *a/b* ratio, stomatal conductance, and dark respiration (CO_2 evolution in darkness) did not differ significantly between genotypes in SD and increased in LD in the wild type only. Hence, physiological parameters showed that growth impairment in *ndufs8.1 ndufs8.2* did not come from gas-exchange alteration (photosynthetic or photorespiratory effects) in either SD or LD, but photoperiod acclimation of photosynthetic parameters appeared to be compromised in the mutant.

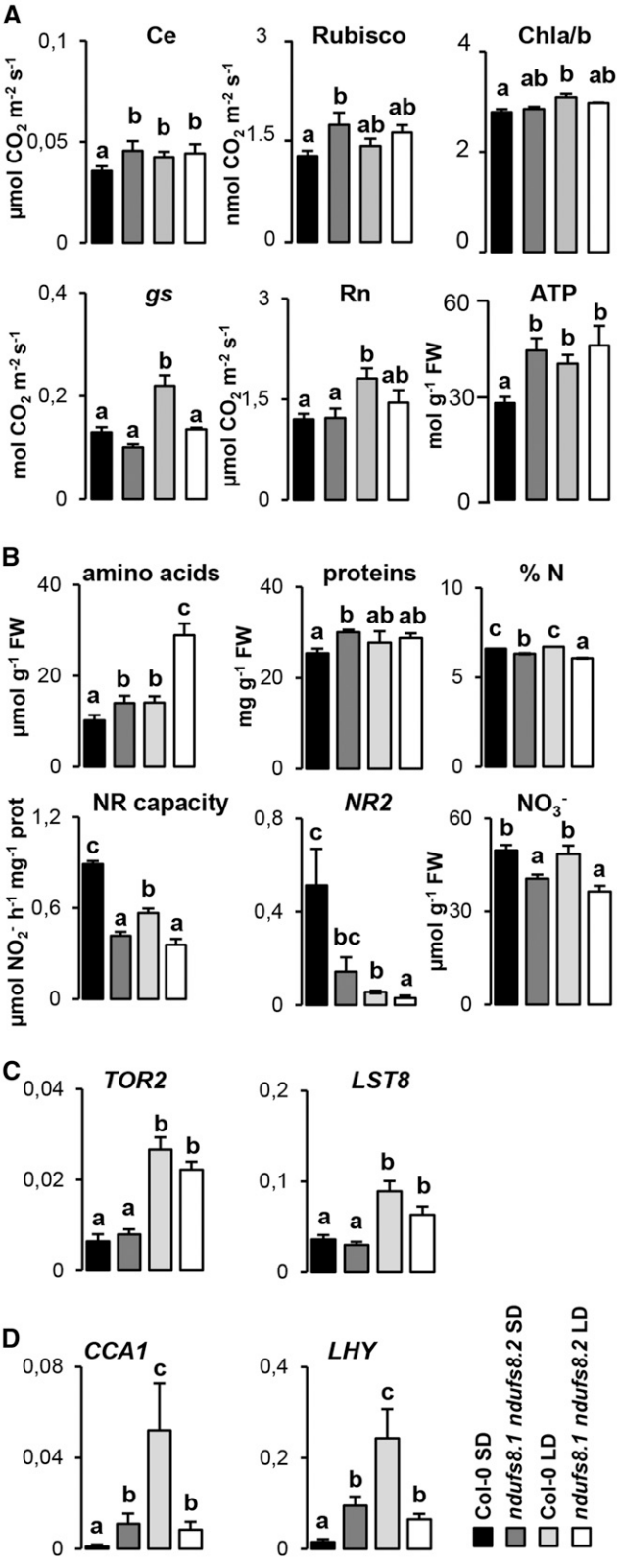

Figure 8. Analysis of growth-related parameters in Col-0 and *ndufs8.1 ndufs8.2*. Leaves were sampled from Col-0 and *ndufs8.1 ndufs8.2* plants at the middle of the light period on day 12. A, Carbon exchange-related parameters determined on leaves of 2- to 3-month-old rosette plants at the same developmental stage. Carboxylation efficiency (Ce; μmol CO_2 m^{-2} s^{-1}), stomatal conductance for CO_2 (*gs*; mol m^{-2} s^{-1}) calculated at growth illumination, Rubisco capacity (in vitro-measured maximum activity; nmol CO_2 min^{-1} mg^{-1} protein), chlorophyll *a*/*b* ratios, night respiration (Rn; μmol CO_2 m^{-2} s^{-1}), and total leaf ATP (nmol g^{-1} fresh weight [FW]) are means + SE of three to six measurements on different plants. Different letters indicate significant differences according to Student's *t* test. B, Nitrogen assimilation-related parameters. Total leaf free amino acids (μmol g^{-1} fresh weight) determined from HPLC quantification (Supplemental Fig. S12), soluble proteins (mg g^{-1} fresh weight), total nitrogen content (%), NR capacity (maximum activity; μmol NO_2 h^{-1} mg^{-1} protein), RT-qPCR analysis of the major nitrate reductase gene (NR2; expression relative to *ACT2*), and nitrate contents (μmol g^{-1} fresh weight) are means + SE of three to six measurements on different plants. Different letters indicate significant differences according to Student's *t* test. C, RT-qPCR analysis of *TOR2*/*LST8* genes of the nutrient-dependent TOR pathway using *ACT2* as a reference. Data are means + SE of three to six measurements on different plants. Different letters indicate significant differences according to Student's *t* test. D, RT-qPCR analysis of *CCA1*/*LHY* clock regulators. Data are means + SE of six measurements on different plants. Different letters indicate significant differences according to Student's *t* test.

In contrast to carbon assimilation, nitrogen assimilation was markedly affected in the *ndufs8.1 ndufs8.2* mutant (Fig. 8B). Despite an increase in the mutant of total amino acids (i.e. 20% higher than in the wild type under SD and about 2-fold higher under LD) and protein contents (under SD), total nitrogen content (%) was reduced slightly under both photoperiods (Fig. 8B). Moreover, maximum nitrate reductase (NR) activity, transcript levels of the major nitrate reductase gene (*NR2*), and nitrate contents were lower in the mutant than in the wild type under SD. Since nitrogen assimilation was not affected significantly by photoperiod in the mutant whereas it was lower in LD than in SD plants in the wild type (also observed by Gibon et al. [2009]), this resulted in lesser phenotypic differences under LD. In addition, we examined the expression of *TOR2* and *LST8*, two key genes of the TOR pathway, which were found previously to be involved in growth and photoperiod adaptation (Moreau et al., 2012). Both genes were up-regulated in LD compared with SD in both *ndufs8.1 ndufs8.2* and the wild type, thus suggesting that the accelerated growth rate in LD might benefit from the TOR pathway independently of CI activity (Fig. 8C), although posttranscriptional changes might be involved. We also measured transcript levels of *CCA1* and *LHY* clock regulators, which are important for growth and flowering (for review, see Nagel and Kay, 2012). Remarkably, levels of both transcripts were significantly higher in the mutant than in the wild type under SD but lower under LD due to their stimulation by LD in the wild type (Fig. 8D). Although these expression profiles would require a comprehensive analysis of the full diurnal cycle and other clock regulators, they suggest that the genetic control of the circadian rhythm might be altered in *ndufs8.1 ndufs8.2* plants. Taken together, these results show that carbon and

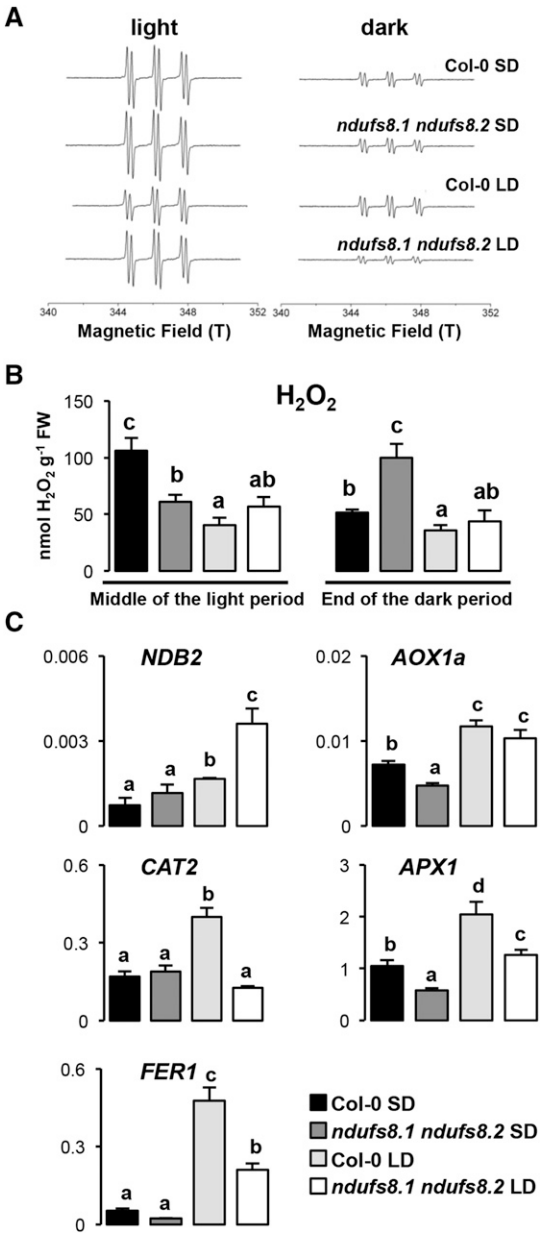

Figure 9. ROS content and expression levels of antioxidant enzymes in Col-0 and *ndufs8.1 ndufs8.2* plants maintained under SD and LD conditions. A, Typical EPR spectroscopy results, determined on leaf discs sampled from SD12/LD12 plants, as described by Michelet and Krieger-Liszkay (2012). B, Total soluble ROS pools (hydrogen peroxide [H_2O_2] equivalents) detected by luminol chemiluminescence in leaves sampled from SD12/LD12 plants at the middle of the light period (left) and at the end of the dark period (right). Data are means + SE of measurements on four to six different plants. Different letters indicate significant differences according to Student's *t* test. FW, Fresh weight. C, RT-qPCR analysis of redox enzymes of leaves sampled from SD12/LD12 plants at the middle of the light period. *ACT2* was used as a reference. Data are means + SE of measurements on three to six different plants. Different letters indicate statistical differences according to Student's *t* test.

nitrogen metabolism are less affected by the SD-to-LD transfer in *ndufs8.1 ndufs8.2* than in the wild type, in possible relation to an altered circadian rhythm in the mutant.

The Photoperiodic Regime Differentially Modulates Redox Homeostasis in the Wild Type and the *ndufs8.1 ndufs8.2* Mutant

The signaling of the photoperiod response has been proposed to be under redox control in Arabidopsis (Lepistö and Rintamäki, 2012). ROS accumulation has been observed previously in various Arabidopsis CI mutants, including *ndufs4* (Meyer et al., 2009; Keren et al., 2012; Soto et al., 2015), but not in the *N. sylvestris* CMSII mutant (Dutilleul et al., 2003b). In this work, the high heterogeneity between individual illuminated leaves prevented us from demonstrating any consistent differences in ROS content between *ndufs8.1 ndufs8.2* and the wild type under both photoperiods, using NBT and diaminobenzidine staining of superoxide and hydrogen peroxide, respectively (Supplemental Fig. S15). Therefore, we used spin-trapping electron paramagnetic resonance (EPR) spectroscopy. A typical EPR comparison of SD and LD plants is shown in Figure 9A, indicating no difference between wild-type and mutant illuminated leaf discs (during 60 min) of SD plants. In both genotypes, the ROS content was low after a dark period (60 min), reflecting the absence of photosynthesis. In the wild type, the amount of apoplastic ROS diffusing to the medium was visibly lower in LD than in SD, as reported previously (Michelet and Krieger-Liszkay, 2012). By contrast, there was no clear photoperiod effect on ROS amounts in the *ndufs8.1 ndufs8.2* mutant. We then determined leaf endogenous ROS content using luminol chemiluminescence, both at the middle of the light period and at the end of the dark period (Fig. 9B). In good agreement with the EPR results, the luminescence signal was significantly lower in LD than in SD in wild-type illuminated leaves, while it was not markedly different in the mutant. Therefore, although the ROS content of illuminated leaves was lower in *ndufs8.1 ndufs8.2* than in the wild type under SD, they were similar in both genotypes under LD. As observed in the light, ROS contents of both genotypes were lower in LD than in SD at the end of the dark period. However, in contrast to the middle of the light period, dark ROS content tended to be higher in the mutant than in the wild type, maybe reflecting altered mitochondrial metabolism.

We further examined transcript levels of oxidative stress markers in different cell compartments: mitochondrial alternative oxidase *AOX1a* (Saisho et al., 1997) and external NAD(P)H dehydrogenase *NDB2* (Michalecka et al., 2003; Yoshida and Noguchi, 2009), chloroplastic ferritin *FER1* (op den Camp et al., 2003), cytosolic ascorbate peroxidase *APX1* (Koussevitzky et al., 2008), and peroxisomal catalase *CAT2* (Noctor et al., 2007). In illuminated SD leaves, the expression levels of antioxidant enzymes were not higher in the

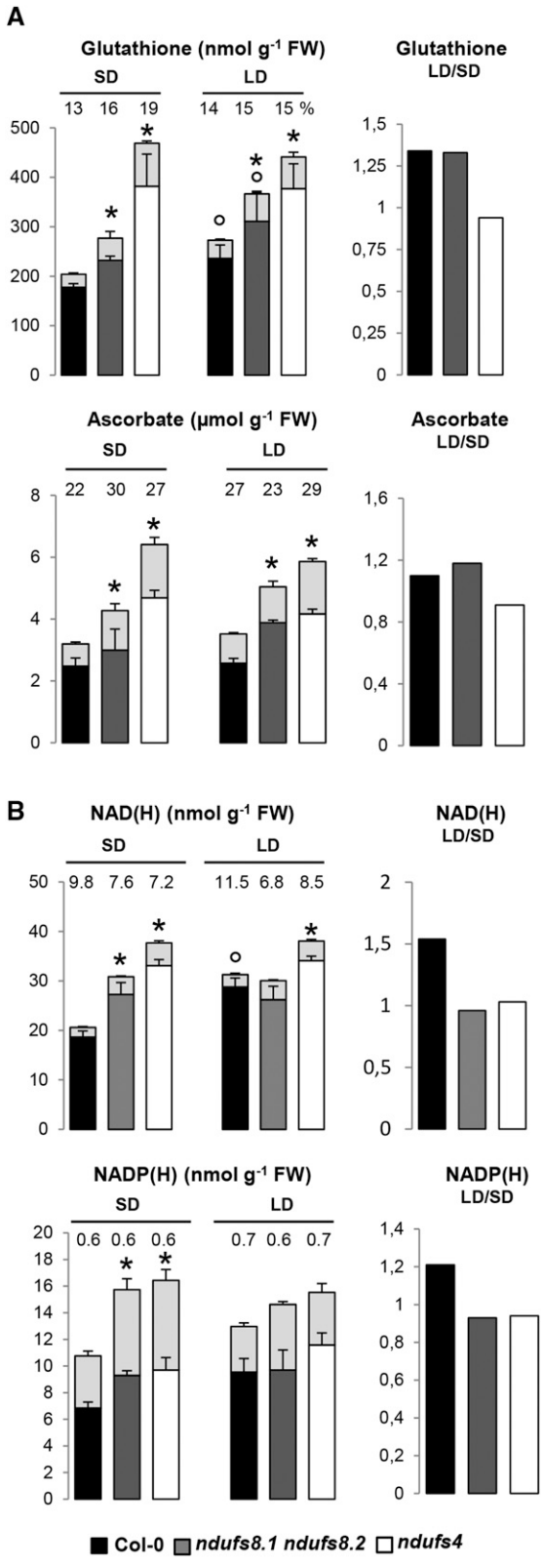

Figure 10. Pools of foliar redox buffers and cofactors in Col-0, *ndufs8.1 ndufs8.2*, and *ndufs4* plants. Leaves were sampled from SD6/LD6 plants at the middle of the day period. Black columns, Col-0; dark gray columns, *ndufs8.1 ndufs8.2*; white columns, *ndufs4*. A, Redox buffers. Left, Total leaf content of reduced and oxidized (top, light gray) forms of glutathione (nmol g^{-1} fresh weight [FW]) and ascorbate (μmol g^{-1} fresh weight). Redox state (% of oxidized forms) is indicated above the histograms. Data are means + SE from at least four extracts from different plants. Asterisks indicate significant differences ($P < 0.05$) between wild-type and mutant total pools according to Student's *t* test; circles indicate significant differences between SD and LD values for the same genotype. Right, LD-SD ratios in the three genotypes. B, Redox cofactors. Left, Total leaf content of oxidized and reduced (top, light gray) forms of NAD(H) and NAD(P)H (nmol g^{-1} fresh weight). $NAD(P)^+$-NAD(P)H ratios are indicated above the histograms. Results are means + SE of eight extracts from different plants. Asterisks indicate significant differences ($P < 0.05$) between wild-type and mutant total pools according to Student's *t* test; the circle indicates a significant difference between SD and LD values for the same genotype. Right, LD-SD ratios in the three genotypes.

ndufs8.1 ndufs8.2 mutant than in the wild type, and they were increased under LD in both genotypes, except for *CAT2* mRNAs, which were increased only in the wild type (Fig. 9C). Although *NDB2* transcripts accumulated proportionally more in the mutant than in the wild type, *AOX1a* was similar in both genotypes, regardless of the photoperiod. This was unexpected, since the AOX protein was found to be more abundant in the mutant under greenhouse conditions (Fig. 3C). In order to examine whether *AOX1a* transcript accumulation might respond to light intensity, SD and LD plants were transferred to 200 μmol m^{-2} s^{-1} PAR for 3 d. Under these conditions, *AOX1a* transcripts appeared to be markedly higher in the mutant than in the wild type in LD, while *CAT2* levels were less abundant (Supplemental Fig. S16A), showing a crossed effect of illumination and photoperiod. When plants were grown in the greenhouse in LD, *AOX1a* and *NDB2* mRNAs also were more abundant in the mutant than in the wild type at the middle of the light period, in contrast to other redox markers (Supplemental Fig. S16B). In addition, transcript levels of *AOX1a*, *NDB2*, *APX1*, and *BONZOI-ASSOCIATED PROTEIN1*, a marker of oxidative stress in the chloroplastic compartment (op den Camp et al., 2003), were considerably lower at the end of the dark period than at the middle of the light period in both genotypes (Supplemental Fig. S16B).

Previous work has shown that the redox homeostasis of CMSII plants in the LD condition was associated with the activation of the enzymatic antioxidant system (Dutilleul et al., 2003b). Similarly, we found higher detoxification activities in *ndufs8.1 ndufs8.2* than in wild-type plants under both photoperiods (Supplemental Fig. S17). Both CAT (the major hydrogen peroxide-detoxifying enzyme in plant leaves; Willekens et al., 1997) and nonchloroplastic ascorbate peroxidase (i.e. cytoplasmic cAPX) activities were significantly higher in the mutant under SD, whereas glutathione reductase (GR; a key enzyme of the ascorbate-glutathione cycle; Foyer and Noctor, 2011) was higher under LD. In both genotypes, antioxidant activities were hardly affected by photoperiod, except cAPX, which was clearly inhibited under LD. In addition, the mutant had higher

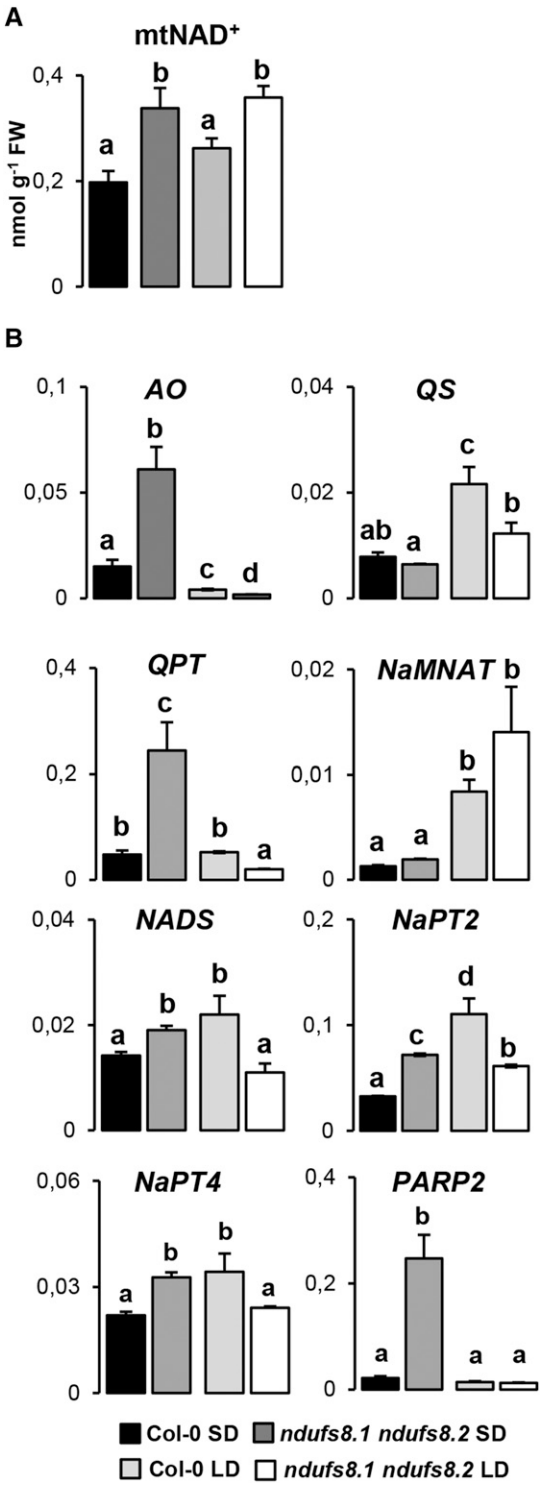

Figure 11. Pools of mitochondrial NAD^+ and transcriptional analysis of NAD^+ biosynthetic genes. In all experiments, leaves were sampled from SD12/LD12 Col-0 and *ndufs8.1 ndufs8.2* plants at the middle of the day period. A, NAD+ (nmol g^{-1} fresh weight [FW]) contents of mitochondrial preparations. Results are means + SE of three extracts from different plants. B, RT-qPCR analyses of NAD^+ biosynthetic genes were carried out using *ACT2* as a reference. Results are means + SE of at least six extracts from different plants. Different letters indicate significant differences according to Student's *t* test.

levels of anthocyanins (involved in redox control in Arabidopsis; Vanderauwera et al., 2005) than in the wild type under both photoperiods, especially during the first 3 d following transfer from SD to LD (Supplemental Fig. S17). Hence, our results indicate that the *ndufs8.1 ndufs8.2* mutant does not exhibit a general oxidative stress in either SD or LD, likely because of the induction of antioxidant activities. However, the photoperiod and light/dark responses appeared to be altered, possibly reflecting some differences in the subcellular distribution of ROS, in particular mitochondrial ROS accumulation.

Photoperiod Differentially Modulates Soluble Antioxidants and Redox Cofactors in Wild-Type, *ndufs8.1 ndufs8.2*, and *ndufs4* Plants

In addition to the high activity of antioxidant enzymes in CMSII (Dutilleul et al., 2003b; Vidal et al., 2007), CI mutants contain more soluble redox buffers than the wild type in the LD condition (Dutilleul et al., 2005; Kühn et al., 2015). Here, we found that total leaf glutathione (reduced and oxidized forms) and ascorbate (reduced and oxidized forms) were higher in both *ndufs8.1 ndufs8.2* and *ndufs4* mutants than in the wild type under both SD and LD, accompanied by slightly higher oxidation (Fig. 10A). Noticeably, levels of both redox buffers were higher in *ndufs4* than in *ndufs8.1 ndufs8.2* in SD. Transfer to LD resulted in a 30% glutathione increase in the wild type and *ndufs8.1 ndufs8.2*, whereas levels were unchanged in *ndufs4*. No significant differences in ascorbate content between SD and LD conditions were observed independently of genotype.

In contrast to redox buffers, NAD(H) content was higher in *ndufs8.1 ndufs8.2* than in the wild type under the SD condition only, whereas *ndufs4* displayed higher contents under both photoperiods (Fig. 10B). A clear buildup in total leaf NAD(H) was observed under LD in the wild type but not in the mutants. Under both photoperiods, the NAD pool was more reduced (larger NADH-NAD^+ ratio) in the mutants than in Col-0. Interestingly, mitochondrial NAD^+ levels determined in Percoll-purified leaf mitochondria were not significantly affected by the photoperiod and were higher in the mutant than in the wild type under both SD and LD (Fig. 11A). Total leaf NADP(H) contents also were higher in the mutants than in the wild type under SD, and a slight photoperiod effect was observed in the wild type only (Fig. 10B).

In order to determine whether NAD^+ contents might be regulated at the transcriptional level, we performed RT-qPCR analyses of genes involved in either de novo NAD^+ biosynthesis or NAD^+ recycling (Noctor et al., 2006): Asp oxidase (*AO*; the first enzyme of the de novo pathway in plants; Katoh et al., 2006), quinolinate synthase (*QS*), quinolinate phosphoribosyltransferase (*QPT*), nicotinate mononucleotide adenylyltransferase (*NaMNAT*), NAD synthetase (*NADS*), and nicotinate phosphoribosyltranferases (*NaPT2/4*). We also examined the expression of poly-ADP-ribose polymerase2 (*PARP2*) that uses NAD^+

as a substrate in stress responses (Schreiber et al., 2006). There were considerable differences in gene expression between genotypes and photoperiods (Fig. 11B). Under SD, the high leaf NAD^+ content of the mutant (compared with the wild type) was accompanied by an accumulation of *AO*, *QPT*, *NADS*, *NaPT2/4*, and *PARP2* transcripts. In Col-0, *NADS*, *QS*, *NaMNAT*, and *NaPT2/4* transcripts were more abundant in LD than in SD, thereby matching the higher NAD^+ content. In contrast, *AO*, *NADS*, *QPT*, *NaPT2/4*, and *PARP2* transcript levels were lower in the mutant in LD than in SD.

Hence, the loss of CI activity in both mutants is associated with (1) the accumulation of redox cofactors under SD conditions and (2) impaired redox acclimation to the LD condition.

DISCUSSION

Lack of the NDUFS8 Subunit Results in Holo-CI Misassembly and Remodeling of the Respiratory Chain

The NDUFS8 CI subunit is highly conserved from bacteria to eukaryotes, including plants (Klodmann et al., 2010). It is located in the Q module and binds two 2S-4Fe clusters involved in electron transfer to ubiquinone (Efremov et al., 2010). NDUFS8 was found to be required for holoenzyme assembly and activity in bacteria and humans (Procaccio and Wallace, 2004). In contrast to other species investigated (except *Brassica rapa*), Arabidopsis NDUFS8 is encoded by two genes, *NDUFS8.1* and *NDUFS8.2* (Fig. 1A) expressed in different tissues (Schmid et al., 2005; Qin et al., 2009), but their respective roles have not been established so far. We found that *NDUFS8.2* is about 2.5 times more expressed than *NDUFS8.1* in Col-0 seedlings and rosette leaves (Fig. 1C). Despite the lack of visible compensation at the transcript level, neither single mutant showed any apparent difference in CI assembly/activity (Fig. 2), indicating that posttranscriptional/translational controls occurred or, alternatively, that NDUFS8 amount was not limiting. These results indicate that the two NDUFS8 subunits have similar roles in CI assembly, forming complexes able to display normal NADH dehydrogenase activity. Interestingly, although no phenotypic alterations were observed in single mutants grown under greenhouse conditions, in vitro-germinated seedlings display a slightly reduced growth rate, suggesting that the presence of both subunits is beneficial at some development stages, in particular before autotrophy. Further investigations are required to establish potential differences in the composition of the CI complex in different tissues and environments.

In contrast to the single mutants, the *ndufs8.1 ndufs8.2* double mutant has undetectable levels of both transcripts (Fig. 1C) and lacks detectable holo-CI assembly/activity. This clearly indicates the absence (or only residual amounts) of the NDUFS8 subunit in the double mutant and its central role in holo-CI assembly in plants. Although traces of holo-CI could not be detected using immunochemistry using anti-NAD9- and anti-CA2 antiserum or NDH/NBT in-gel assays in *ndufs8.1 ndufs8.2*, very low levels of polypeptides potentially corresponding to CI subunits can be distinguished using two-dimensional BN/SDS-PAGE (Supplemental Fig. S1), suggesting that substoichiometric amounts of the complex might indeed be present. Furthermore, subcomplexes might be assembled, as reported for many CI mutants lacking either peripheral or membrane subunits in plants (Karpova and Newton, 1999; Brangeon et al., 2000; Pineau et al., 2008; Meyer et al., 2009; Kühn et al., 2015; Soto et al., 2015) and humans (Vogel et al., 2007). A specific mitochondrial CA signal was as abundant in *ndufs8.1 ndufs8* than in Col-0 mitochondrial proteins (Fig. 3C), suggesting that subcomplexes associated with the CA domain (possibly assembly intermediates; Wang et al., 2012) might be present in this mutant, as reported previously in *ndufs4* (Kühn et al., 2015).

Besides potential traces of holo-CI, the induction of alternative respiratory enzymes might be crucial to sustain respiration in *ndufs8.1 ndufs8.2*. In addition to complex II (succinate dehydrogenase), nonphosphorylating alternative NAD(P)H dehydrogenases (type II dehydrogenases), located on the inner and outer surfaces of the inner mitochondrial membrane, are essential for plant growth and metabolism (Liu et al., 2009; Wallström et al., 2014). Their activity depends on plant metabolic status, such as NADH and Ca^{2+} concentration (Rasmusson et al., 2008). The stimulation of both internal and external enzymes was reported in the *N. sylvestris* CMSII and NMS1 mutants (Sabar et al., 2000), and induction of external enzymes was reported in maize NCS2 (Marienfeld and Newton, 1994) and in *ndufs4* (Meyer et al., 2009). Similar to CMSII and *ndufs4* mutants (Meyer et al., 2009; Kühn et al., 2015), total respiration measured either as oxygen consumption (Fig. 3A) or as CO_2 emission (Fig. 8A) was not altered in *ndufs8.1 ndufs8.2* LD leaves, indicating that the electron flux through alternative NAD(P)H dehydrogenase(s) was stimulated in the mutant. Consistently, we found an accumulation of mitochondrial NAD(H) in *ndufs8.1 ndufs8.2* (Fig. 11A), as would be expected considering the low affinity for NADH of these enzymes (Møller, 2001). Also, as reported for other CI mutants, including *ndufs4* (Sabar et al., 2000; Karpova et al., 2002; Meyer et al., 2009; Keren et al., 2012; Cohen et al., 2014), increased AOX protein content and capacity were observed in *ndufs8.1 ndufs8.2* (Fig. 3, B and C). Interestingly, AOX accumulation was accompanied by reduced aconitase transcript levels (Supplemental Fig. S13) and increased content in citrate (Figs. 6 and 7; Supplemental Fig. S9), a well-known AOX activator (Vanlerberghe and McIntosh, 1996). High electron partitioning to AOX could have allowed the reoxidation of excess NADH in the mitochondrial matrix caused by CI impairment, while the COX pathway is essentially controlled by ATP (Florez-Sarasa et al., 2007). Here, since alternative pathways are nonphosphorylating (not coupled to H^+ translocation), the ATP yield of mitochondrial electron transport is expected to be reduced in *ndufs8.1 ndufs8.2*, as reported in CMSII (Sabar et al., 2000) and *ndufs4* (Meyer et al., 2009). In

summary, there is an induction of alternative respiratory pathways in *ndufs8.1 ndufs8.2* similar to most CI mutants investigated so far. However, in contrast to CMSII (Priault et al., 2007; Vidal et al., 2007), the in vivo electron partition to AOX is increased in *ndufs8.1 ndufs8.2*.

The Large Reduction of CI Activity Results in Similar Phenotypes in *ndufs8.1 ndufs8.2* and *ndufs4* Mutants Grown under the LD Condition

Plant CI mutants have different phenotypes, from mild (growth retardation only, as in *ndufs4*) to severe (morphological defects, as in *N. sylvestris* CMSII and NMS1 and maize *ncs2*) or even near lethal (*nMat* and *ndufv1*; see introduction). Here, we found that the *ndufs8.1 ndufs8.2* double mutant displays a mild phenotype, without phenotypic alterations at the adult stage in flowering conditions (LD; Supplemental Fig. S3). The slow-growing phenotype is clearly related to holo-CI highly reduced contents in the double mutant, as both single mutants had CI assembly/activity and growth rates identical to the wild type. This also indicates the absence of unidentified insertions in the mutants, at least insertions with phenotypic consequences. Despite very slight differences in germination (+30%) and seedling growth rates (+20%), *ndufs8.1 ndufs8.2* plants were similar to *ndufs4* plants at subsequent developmental stages (Supplemental Figs. S3 and S4). The mild phenotype of the *ndufs4* mutant has been suggested to result from persisting trace amounts of CI activity (Kühn et al., 2015). Although we were unable to detect an NDH/NBT signal around 1 MD in *ndufs8.1 ndufs8.2* BN/PAGE (Fig. 2), low levels of CI activity cannot be excluded, since substoichiometric amounts of putative CI subunits are detected by two-dimensional BN/SDS-PAGE (Supplemental Fig. S1). Nevertheless, it is not possible to estimate accurately possible differences in substoichiometric holo-CI levels between *ndufs8.1 ndufs8.2* and *ndufs4* mutants due to the limited sensitivity of the detection methods (discussed in Keren et al., 2012).

As for other CI mutants, the lower efficiency of the respiratory chain (discussed above) might explain the slow-growth phenotype of *ndufs8.1 ndufs8.2* LD plants. Similar to *nMat*, *ndufs4*, and *ndufv1* mutants (Keren et al., 2012; Kühn et al., 2015), Suc supplementation improves the in vitro development of *ndufs8.1 ndufs8.2* seedlings (Supplemental Fig. S3D), suggesting that photosynthetic ATP might compensate for lower mitochondrial ATP production. Nevertheless, as reported previously for CMSII (Szal et al., 2008; Djebbar et al., 2012) and *ndufs4* (Meyer et al., 2009), total leaf ATP of illuminated leaves was not affected in *ndufs8.1 ndufs8.2* (Fig. 3B), indicating either the activation of alternative mechanisms of ATP production as substrate-level phosphorylation at the level of mitochondrial enzymes, as proposed by Kühn et al. (2015), or reduced rates of cellular processes resulting in a lower ATP consumption. Regardless of the exact specific mechanism(s) involved, the growth retardation phenotype of CI mutants in the LD condition is unlikely to be related to energy limitation.

Oxidative stress also might be involved in the reduced growth of CI mutants. Accordingly, ROS accumulation has been reported to occur in several Arabidopsis CI mutants, including *ndufs4* (Meyer et al., 2009), in possible relation to increased mitochondrial ROS generation by the remodeled respiratory chain. High levels of AOX proteins and capacities in all CI mutants investigated so far are in line with this hypothesis. However, like CMSII and NMS1 mutants (Dutilleul et al., 2003b), ROS accumulation could not be observed in illuminated leaves of *ndufs8.1 ndufs8.2* using various methods (Fig. 9; Supplemental Fig. S15), likely due to the overactivation of antioxidant enzymes (Supplemental Fig. S17). Therefore, a marked oxidative stress is unlikely to have impeded growth rates under LD in this mutant, although such an effect cannot be excluded in *ndufs4*.

Metabolic perturbations associated with respiration reorchestration might account for the slow-growth phenotypes of *ndufs8.1 ndufs8.2* and *ndufs4* mutants. In fact, mitochondria are known to play a key role in the nitrogen/carbon balance (Foyer et al., 2011), which is affected in CMSII, with a marked increase in amino acids plausibly caused by high NAD(H) content (Dutilleul et al., 2005; Hager et al., 2010; Djebbar et al., 2012). Similarly, we found here that, despite lower values for parameters associated with nitrate assimilation (i.e. *NR* transcripts, NR activity, and NO_3^- content), amino acids accumulated in both mutants, with the notable exception of Asp (which appeared to be decreased except at the end of the night; Fig. 6; Supplemental Fig. S9). However, we did not observe a significant NAD(H) buildup in *ndufs8.1 ndufs8.2* leaves compared with the wild type in LD (Fig. 10B), suggesting that an increase in NAD(H) content per se is not the cause of amino acid accumulation in the mutants. Rather, amino acid accumulation clearly paralleled that of carbon skeletons generated by tricarboxylic acid cycle activity (citrate, succinate, fumarate, and malate) in both mutants. This suggests that, in the light, when a partial tricarboxylic acid cycle is believed to operate (Tcherkez et al., 2009; Sweetlove et al., 2010), the metabolism in mutants is associated with (1) a stimulation of both cytosolic and mitochondrial malate dehydrogenases (whereby oxaloacetate is reduced rapidly to malate) because of over-NADH(H) (Heldt et al., 2005; Tomaz et al., 2010) and (2) an increased phospho*enol*-pyruvate carboxylase activity (O'Leary et al., 2011), as reported in CMSII mutants (Dutilleul et al., 2005), at the expense of Asp accumulation. In the night, the operation of the full (cyclic) tricarboxylic acid cycle, and thus the lower reduction of oxaloacetate to malate, would account for the high Asp observed in the *ndufs8.1 ndufs8.2* mutant.

Hence, our results show a similar impact of reduced CI activity in both *ndufs8.1 ndufs8.2* and *ndufs4* mutants at developmental, physiological, and metabolic levels in relation to NAD(H) overreduction.

The Growth Retardation Phenotype Is More Pronounced in *ndufs4* Than in *ndufs8.1 ndufs8.2* Plants Grown in the SD Condition, in Possible Relation to Higher Oxidative Stress

All plant CI mutants characterized so far display growth retardation in LD, associated with various physiological and metabolic alterations, but their phenotype in SD has never been documented. Here, we show that *ndufs8.1 ndufs8.2* and *ndufs4* plants had a retarded growth phenotype under both LD and SD conditions (Supplemental Fig. S4). However, in contrast to LD, the retardation phenotype was more marked in *ndufs4* than in *ndufs8.1 ndufs8.2* plants under SD, sometimes associated with necrotic spots. Although the accumulation of total soluble redox buffers, glutathione and ascorbate, was observed in mutants under both SD and LD, redox buffers were in significantly higher amounts in *ndufs4* compared with *ndufs8.1 ndufs8.2* under SD (Fig. 10A), strongly suggesting enhanced oxidative stress. This effect might have originated from a less activated mitochondrial antioxidant system in *ndufs4* compared with *ndufs8.1 ndufs8.2*. In fact, in contrast to *ndufs4* (Meyer et al., 2009), *NDB2* and *AOX1a* transcripts accumulated in *ndufs8.1 ndufs8.2* either under our standard illumination condition (100 μmol photons m^{-2} s^{-1}; Fig. 9C) or in high light (Supplemental Fig. S16). Redox differences between *ndufs4* and *ndufs8.1 ndufs8.2* might result from the nature and/or location of the lacking CI subunit. In *ndufs4*, a large accumulation of the CA domain, which was proposed to be involved in plant CO_2 transport (Zabaleta et al., 2012) and carbon metabolism (Soto et al., 2015; Fromm et al., 2016), might result in increased mitochondrial ROS production, as reported in animals (Price et al., 2012). NDUFS4 and NDUFS7 are located in different CI modules (N and Q, respectively), and in human cell lines, mitochondrial metabolism was differentially affected in mutants affected in the two modules, in relation to the differential accumulation of assembly intermediates (Leman et al., 2015).

Untargeted metabolomics showed that the reduced growth of *ndufs4* compared with *ndufs8.1 ndufs8.2* SD plants was accompanied by much larger differences in global metabolism under SD than under LD (Fig. 5), in particular by higher levels of many amino acids (Fig. 6), as reported previously for low-nitrogen-adapted plants (Tschoep et al., 2009). It is interesting that the metabolomics signature of *ndufs4* SD leaves has some similarities to that of plants under anoxic stress (de Sousa and Sodek, 2002; Sweetlove et al., 2010). Similarity to the anoxic response also can be found in the citrate accumulation, low level of aconitase transcripts, and increased AOX capacity in *ndufs8.1 ndufs8.2* (Figs. 3 and 6; Supplemental Fig. S13), as shown by Gupta et al. (2012). Also, the CMSII mutant displays an up-regulation of fermentation pathways (Shah et al., 2013).

Overall results indicate that redox state is more compromised in *ndufs4* in the SD than in the LD condition, possibly resulting in the redirection of tricarboxylic acid fluxes toward amino acid synthesis at the expense of oxidative phosphorylation, thereby explaining the lower growth rates.

Growth and Metabolic Acclimation to LD Depend on CI Activity

The rapid growth acceleration observed in Col-0 plants after their transfer to LD (already visible at day 3; Fig. 4) was clearly reduced in the *ndufs8.1 ndufs8.2* mutant. Moreover, physiological changes associated with the SD-to-LD transition in the wild type (such as increased leaf mass area, palisade cell width, stomatal conductance, carboxylation efficiency, dark respiration, and total ATP and decreases in nitrogen assimilation and total ROS levels) were not observed (or were highly reduced) in the mutant (Fig. 8; Supplemental Fig. S5), thereby showing an impaired acclimation to LD. Despite marked growth differences between *ndufs8.1 ndufs8.2* and *ndufs4* under SD conditions, the growth response of both mutants, taken at a similar developmental stage (nine-leaf stage), to the SD-to-LD transition was comparably impaired compared with the wild type (Fig. 4). Untargeted metabolomics (HILIC-qTOF-MS) and GC-time of flight analyses confirmed that metabolism was less affected in both mutants than in the wild type upon SD-to-LD transfer (Fig. 5). The differential photoperiod effect on tricarboxylic acid intermediates, amino acids, and redox buffers in mutants (Figs. 6 and 10A) likely reflected their different metabolic and redox states under SD (as discussed above). That is, it is unlikely that the altered content in respiratory metabolites was the cause of the impaired photoperiod acclimation.

Rather, we found a clear correlation between the lack of NAD(H) accumulation and impaired LD acclimation in both *ndufs8.1 ndufs8.2* and *ndufs4* mutants. In fact, in contrast to the wild type, NAD(H) contents (1) were high under the SD condition, as would be anticipated considering the high K_m(NADH) values of alternative NADH dehydrogenases, and (2) did not increase significantly in both mutants under LD (Fig. 10B). Presumably, NAD^+ accumulation in wild-type plants transferred to LD came from a complex set of interactions between biosynthesis, oxidation by the mitochondrial electron transport chain (higher dark respiration), and degradation. $NADH^+$ consumption under LD is suggested by the decreased levels of *PARP2* transcripts (Fig. 11B). Also, in *ndufs8.1 ndufs8.2*, there was higher expression of several transcripts encoding NAD^+ biosynthesis enzymes under SD and a clear depressing effect of LD, suggesting the repression of NAD^+ neosynthetic/recycling pathways under LD.

Overall, our data show that the physiological and metabolic reorchestration accompanying LD acclimation in Arabidopsis is similarly compromised in both *ndufs8.1 ndufs8.2* and *ndufs4* mutants, thereby strongly suggesting that it results from reduced CI activity.

Signaling Mechanisms Possibly Involved in the Impaired LD Acclimation of CI Mutants

Changes in the composition of mitochondrial enzymes in CI mutants are expected to generate increased ROS by the mitochondrial electron transport chain. In

fact, ROS were reported previously to accumulate in several plant CI mutants (Meyer et al., 2009; Keren et al., 2012) and in human cell lines lacking CI peripheral arm subunits (Verkaart et al., 2007; Miwa et al., 2014), where they were produced by matrix intermediates (Leman et al., 2015). Although total ROS levels were similar in *ndufs8.1 ndufs8.2* and the wild type in the middle of the light period, they were higher in the mutant than in the wild type at the end of night period (Fig. 9B), thus suggesting increased generation of mitochondrial ROS by the respiratory chain. A general role of mitochondrial ROS in plant signaling is well documented (Huang et al., 2016). In humans, mitochondrial ROS were reported to induce pyruvate dehydrogenase activity by inactivating pyruvate dehydrogenase kinase2 (Hurd et al., 2012), thereby supporting a pathway through which mitochondrial ROS may regulate respiratory metabolism. Therefore, a specific signaling role for mitochondrial ROS in the photoperiod response is possible.

Also, glutathione levels and redox state have been reported to regulate daylength transcriptional responses in the *cat2* mutants (Queval et al., 2007). Here, we found that, although antioxidants were higher in both mutants, they were differentially affected by photoperiod: glutathione and ascorbate accumulated under LD in the wild type and in *ndufs8.1 ndufs8.2* but not in *ndufs4*, maybe because of the high content in SD (Fig. 10A). Therefore, antioxidants per se are unlikely to be involved in the impairment of the photoperiod response in CI mutants. In contrast, NAD(H) increased in LD in the wild type but not in both mutants, thereby correlating to growth rates in the three genotypes (see above). NAD^+ is known to be involved in the control of Arabidopsis growth (Hashida et al., 2009). In addition to its well-established role in redox homeostasis and oxidative phosphorylation, a considerable body of evidence indicates that NAD^+ is a crucial signaling molecule (Pétriacq et al., 2012, 2013, 2016; Sassone-Corsi, 2012) driving mitochondrial oxidative metabolism in mammals (Mouchiroud et al., 2013; Rey and Reddy, 2013). In animals, the inhibition of nicotinamide phosphoribosyl transferase, involved in nicotinamide recycling into NAD^+, has been found to impede glycolysis and tricarboxylic acid cycle activity and lead to ATP depletion (Tan et al., 2013).

A slight but consistent overreduction of NAD(H) was observed in both Arabidopsis mutants (NAD^+/NADH around 7%–8% under all conditions, compared with 10%–11% in the wild type; Supplemental Fig. S10B), as found previously in CMSII (Hager et al., 2010). Reduction levels of pyridine nucleotides are believed to exert a control on tricarboxylic acid fluxes (Igamberdiev and Gardeström, 2003; Araújo et al., 2012), for example by controlling mitochondrial MDH activity (Tomaz et al., 2010). This effect could explain the lack of significant respiratory increase in *ndufs8.1 ndufs8.2* under LD (Fig. 8A). Overreduction of the NAD pool in mutants might stem from the induction of alternative NAD(P)H dehydrogenase activities (Liu et al., 2009; Rasmusson and Wallström, 2010; Wallström et al., 2014) and/or the activation of redox shuttles (Shen et al., 2006). A redox effect may have then resulted in alterations of the circadian clock (Stangherlin and Reddy, 2013; Shim and Imaizumi, 2015). Indeed, NAD^+ is a clock-regulated metabolite in animals (Peek et al., 2013), and alteration of clock regulator expression during LD acclimation (Fig. 8D) and the dramatic increase in anthocyanins (Supplemental Fig. S17), which are regulated by cryptochromes (Ahmad et al., 1995), might reflect perturbation of the circadian clock in the *ndufs8.1 ndufs8.2* mutant. This would be similar to what was reported in mutants affected in promoter regions of genes encoding mitochondrial proteins (Giraud et al., 2010). Interestingly, diurnal rhythms of *AOX* expression are highly perturbed in the CMSII mutant, possibly reflecting an impaired circadian cycle (Dutilleul et al., 2003b). Conversely, it has been shown that Arabidopsis mutants affected in circadian clock regulation exhibit dramatic changes in the mitochondrial metabolome, in particular tricarboxylic acid derivatives (Fukushima et al., 2009). Thus, we hypothesize that an impairment in the circadian clock occurred in the CI mutants examined here, thus leading to metabolic perturbations (Peek et al., 2012; Haydon et al., 2015), and limited growth enhancement under LD conditions. Nevertheless, the specific signaling mechanisms linking CI to circadian clock regulation need further investigation.

CONCLUSION

In summary, our study provides compelling evidence that photoperiod influences the phenotype of Arabidopsis CI mutants. Despite the lower growth of *ndufs4* in SD (possibly related to a higher oxidative stress), *ndufs8.1 ndufs8.2* and *ndufs4* showed an impaired acclimation to LD after growth in SD, associated with a differential reorchestration of metabolism. We propose that highly reduced CI activity (i.e. oxidation of mitochondrial NADH) affects photoperiod acclimation via mitochondrial ROS and/or NAD(H) content and redox state.

MATERIALS AND METHODS

Plant Material

Arabidopsis (*Arabidopsis thaliana*) seeds of the SAIL_227F03 line carrying a T-DNA insertion in the *At1g16700* gene (further referred to as *NDUFS8.1*) and of the SALK_062179 line carrying an insertion in the *At1g79010* gene (further referred to as *NDUFS8.2*) were selected using the T-DNA Express Arabidopsis gene-mapping tool (http://signal.salk.edu/cgi-bin/tdnaexpress; Alonso et al., 2003) and ordered from the Nottingham Arabidopsis Stock Centre. Both mutant lines come from a T-DNA-mutagenized population in the Col-0 Arabidopsis ecotype. Primers used are listed in Supplemental Table S1. For initial characterization of single and double mutants, plants were grown in greenhouses under a 16-h photoperiod, at a day/night temperature regime of 23°C/17°C, under natural illumination supplemented with artificial lighting as described by Vidal et al. (2007). In addition, seeds of the *ndufs4* mutant were provided by E.H. Meyer. For LD/SD comparisons, wild-type and *ndufs8.1 ndufs8.2/ndufs4* seeds were sown at 1-week intervals, and seedlings were grown in controlled chambers in SD (8-h/

16-h day/night) at 100 μmol m^{-2} s^{-1} PAR to the eight- to nine-leaf stage (referred to as SD0). After this time point, rosette plantlets were either transferred to LD (16 h/8 h) or maintained under SD conditions under the same illumination conditions. Li-Cor fluorometer measurements were performed on well-developed leaves of 2- to 3-month-old rosette plants (minimum 2 cm^2 area). In all cases, experiments were carried out on mutant and Col-0 plants of similar development.

RNA Isolation and RT-PCR Analysis

Total RNA was prepared using the Trizol reagent (Invitrogen) following the manufacturer's recommendations. RNA (1 μg) was treated with RQ1 RNase-Free DNase (Promega) and reverse transcribed using random hexamers and the SuperScript III first-strand kit (Invitrogen) following the manufacturer's recommendations. The LightCycler 480 detection system (Roche Applied Science) was used to perform quantitative real-time PCR. Relative mRNA abundance was calculated using the comparative delta-cycle threshold method and normalized to the corresponding *ACT2* (*At3g18780*) gene levels. The sequences of primers used in this study are listed in Supplemental Table S1.

CO_2-Exchange Measurements

Responses of A to photon flux density (light curves) and internal CO_2 molar fraction (A/C_i curves) performed under ambient (21%) oxygen content were measured on attached leaves with an open infrared gas analysis system equipped with a leaf chamber fluorometer (Li-Cor 6400-40; Li-Cor) as described by Priault et al. (2006a). Leaves were dark adapted for at least 30 min before determining dark respiration.

Oxygen Respiratory Measurements

Oxygen isotope discrimination experiments were performed as described by Florez-Sarasa et al. (2007) under controlled conditions (12-h/12-h photoperiod), except that plants were grown under 80 μmol m^{-2} s^{-1} and oxygen-isotope fractionation calculations were made as described by Guy et al. (1989) and Ribas-Carbo et al. (1995). The AOX pathway capacity was measured on leaf tissues as described by Florez-Sarasa et al. (2009).

Preparation of Crude Leaf and Root Membrane Extracts, BN Electrophoresis, Western-Blot Analyses, and Determination of In-Gel NADH Dehydrogenase Activity

Extraction of total and mitochondrial proteins, BN/PAGE, two-dimensional BN/SDS electrophoresis, determination of in-gel NADH dehydrogenase activity of CI, and protein silver staining were performed as described previously (Pineau et al., 2008). Gels were electroblotted onto nitrocellulose membranes for SDS-PAGE and onto polyvinylidene difluoride membranes for BN/PAGE. Immunodetections were performed using wheat (*Triticum aestivum*) anti-NAD9 antibody (a gift from J.M. Grienenberger), anti-CA2 antibody directed against the C-terminal half of the mitochondrial CA2 (*At1g47260*) from Arabidopsis (a gift from E. Zabaleta), and mouse monoclonal *Sauromatum guttatum* anti-AOX antibody (a gift from A.H. Millar). Immunosignals were visualized by enhanced chemiluminescence according to the manufacturer's instructions (Roche Diagnostics).

Minipreparations of Percoll-Purified Leaf Mitochondria

One gram of fresh material was used to obtain crude leaf mitochondrial preparations, as described by Vidal et al. (2007). Mitochondria were further purified on a three-layer Percoll gradient (13%, 25%, and 45% [w/v] Percoll), performed in 2-mL Eppendorf tubes, using the protocol designed for the purification of *Nicotiana sylvestris* pollen mitochondria (De Paepe et al., 1993). The pyridine redox state could not be determined in mitochondrial extracts due to the oxidation of preparations during Percoll purification.

Rubisco Radioisotopic Assay

Total Rubisco activity was determined from the rate of $^{14}CO_2$ incorporation into acid-stable compounds and subsequent liquid scintillation counting of ^{14}C, according to Seemann and Sharkey (1986). Details are given in Supplemental Methods S1.

Antioxidant Activities

All enzymes were extracted from washed leaves in 50 mM potassium phosphate, pH 7.5, and measurements of activities of glycolate oxidase (EC 1.1.3.1), CAT (EC 1.11.1.6), APX (EC 1.11.1.11), and GR (EC 1.6.4.2) were as described by Streb et al. (1997). For APX activity, only the cytoplasmic form was determined.

Pigment Contents

Chlorophyll a/b contents were measured from 80% acetone extracts with extinction coefficients reported by Porra (2002).

Determination of Soluble Antioxidants in Leaf and Mitochondrial Extracts

Oxidized and reduced forms of glutathione, ascorbate, NAD, and NADP were measured in total leaf extracts or Percoll-purified mitochondrial preparations, by plate-reader assay, as described by Queval and Noctor (2007) and modified by Pétriacq et al. (2012). The pyridine redox state could not be determined in mitochondrial extracts due to their oxidation during Percoll purification (Vidal et al., 2007).

Untargeted Metabolomics by HILIC-MS

Polar metabolites were detected by HILIC coupled to qTOF-MS using a method from Paglia et al. (2012) that was modified by Pétriacq et al. (2016). Details are given in Supplemental Methods S1.

Targeted Metabolic Profiling by GC-MS

GC coupled to time-of-flight MS profiling and quantitative analysis of amino acids by HPLC were performed as described in detail by Noctor et al. (2007) and Tcherkez et al. (2010) using the isotopic facility structure of the Plateforme Metabolisme Metabolome. Details are given in Supplemental Methods S1.

ATP contents were quantified using the ENLITEN ATP Assay System Bioluminescence Detection Kit (Promega) using the manufacturer's instructions.

ROS Determination

In situ ROS detection was performed using NBT and diaminobenzidine stains, detecting superoxide and hydrogen peroxide, respectively, as described by Dutilleul et al. (2003b). Room-temperature spin-trapping EPR spectroscopy was carried out to measure apoplastic ROS, as described by Michelet and Krieger-Liszkay (2012). Details are given in Supplemental Methods S1. Luminol chemiluminescence was performed on leaves as described by Pétriacq et al. (2016). Results were calibrated using hydrogen peroxide as the ROS source.

NR Activity and Nitrate Determination

NR activity was determined as described by Fresneau et al. (2007) on desalted extracts purified with a NAP-5 column (Sephadex G-25; GE Healthcare). Nitrate ion contents were determined as described by Cataldo et al. (1975). Details are given in Supplemental Methods S1.

Anthocyanin Determination

Anthocyanin content was determined according to Vanderauwera et al. (2005) and expressed as optical density at 530 nm mg^{-1} fresh weight.

Electron Microscopy

Leaf samples were processed as described by Hawes and Satiat-Jeunemaitre (2001). Details are given in Supplemental Methods S1.

Statistical Methods

Significant differences ($P < 0.05$) were calculated using Student's t test.

Accession Numbers

Sequence data from this article can be found in the GenBank/EMBL data libraries under accession numbers At1g16700 and At1g79010 and in Supplemental Table S1.

Supplemental Data

The following supplemental materials are available.

Supplemental Figure S1. Resolution by two-dimensional BN/SDS-PAGE of root membrane proteins of Col-0 and the *ndufs8.1 ndufs8.2* double mutant.

Supplemental Figure S2. Electron microscopy of mitochondria in Col-0 and *ndufs8.1 ndufs8.2* leaves.

Supplemental Figure S3. Phenotypes of *ndufs8.1* and *ndufs8.2* single mutants, the *ndufs8.1 ndufs8.2* double mutant, and the *ndufs4* mutant.

Supplemental Figure S4. Col-0, *ndufs8.1 ndufs8.2*, and *ndufs4* plants grown in SD and LD conditions.

Supplemental Figure S5. Dimensions of leaf cells of Col-0 and *ndufs8.1 ndufs8.2* plants in SD and LD conditions.

Supplemental Figure S6. Micrographs of chloroplast ultrastructure in Col-0 and *ndufs8.1 ndufs8.2* plants.

Supplemental Figure S7. Changes in the contents of sugars and tricarboxylic acid derivatives in Col-0 and *ndufs8.1 ndufs8.2* plants during the day/night cycle analyzed using GC-MS.

Supplemental Figure S8. Changes in the contents of amino acids in Col-0 and *ndufs8.1 ndufs8.2* plants during the day/night cycle analyzed by GC-MS (part 1).

Supplemental Figure S9. Changes in the contents of amino acids in Col-0 and *ndufs8.1 ndufs8.2* plants during the day/night cycle analyzed by GC-MS (part 2).

Supplemental Figure S10. Heat map and hierarchical clustering (cosine correlation) of metabolites found to be significant with respect to photoperiod (SD/LD) in a two-way ANOVA (GC-MS metabolomics).

Supplemental Figure S11. Metabolomic pattern in Col-0 and *ndufs8.1 ndufs8.2* plants and photoperiod-genotype interaction.

Supplemental Figure S12. HPLC quantitation of amino acids in Col-0 and *ndufs8.1 ndufs8.2* leaves.

Supplemental Figure S13. Transcriptional analysis of tricarboxylic acid-related enzymes in Col-0 and *ndufs8.1 ndufs8.2* leaves.

Supplemental Figure S14. Gas-exchange measurements of Col-0 and *ndufs8.1 ndufs8.2* plants maintained under SD and LD conditions.

Supplemental Figure S15. In situ detection of leaf superoxide and hydrogen peroxide in Col-0 and *ndufs8.1 ndufs8.2* plants grown under LD and SD conditions.

Supplemental Figure S16. Transcriptional analysis of redox enzymes in Col-0 and *ndufs8.1 ndufs8.2* plants under various illumination conditions.

Supplemental Figure S17. Cellular antioxidant activities and anthocyanin contents of Col-0 and *ndufs8.1 ndufs8.2* mutant plants maintained under SD and LD conditions.

Supplemental Table S1. Sequences of primers and accession numbers of genes used in this study.

Supplemental Methods S1. Supplemental Materials and Methods.

ACKNOWLEDGMENTS

We thank Béatrice Satiat Jeunemaître for help in ME analyses; Sophie Chailloux, Dorothée Thominet, and Ouardia Layoune for excellent technical help; A.H. Millar for the anti-AOX antibody, J.M. Grienenberger for the wheat anti-NAD9 antibody, and E. Zabaleta for the Arabidopsis anti-CA2 antibody; and E.H. Meyer for the gift of *ndufs4* seeds.

Received September 28, 2016; accepted November 16, 2016; published November 16, 2016.

LITERATURE CITED

Ahmad M, Lin C, Cashmore AR (1995) Mutations throughout an Arabidopsis blue-light photoreceptor impair blue-light-responsive anthocyanin accumulation and inhibition of hypocotyl elongation. Plant J **8:** 653–658

Alonso JM, Stepanova AN, Leisse TJ, Kim CJ, Chen H, Shinn P, Stevenson DK, Zimmerman J, Barajas P, Cheuk R, et al (2003) Genome-wide insertional mutagenesis of Arabidopsis thaliana. Science **301:** 653–657

Araújo WL, Nunes-Nesi A, Nikoloski Z, Sweetlove LJ, Fernie AR (2012) Metabolic control and regulation of the tricarboxylic acid cycle in photosynthetic and heterotrophic plant tissues. Plant Cell Environ **35:** 1–21

Becker B, Holtgrefe S, Jung S, Wunrau C, Kandlbinder A, Baier M, Dietz KJ, Backhausen JE, Scheibe R (2006) Influence of the photoperiod on redox regulation and stress responses in Arabidopsis thaliana L. (Heynh.) plants under long- and short-day conditions. Planta **224:** 380–393

Brangeon J, Sabar M, Gutierres S, Combettes B, Bove J, Gendy C, Chétrit P, Des Francs-Small CC, Pla M, Vedel F, et al (2000) Defective splicing of the first nad4 intron is associated with lack of several complex I subunits in the Nicotiana sylvestris NMS1 nuclear mutant. Plant J **21:** 269–280

Cataldo DA, Maroon M, Schrader LE, Youngs VL (1975) Rapid colorimetric determination of nitrate in plant tissue by nitration of salicylic acid. Commun Soil Sci Plant Anal **6:** 71–80

Cohen S, Zmudjak M, Colas des Francs-Small C, Malik S, Shaya F, Keren I, Belausov E, Many Y, Brown GG, Small I, et al (2014) nMAT4, a maturase factor required for nad1 pre-mRNA processing and maturation, is essential for holocomplex I biogenesis in Arabidopsis mitochondria. Plant J **78:** 253–268

Colas des Francs-Small C, Small I (2014) Surrogate mutants for studying mitochondrially encoded functions. Biochimie **100:** 234–242

de Longevialle AF, Meyer EH, Andrés C, Taylor NL, Lurin C, Millar AH, Small ID (2007) The pentatricopeptide repeat gene OTP43 is required for trans-splicing of the mitochondrial nad1 intron 1 in *Arabidopsis thaliana*. Plant Cell **19:** 3256–3265

De Paepe R, Chétrit P, Vitart V, Ambard-Bretteville F, Prat D, Vedel F (1990) Several nuclear genes control both male sterility and mitochondrial protein synthesis in Nicotiana sylvestris protoclones. Mol Gen Genet **222:** 206–210

De Paepe R, Forchioni A, Chétrit P, Vedel F (1993) Specific mitochondrial proteins in pollen: presence of an additional ATP synthase beta subunit. Proc Natl Acad Sci USA **90:** 5934–5938

de Sousa CAF, Sodek L (2002) The metabolic response of plants to oxygen deficiency. Braz J Plant Physiol **14:** 83–94

Djebbar R, Rzigui T, Pétriacq P, Mauve C, Priault P, Fresneau C, De Paepe M, Florez-Sarasa I, Benhassaine-Kesri G, Streb P, et al (2012) Respiratory complex I deficiency induces drought tolerance by impacting leaf stomatal and hydraulic conductances. Planta **235:** 603–614

Dutilleul C, Driscoll S, Cornic G, De Paepe R, Foyer CH, Noctor G (2003a) Functional mitochondrial complex I is required by tobacco leaves for optimal photosynthetic performance in photorespiratory conditions and during transients. Plant Physiol **131:** 264–275

Dutilleul C, Garmier M, Noctor G, Mathieu C, Chétrit P, Foyer CH, de Paepe R (2003b) Leaf mitochondria modulate whole cell redox homeostasis, set antioxidant capacity, and determine stress resistance through altered signaling and diurnal regulation. Plant Cell **15:** 1212–1226

Dutilleul C, Lelarge C, Prioul JL, De Paepe R, Foyer CH, Noctor G (2005) Mitochondria-driven changes in leaf NAD status exert a crucial influence on the control of nitrate assimilation and the integration of carbon and nitrogen metabolism. Plant Physiol **139:** 64–78

Efremov RG, Baradaran R, Sazanov LA (2010) The architecture of respiratory complex I. Nature **465:** 441–445

Florez-Sarasa I, Ostaszewska M, Galle A, Flexas J, Rychter AM, Ribas-Carbo M (2009) Changes of alternative oxidase activity, capacity and protein content in leaves of Cucumis sativus wild-type and MSC16 mutant grown under different light intensities. Physiol Plant **137:** 419–426

Florez-Sarasa ID, Bouma TJ, Medrano H, Azcon-Bieto J, Ribas-Carbo M (2007) Contribution of the cytochrome and alternative pathways to growth respiration and maintenance respiration in Arabidopsis thaliana. Physiol Plant **129:** 143–151

Foyer CH, Noctor G (2011) Ascorbate and glutathione: the heart of the redox hub. Plant Physiol **155:** 2–18

Foyer CH, Noctor G, Hodges M (2011) Respiration and nitrogen assimilation: targeting mitochondria-associated metabolism as a means to enhance nitrogen use efficiency. J Exp Bot **62:** 1467–1482

Fresneau C, Ghashghaie J, Cornic G (2007) Drought effect on nitrate reductase and sucrose-phosphate synthase activities in wheat (Triticum durum L.): role of leaf internal CO_2. J Exp Bot **58:** 2983–2992

Fromm S, Göing J, Lorenz C, Peterhänsel C, Braun HP (2016) Depletion of the "gamma-type carbonic anhydrase-like" subunits of complex I affects central mitochondrial metabolism in Arabidopsis thaliana. Biochim Biophys Acta **1857:** 60–71

Fukushima A, Kusano M, Nakamichi N, Kobayashi M, Hayashi N, Sakakibara H, Mizuno T, Saito K (2009) Impact of clock-associated Arabidopsis pseudo-response regulators in metabolic coordination. Proc Natl Acad Sci USA **106:** 7251–7256

Galle A, Florez-Sarasa I, Thameur A, de Paepe R, Flexas J, Ribas-Carbo M (2010) Effects of drought stress and subsequent rewatering on photosynthetic and respiratory pathways in Nicotiana sylvestris wild type and the mitochondrial complex I-deficient CMSII mutant. J Exp Bot **61:** 765–775

Gibon Y, Bläsing OE, Palacios-Rojas N, Pankovic D, Hendriks JHM, Fisahn J, Höhne M, Günther M, Stitt M (2004) Adjustment of diurnal starch turnover to short days: depletion of sugar during the night leads to a temporary inhibition of carbohydrate utilization, accumulation of sugars and post-translational activation of ADP-glucose pyrophosphorylase in the following light period. Plant J **39:** 847–862

Gibon Y, Pyl ET, Sulpice R, Lunn JE, Höhne M, Günther M, Stitt M (2009) Adjustment of growth, starch turnover, protein content and central metabolism to a decrease of the carbon supply when Arabidopsis is grown in very short photoperiods. Plant Cell Environ **32:** 859–874

Giraud E, Ng S, Carrie C, Duncan O, Low J, Lee CP, Van Aken O, Millar AH, Murcha M, Whelan J (2010) TCP transcription factors link the regulation of genes encoding mitochondrial proteins with the circadian clock in *Arabidopsis thaliana*. Plant Cell **22:** 3921–3934

Gupta KJ, Shah JK, Brotman Y, Jahnke K, Willmitzer L, Kaiser WM, Bauwe H, Igamberdiev AU (2012) Inhibition of aconitase by nitric oxide leads to induction of the alternative oxidase and to a shift of metabolism towards biosynthesis of amino acids. J Exp Bot **63:** 1773–1784

Gutierres S, Sabar M, Lelandais C, Chetrit P, Diolez P, Degand H, Boutry M, Vedel F, de Kouchkovsky Y, De Paepe R (1997) Lack of mitochondrial and nuclear-encoded subunits of complex I and alteration of the respiratory chain in Nicotiana sylvestris mitochondrial deletion mutants. Proc Natl Acad Sci USA **94:** 3436–3441

Guy RD, Berry JA, Fogel ML, Hoering TC (1989) Differential fractionation of oxygen isotopes by cyanide-resistant and cyanide-sensitive respiration in plants. Planta **177:** 483–491

Hager J, Pellny TK, Mauve C, Lelarge-Trouverie C, De Paepe R, Foyer CH, Noctor G (2010) Conditional modulation of NAD levels and metabolite profiles in Nicotiana sylvestris by mitochondrial electron transport and carbon/nitrogen supply. Planta **231:** 1145–1157

Hashida SN, Takahashi H, Uchimiya H (2009) The role of NAD biosynthesis in plant development and stress responses. Ann Bot (Lond) **103:** 819–824

Hawes CR, Satiat-Jeunemaitre B, editors (2001) Plant Cell Biology: A Practical Approach, Ed 2. Oxford University Press, Oxford

Haydon MJ, Román Á, Arshad W (2015) Nutrient homeostasis within the plant circadian network. Front Plant Sci **6:** 299

Heldt HW (2005) Plant Biochemistry, Ed 3. Elsevier Academic Press, Heidelberg, Germany

Huang S, Van Aken O, Schwarzländer M, Belt K, Millar AH (2016) The roles of mitochondrial reactive oxygen species in cellular signaling and stress response in plants. Plant Physiol **171:** 1551–1559

Hurd TR, Collins Y, Abakumova I, Chouchani ET, Baranowski B, Fearnley IM, Prime TA, Murphy MP, James AM (2012) Inactivation of pyruvate dehydrogenase kinase 2 by mitochondrial reactive oxygen species. J Biol Chem **287:** 35153–35160

Igamberdiev AU, Gardeström P (2003) Regulation of NAD- and NADP-dependent isocitrate dehydrogenases by reduction levels of pyridine nucleotides in mitochondria and cytosol of pea leaves. Biochim Biophys Acta **1606:** 117–125

Karpova OV, Kuzmin EV, Elthon TE, Newton KJ (2002) Differential expression of alternative oxidase genes in maize mitochondrial mutants. Plant Cell **14:** 3271–3284

Karpova OV, Newton KJ (1999) A partially assembled complex I in NAD4-deficient mitochondria of maize. Plant J **17:** 511–521

Katoh A, Uenohara K, Akita M, Hashimoto T (2006) Early steps in the biosynthesis of NAD in Arabidopsis start with aspartate and occur in the plastid. Plant Physiol **141:** 851–857

Keren I, Tal L, des Francs-Small CC, Araújo WL, Shevtsov S, Shaya F, Fernie AR, Small I, Ostersetzer-Biran O (2012) nMAT1, a nuclear-encoded maturase involved in the trans-splicing of nad1 intron 1, is essential for mitochondrial complex I assembly and function. Plant J **71:** 413–426

Klodmann J, Sunderhaus S, Nimtz M, Jänsch L, Braun HP (2010) Internal architecture of mitochondrial complex I from *Arabidopsis thaliana*. Plant Cell **22:** 797–810

Koussevitzky S, Suzuki N, Huntington S, Armijo L, Sha W, Cortes D, Shulaev V, Mittler R (2008) Ascorbate peroxidase 1 plays a key role in the response of Arabidopsis thaliana to stress combination. J Biol Chem **283:** 34197–34203

Kühn K, Obata T, Feher K, Bock R, Fernie AR, Meyer EH (2015) Complete mitochondrial complex I deficiency induces an up-regulation of respiratory fluxes that is abolished by traces of functional complex I. Plant Physiol **168:** 1537–1549

Leman G, Gueguen N, Desquiret-Dumas V, Kane MS, Wettervald C, Chupin S, Chevrollier A, Lebre AS, Bonnefont JP, Barth M, et al (2015) Assembly defects induce oxidative stress in inherited mitochondrial complex I deficiency. Int J Biochem Cell Biol **65:** 91–103

Lepistö A, Rintamäki E (2012) Coordination of plastid and light signaling pathways upon development of Arabidopsis leaves under various photoperiods. Mol Plant **5:** 799–816

Liu Y, He J, Chen Z, Ren X, Hong X, Gong Z (2010) ABA overly-sensitive 5 (ABO5), encoding a pentatricopeptide repeat protein required for cis-splicing of mitochondrial nad2 intron 3, is involved in the abscisic acid response in Arabidopsis. Plant J **63:** 749–765

Liu YJ, Nunes-Nesi A, Wallström SV, Lager I, Michalecka AM, Norberg FEB, Widell S, Fredlund KM, Fernie AR, Rasmusson AG (2009) A redox-mediated modulation of stem bolting in transgenic *Nicotiana sylvestris* differentially expressing the external mitochondrial NADPH dehydrogenase. Plant Physiol **150:** 1248–1259

Marienfeld JR, Newton KJ (1994) The maize NCS2 abnormal growth mutant has a chimeric nad4-nad7 mitochondrial gene and is associated with reduced complex I function. Genetics **138:** 855–863

Meyer EH, Solheim C, Tanz SK, Bonnard G, Millar AH (2011) Insights into the composition and assembly of the membrane arm of plant complex I through analysis of subcomplexes in Arabidopsis mutant lines. J Biol Chem **286:** 26081–26092

Meyer EH, Tomaz T, Carroll AJ, Estavillo G, Delannoy E, Tanz SK, Small ID, Pogson BJ, Millar AH (2009) Remodeled respiration in ndufs4 with low phosphorylation efficiency suppresses Arabidopsis germination and growth and alters control of metabolism at night. Plant Physiol **151:** 603–619

Michalecka AM, Svensson AS, Johansson FI, Agius SC, Johanson U, Brennicke A, Binder S, Rasmusson AG (2003) Arabidopsis genes encoding mitochondrial type II NAD(P)H dehydrogenases have different evolutionary origin and show distinct responses to light. Plant Physiol **133:** 642–652

Michelet L, Krieger-Liszkay A (2012) Reactive oxygen intermediates produced by photosynthetic electron transport are enhanced in short-day grown plants. Biochim Biophys Acta **1817:** 1306–1313

Miwa S, Jow H, Baty K, Johnson A, Czapiewski R, Saretzki G, Treumann A, von Zglinicki T (2014) Low abundance of the matrix arm of complex I in mitochondria predicts longevity in mice. Nat Commun **5:** 3837

Møller IM (2001) Plant mitochondria and oxidative stress: electron transport, NADPH turnover, and metabolism of reactive oxygen species. Annu Rev Plant Physiol Plant Mol Biol **52:** 561–591

Moreau M, Azzopardi M, Clément G, Dobrenel T, Marchive C, Renne C, Martin-Magniette ML, Taconnat L, Renou JP, Robaglia C, et al (2012) Mutations in the *Arabidopsis* homolog of LST8/GβL, a partner of the target of rapamycin kinase, impair plant growth, flowering, and metabolic adaptation to long days. Plant Cell **24:** 463–481

Mouchiroud L, Houtkooper RH, Moullan N, Katsyuba E, Ryu D, Cantó C, Mottis A, Jo YS, Viswanathan M, Schoonjans K, et al (2013) The NAD(+)/sirtuin pathway modulates longevity through activation of mitochondrial UPR and FOXO signaling. Cell **154:** 430–441

Nagel DH, Kay SA (2012) Complexity in the wiring and regulation of plant circadian networks. Curr Biol **22:** R648–R657

Noctor G, Bergot G, Mauve C, Thominet D, Lelarge-Trouverie C, Prioul JL (2007) A comparative study of amino acid measurement in leaf extracts by gas chromatography-time of flight-mass spectrometry and high performance liquid chromatography with fluorescence detection. Metabolomics **3:** 161–174

Noctor G, Queval G, Gakière B (2006) NAD(P) synthesis and pyridine nucleotide cycling in plants and their potential importance in stress conditions. J Exp Bot **57:** 1603–1620

O'Leary B, Park J, Plaxton WC (2011) The remarkable diversity of plant PEPC (phosphoenolpyruvate carboxylase): recent insights into the physiological functions and post-translational controls of non-photosynthetic PEPCs. Biochem J **436:** 15–34

op den Camp RGL, Przybyla D, Ochsenbein C, Laloi C, Kim C, Danon A, Wagner D, Hideg E, Göbel C, Feussner I, et al (2003) Rapid induction of distinct stress responses after the release of singlet oxygen in *Arabidopsis*. Plant Cell **15:** 2320–2332

Paglia G, Hrafnsdóttir S, Magnúsdóttir M, Fleming RMT, Thorlacius S, Palsson BØ, Thiele I (2012) Monitoring metabolites consumption and secretion in cultured cells using ultra-performance liquid chromatography quadrupole-time of flight mass spectrometry (UPLC-Q-ToF-MS). Anal Bioanal Chem **402:** 1183–1198

Peek CB, Affinati AH, Ramsey KM, Kuo HY, Yu W, Sena LA, Ilkayeva O, Marcheva B, Kobayashi Y, Omura C, et al (2013) Circadian clock NAD+ cycle drives mitochondrial oxidative metabolism in mice. Science **342:** 1243417

Peek CB, Ramsey KM, Marcheva B, Bass J (2012) Nutrient sensing and the circadian clock. Trends Endocrinol Metab **23:** 312–318

Pellny TK, Van Aken O, Dutilleul C, Wolff T, Groten K, Bor M, De Paepe R, Reyss A, Van Breusegem F, Noctor G, et al (2008) Mitochondrial respiratory pathways modulate nitrate sensing and nitrogen-dependent regulation of plant architecture in Nicotiana sylvestris. Plant J **54:** 976–992

Perales M, Eubel H, Heinemeyer J, Colaneri A, Zabaleta E, Braun HP (2005) Disruption of a nuclear gene encoding a mitochondrial gamma carbonic anhydrase reduces complex I and supercomplex I + III2 levels and alters mitochondrial physiology in Arabidopsis. J Mol Biol **350:** 263–277

Pétriacq P, de Bont L, Hager J, Didierlaurent L, Mauve C, Guérard F, Noctor G, Pelletier S, Renou JP, Tcherkez G, et al (2012) Inducible NAD overproduction in Arabidopsis alters metabolic pools and gene expression correlated with increased salicylate content and resistance to Pst-AvrRpm1. Plant J **70:** 650–665

Pétriacq P, de Bont L, Tcherkez G, Gakière B (2013) NAD: not just a pawn on the board of plant-pathogen interactions. Plant Signal Behav **8:** e22477

Pétriacq P, Ton J, Patrit O, Tcherkez G, Gakière B (2016) NAD acts as an integral regulator of multiple defense layers. Plant Physiol **172:** 1465–1479

Pineau B, Layoune O, Danon A, De Paepe R (2008) L-Galactono-1,4-lactone dehydrogenase is required for the accumulation of plant respiratory complex I. J Biol Chem **283:** 32500–32505

Pineau B, Mathieu C, Gérard-Hirne C, De Paepe R, Chétrit P (2005) Targeting the NAD7 subunit to mitochondria restores a functional complex I and a wild type phenotype in the Nicotiana sylvestris CMS II mutant lacking nad7. J Biol Chem **280:** 25994–26001

Pla M, Mathieu C, De Paepe R, Chétrit P, Vedel F (1995) Deletion of the last two exons of the mitochondrial nad7 gene results in lack of the NAD7 polypeptide in a Nicotiana sylvestris CMS mutant. Mol Gen Genet **248:** 79–88

Porra RJ (2002) The chequered history of the development and use of simultaneous equations for the accurate determination of chlorophylls a and b. Photosynth Res **73:** 149–156

Priault P, Fresneau C, Noctor G, De Paepe R, Cornic G, Streb P (2006a) The mitochondrial CMSII mutation of Nicotiana sylvestris impairs adjustment of photosynthetic carbon assimilation to higher growth irradiance. J Exp Bot **57:** 2075–2085

Priault P, Tcherkez G, Cornic G, De Paepe R, Naik R, Ghashghaie J, Streb P (2006b) The lack of mitochondrial complex I in a CMSII mutant of Nicotiana sylvestris increases photorespiration through an increased internal resistance to CO_2 diffusion. J Exp Bot **57:** 3195–3207

Priault P, Vidal G, De Paepe R, Ribas-Carbo M (2007) Leaf age-related changes in respiratory pathways are dependent on complex I activity in Nicotiana sylvestris. Physiol Plant **129:** 152–162

Price TO, Eranki V, Banks WA, Ercal N, Shah GN (2012) Topiramate treatment protects blood-brain barrier pericytes from hyperglycemia-induced oxidative damage in diabetic mice. Endocrinology **153:** 362–372

Procaccio V, Wallace DC (2004) Late-onset Leigh syndrome in a patient with mitochondrial complex I NDUFS8 mutations. Neurology **62:** 1899–1901

Qin Y, Leydon AR, Manziello A, Pandey R, Mount D, Denic S, Vasic B, Johnson MA, Palanivelu R (2009) Penetration of the stigma and style elicits a novel transcriptome in pollen tubes, pointing to genes critical for growth in a pistil. PLoS Genet **5:** e1000621

Queval G, Issakidis-Bourguet E, Hoeberichts FA, Vandorpe M, Gakière B, Vanacker H, Miginiac-Maslow M, Van Breusegem F, Noctor G (2007) Conditional oxidative stress responses in the Arabidopsis photorespiratory mutant cat2 demonstrate that redox state is a key modulator of daylength-dependent gene expression, and define photoperiod as a crucial factor in the regulation of H_2O_2-induced cell death. Plant J **52:** 640–657

Queval G, Neukermans J, Vanderauwera S, Van Breusegem F, Noctor G (2012) Day length is a key regulator of transcriptomic responses to both CO_2 and H_2O_2 in Arabidopsis. Plant Cell Environ **35:** 374–387

Queval G, Noctor G (2007) A plate reader method for the measurement of NAD, NADP, glutathione, and ascorbate in tissue extracts: application to redox profiling during Arabidopsis rosette development. Anal Biochem **363:** 58–69

Rasmusson AG, Geisler DA, Møller IM (2008) The multiplicity of dehydrogenases in the electron transport chain of plant mitochondria. Mitochondrion **8:** 47–60

Rasmusson AG, Wallström SV (2010) Involvement of mitochondria in the control of plant cell NAD(P)H reduction levels. Biochem Soc Trans **38:** 661–666

Rey G, Reddy AB (2013) Protein acetylation links the circadian clock to mitochondrial function. Proc Natl Acad Sci USA **110:** 3210–3211

Ribas-Carbo M, Berry JA, Yakir D, Giles L, Robinson SA, Lennon AM, Siedow JN (1995) Electron partitioning between the cytochrome and alternative pathways in plant mitochondria. Plant Physiol **109:** 829–837

Robbins NS, Pharr DM (1987) Regulation of photosynthetic carbon metabolism in cucumber by light intensity and photosynthetic period. Plant Physiol **85:** 592–597

Sabar M, De Paepe R, de Kouchkovsky Y (2000) Complex I impairment, respiratory compensations, and photosynthetic decrease in nuclear and mitochondrial male sterile mutants of *Nicotiana sylvestris*. Plant Physiol **124:** 1239–1250

Saisho D, Nambara E, Naito S, Tsutsumi N, Hirai A, Nakazono M (1997) Characterization of the gene family for alternative oxidase from Arabidopsis thaliana. Plant Mol Biol **35:** 585–596

Sassone-Corsi P (2012) NAD+, a circadian metabolite with an epigenetic twist. Endocrinology **153:** 1–5

Schmid M, Davison TS, Henz SR, Pape UJ, Demar M, Vingron M, Schölkopf B, Weigel D, Lohmann JU (2005) A gene expression map of Arabidopsis thaliana development. Nat Genet **37:** 501–506

Schreiber V, Dantzer F, Ame JC, de Murcia G (2006) Poly(ADP-ribose): novel functions for an old molecule. Nat Rev Mol Cell Biol **7:** 517–528

Seemann JR, Sharkey TD (1986) Salinity and nitrogen effects on photosynthesis, ribulose-1,5-bisphosphate carboxylase and metabolite pool sizes in *Phaseolus vulgaris* L. Plant Physiol **82:** 555–560

Shah JK, Cochrane DW, De Paepe R, Igamberdiev AU (2013) Respiratory complex I deficiency results in low nitric oxide levels, induction of hemoglobin and upregulation of fermentation pathways. Plant Physiol Biochem **63:** 185–190

Shen W, Wei Y, Dauk M, Tan Y, Taylor DC, Selvaraj G, Zou J (2006) Involvement of a glycerol-3-phosphate dehydrogenase in modulating the NADH/NAD+ ratio provides evidence of a mitochondrial glycerol-3-phosphate shuttle in *Arabidopsis*. Plant Cell **18:** 422–441

Shim JS, Imaizumi T (2015) Circadian clock and photoperiodic response in Arabidopsis: from seasonal flowering to redox homeostasis. Biochemistry **54:** 157–170

Smith CA, Want EJ, O'Maille G, Abagyan R, Siuzdak G (2006) XCMS: processing mass spectrometry data for metabolite profiling using nonlinear peak alignment, matching, and identification. Anal Chem **78:** 779–787

Soto D, Córdoba JP, Villarreal F, Bartoli C, Schmitz J, Maurino VG, Braun HP, Pagnussat GC, Zabaleta E (2015) Functional characterization of mutants affected in the carbonic anhydrase domain of the respiratory complex I in Arabidopsis thaliana. Plant J **83:** 831–844

Stangherlin A, Reddy AB (2013) Regulation of circadian clocks by redox homeostasis. J Biol Chem **288:** 26505–26511

Streb P, Feierabend J, Bligny R (1997) Resistance to photoinhibition of photosystem II and catalase and antioxidative protection in high mountain plants. Plant Cell Environ **20:** 1030–1040

Sunderhaus S, Dudkina NV, Jänsch L, Klodmann J, Heinemeyer J, Perales M, Zabaleta E, Boekema EJ, Braun HP (2006) Carbonic anhydrase subunits form a matrix-exposed domain attached to the membrane arm of mitochondrial complex I in plants. J Biol Chem **281:** 6482–6488

Sweetlove LJ, Beard KF, Nunes-Nesi A, Fernie AR, Ratcliffe RG (2010) Not just a circle: flux modes in the plant TCA cycle. Trends Plant Sci **15:** 462–470

Szal B, Dabrowska Z, Malmberg G, Gardeström P, Rychter AM (2008) Changes in energy status of leaf cells as a consequence of mitochondrial genome rearrangement. Planta **227:** 697–706

Tan B, Young DA, Lu ZH, Wang T, Meier TI, Shepard RL, Roth K, Zhai Y, Huss K, Kuo MS, et al (2013) Pharmacological inhibition of nicotinamide phosphoribosyltransferase (NAMPT), an enzyme essential for NAD+ biosynthesis, in human cancer cells: metabolic basis and potential clinical implications. J Biol Chem **288:** 3500–3511

Tcherkez G, Mahé A, Gauthier P, Mauve C, Gout E, Bligny R, Cornic G, Hodges M (2009) In folio respiratory fluxomics revealed by ^{13}C isotopic labeling and H/D isotope effects highlight the noncyclic nature of the tricarboxylic acid "cycle" in illuminated leaves. Plant Physiol **151:** 620–630

Tcherkez G, Schäufele R, Nogués S, Piel C, Boom A, Lanigan G, Barbaroux C, Mata C, Elhani S, Hemming D, et al (2010) On the $^{13}C/^{12}C$ isotopic signal of day and night respiration at the mesocosm level. Plant Cell Environ **33:** 900–913

Tomaz T, Bagard M, Pracharoenwattana I, Lindén P, Lee CP, Carroll AJ, Ströher E, Smith SM, Gardeström P, Millar AH (2010) Mitochondrial malate dehydrogenase lowers leaf respiration and alters photorespiration and plant growth in Arabidopsis. Plant Physiol **154:** 1143–1157

Tschoep H, Gibon Y, Carillo P, Armengaud P, Szecowka M, Nunes-Nesi A, Fernie AR, Koehl K, Stitt M (2009) Adjustment of growth and central metabolism to a mild but sustained nitrogen-limitation in Arabidopsis. Plant Cell Environ **32:** 300–318

Vanderauwera S, Zimmermann P, Rombauts S, Vandenabeele S, Langebartels C, Gruissem W, Inzé D, Van Breusegem F (2005) Genome-wide analysis of hydrogen peroxide-regulated gene expression in Arabidopsis reveals a high light-induced transcriptional cluster involved in anthocyanin biosynthesis. Plant Physiol **139:** 806–821

Vanlerberghe GC, McIntosh L (1996) Signals regulating the expression of the nuclear gene encoding alternative oxidase of plant mitochondria. Plant Physiol **111:** 589–595

Verkaart S, Koopman WJH, van Emst-de Vries SE, Nijtmans LGJ, van den Heuvel LWPJ, Smeitink JAM, Willems PHGM (2007) Superoxide production is inversely related to complex I activity in inherited complex I deficiency. Biochim Biophys Acta **1772:** 373–381

Vidal G, Ribas-Carbo M, Garmier M, Dubertret G, Rasmusson AG, Mathieu C, Foyer CH, De Paepe R (2007) Lack of respiratory chain complex I impairs alternative oxidase engagement and modulates redox signaling during elicitor-induced cell death in tobacco. Plant Cell **19:** 640–655

Vogel RO, Smeitink JAM, Nijtmans LGJ (2007) Human mitochondrial complex I assembly: a dynamic and versatile process. Biochim Biophys Acta **1767:** 1215–1227

Wallström SV, Florez-Sarasa I, Araújo WL, Aidemark M, Fernández-Fernández M, Fernie AR, Ribas-Carbó M, Rasmusson AG (2014) Suppression of the external mitochondrial NADPH dehydrogenase, NDB1, in Arabidopsis thaliana affects central metabolism and vegetative growth. Mol Plant **7:** 356–368

Wang Q, Fristedt R, Yu X, Chen Z, Liu H, Lee Y, Guo H, Merchant SS, Lin C (2012) The γ-carbonic anhydrase subcomplex of mitochondrial complex I is essential for development and important for photomorphogenesis of Arabidopsis. Plant Physiol **160:** 1373–1383

Willekens H, Chamnongpol S, Davey M, Schraudner M, Langebartels C, Van Montagu M, Inzé D, Van Camp W (1997) Catalase is a sink for H_2O_2 and is indispensable for stress defence in C_3 plants. EMBO J **16:** 4806–4816

Yoshida K, Noguchi K (2009) Differential gene expression profiles of the mitochondrial respiratory components in illuminated Arabidopsis leaves. Plant Cell Physiol **50:** 1449–1462

Zabaleta E, Martin MV, Braun HP (2012) A basal carbon concentrating mechanism in plants? Plant Sci **187:** 97–104

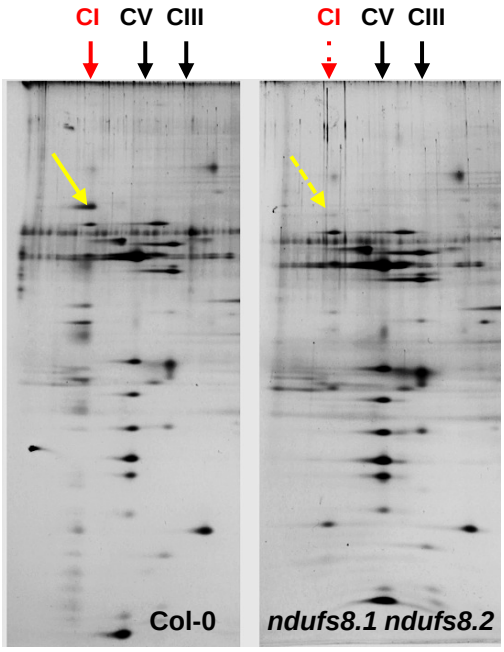

Figure S1. Resolution by two-dimensional (2D) BN-SDS PAGE of root membrane proteins of Col-0 and of the *ndufs8.1 ndufs8.2* double mutant

Total root membrane proteins solubilised with β-dodecylmaltoside were resolved by two-dimensional (2D) BN-SDS PAGE and silver stained according to Pineau et al. (2008). CI denotes complex I; CV, complex V; CIII, complex III. Subunits of CI, in particular the 76 kD subunit (yellow arrow), which are clearly visible on the Col-0 gel are hardly detectable on the *ndufs8.1 ndufs8.2* mutant pattern.

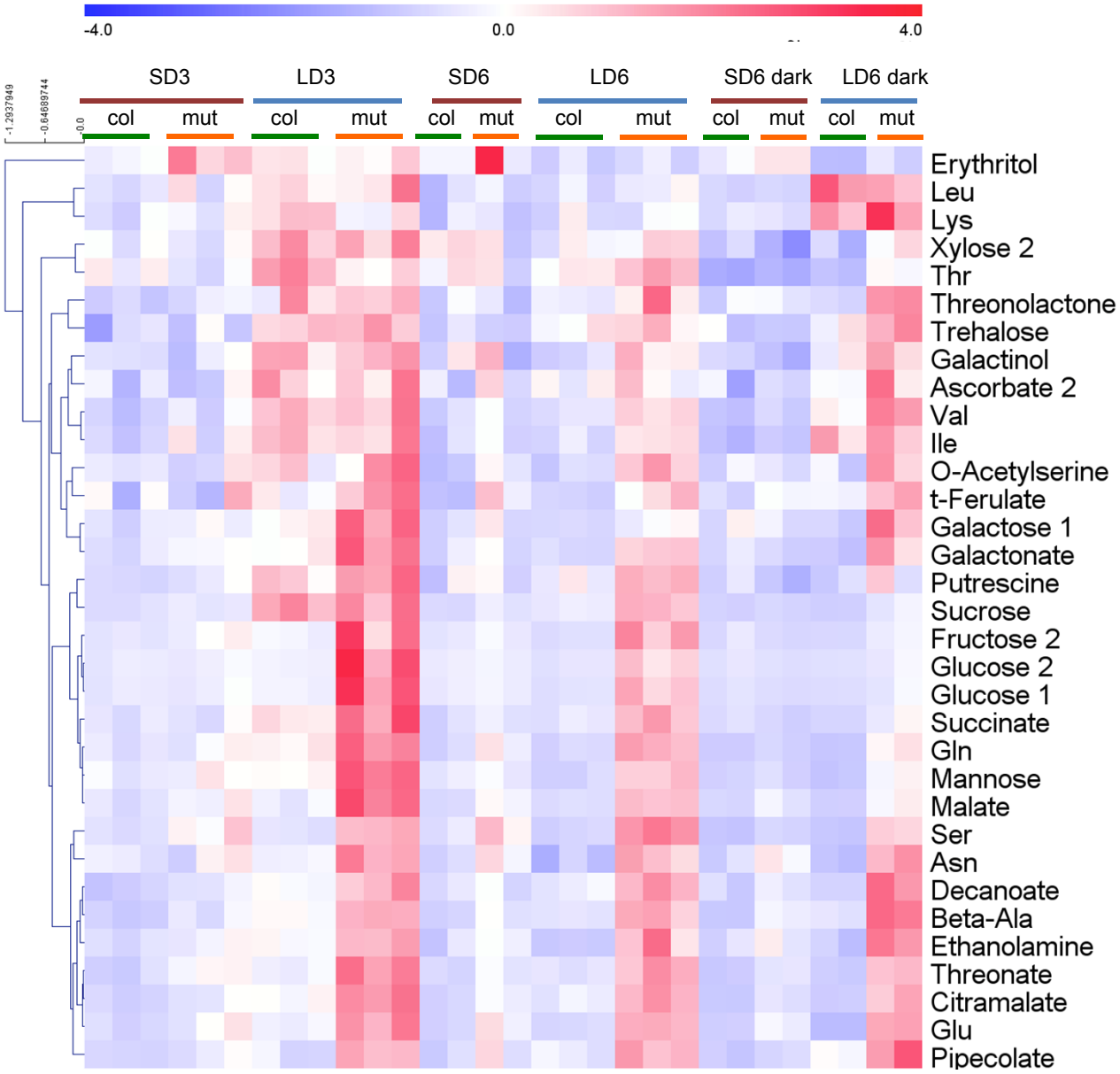

Figure S10. **Heat-map and hierarchical clustering (cosine correlation) of metabolites found to be significant with respect to photoperiod (SD/LD) in a two-way ANOVA (GC-MS metabolomics)**
Col-0 (col) and *ndufs8.1 ndufs8.2* (mut) leaves were sampled from SD3/LD3 at the middle of the light period and from SD6/LD6 plants both at the middle of the light period and at the end of the night period (dark). Metabolomic analyses were carried out 3 times for each condition (*i.e.*, 3 biological replicates). Relative metabolite content are represented as mean-centered values with a color scale (blue, low content; red, high content). Numbers close to metabolite names refer to individual analytes associated with the metabolite of interest.

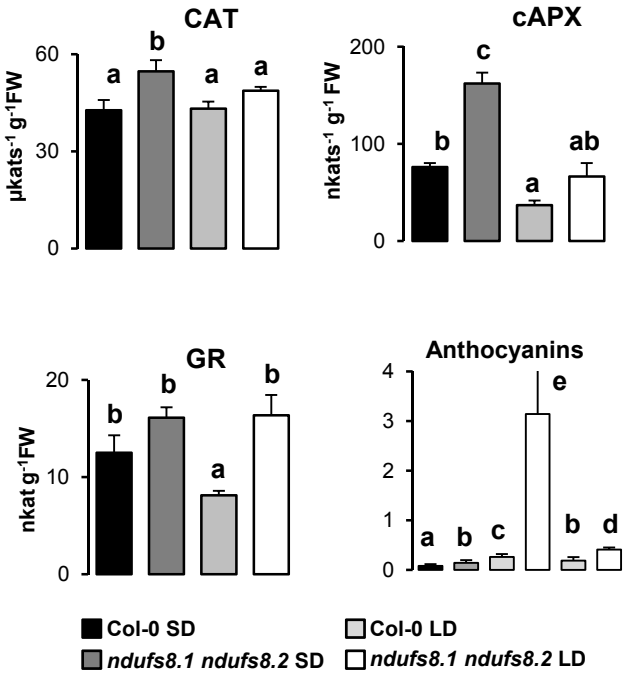

Figure S17. **Cellular antioxidant activities and anthocyanin contents of Col-0 and *ndufs8.1 ndufs8.2* mutant plants maintained under SD and LD conditions**

Leaves of SD12/LD12 plants were sampled at midday. CAT, catalase; cAPX, non-chloroplastic (cytosolic) ascorbate peroxidase; GR, glutathione reductase. Anthocyanin levels of Col-0 and *ndufs8.1 ndufs8.2* leaves are expressed in OD 530 mg FW^{-1}. Columns 1, 3: SD3 plants, columns 3, 4: LD3 plants columns 5, 6: LD6 plants. Results are means +SE of measurements on 4-6 different plants for activities and at least 6 different plants for anthocyanins. Different letters indicate statistically significant differences according to Student *t* test.

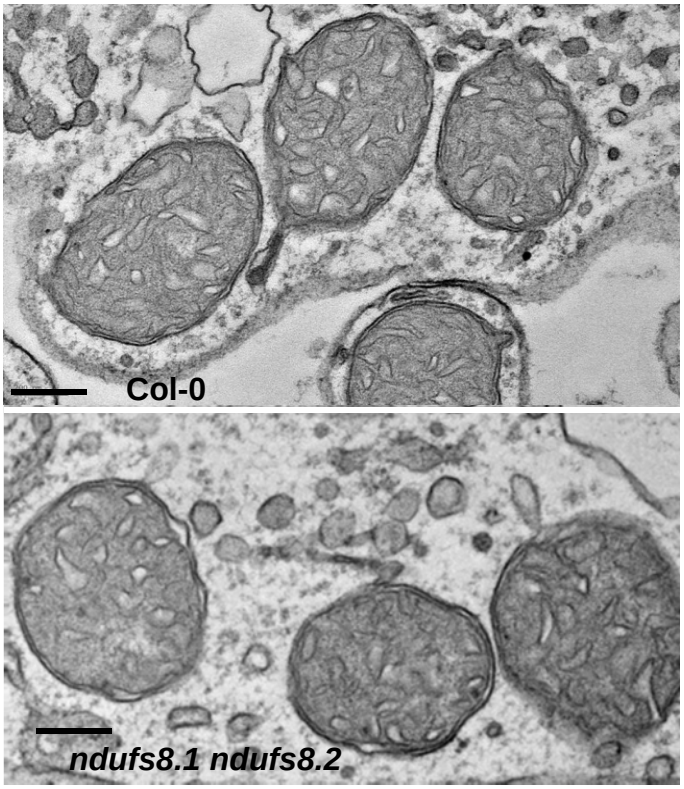

Figure S2. **Electron microscopy of mitochondria in Col-0 and *ndufs8.1 ndufs8.2* leaves.** In both photographs: bar = 0.5 µm.

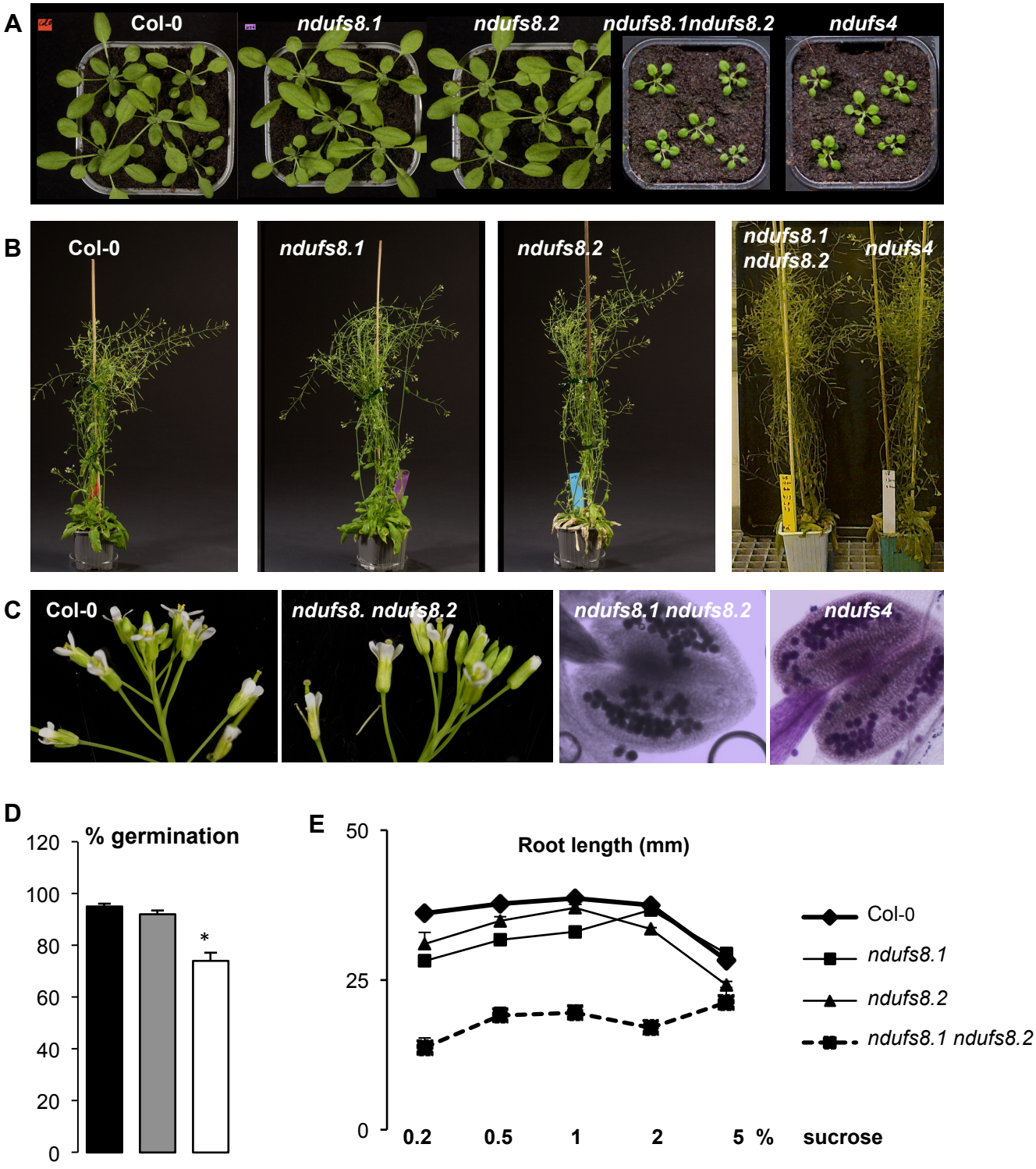

Figure S3. Phenotypes of *ndufs8.1 and ndufs8.2* single mutants, the *ndufs8.1 ndufs8.2* double mutant and the *ndufs4* mutant

A, One month-old plantlets of *ndufs8.1 and ndufs8.2* single mutants, the *ndufs8.1 ndufs8.2* double mutant, and the *ndufs4* mutant compared to Col-0 under long day (LD) condition. Development is delayed in the double mutant only.

B, Adult plants grown in greenhouse under long day (LD) condition. Plant dimensions and formation of siliques are unaffected in both the *ndufs8.1 ndufs8.2* - and the *ndufs4* mutants.

C, Inflorescences of Col-0 and of the *ndufs8.1 ndufs8.2* mutant (two left photographs) and Alexander dye stained pollen of *ndufs8.1 ndufs8.2* and *ndufs4* mutant (two right photographs). Pollen viability is normal in both mutants.

D, % Germination on soil at day 7 after sowing. Black: Col-0; grey: *ndufs8.1 ndufs8.2*; white: *ndufs4;** indicate significant difference between mutant and WT.

E, Root length of *in vitro* germinated plantlets 6 days after sowing on sucrose-containing media.

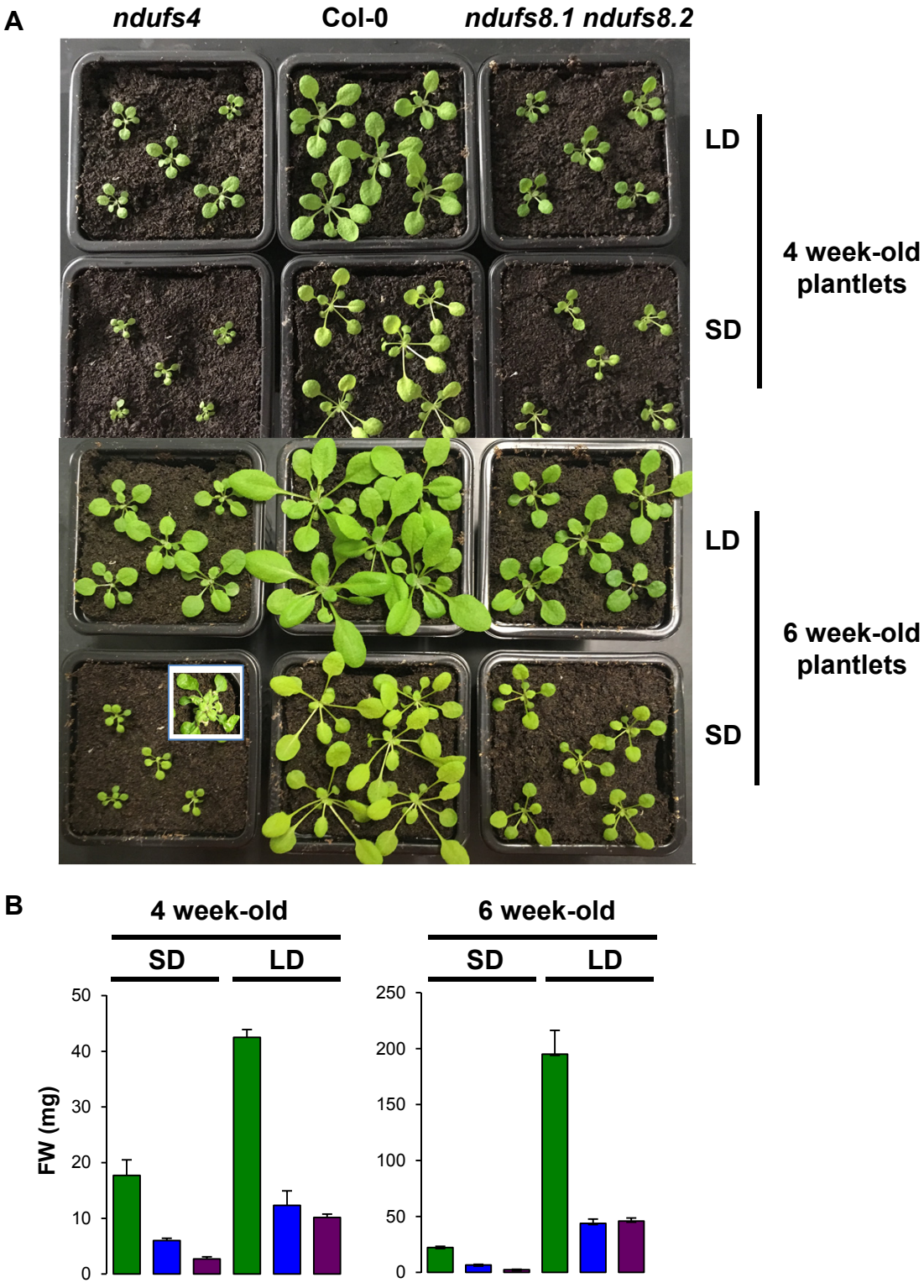

Figure S4. Col-0, *ndufs8.1 ndufs8.2* and *ndufs4* plants grown in SD and LD conditions
Seeds were germinated on soil in greenhouses in either SD or LD condition (100 µmol m^{-2} s^{-1} PAR)
A, Photographs of 4 week- old plantlets and 6 week-old plantlets; inset: *ndufs4* plantlet with necrotic points
B, Histograms of FW (mg). Left : 4 week- old plantlets; right: 6 week-old plantlets; Col-0: green columns; *ndufs8.1 ndufs8.2*: blue columns; *ndufs4*: purple columns

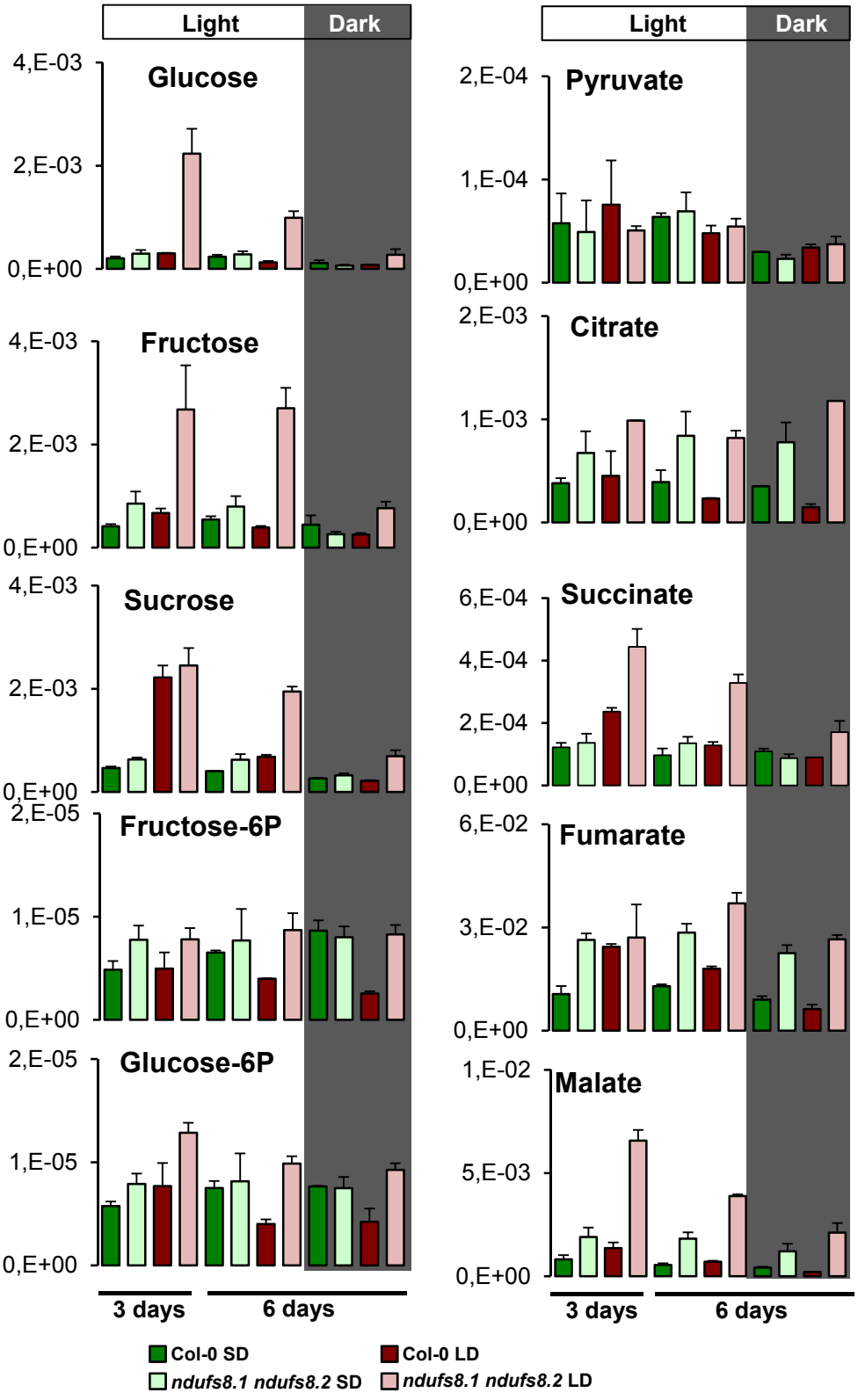

Figure S7. Changes in contents of sugars and TCA derivatives in Col-0 and *ndufs8.1 ndufs8.2* plants during the day/night cycle analyzed using GC-MS. Leaves of SD and LD plants were sampled in the middle of the light period at day 3 (light, columns 1-4), and both in the light (columns 5-8) and at the end of the dark (columns 9-12) at day 6. Levels of metabolites are expressed in relative units.

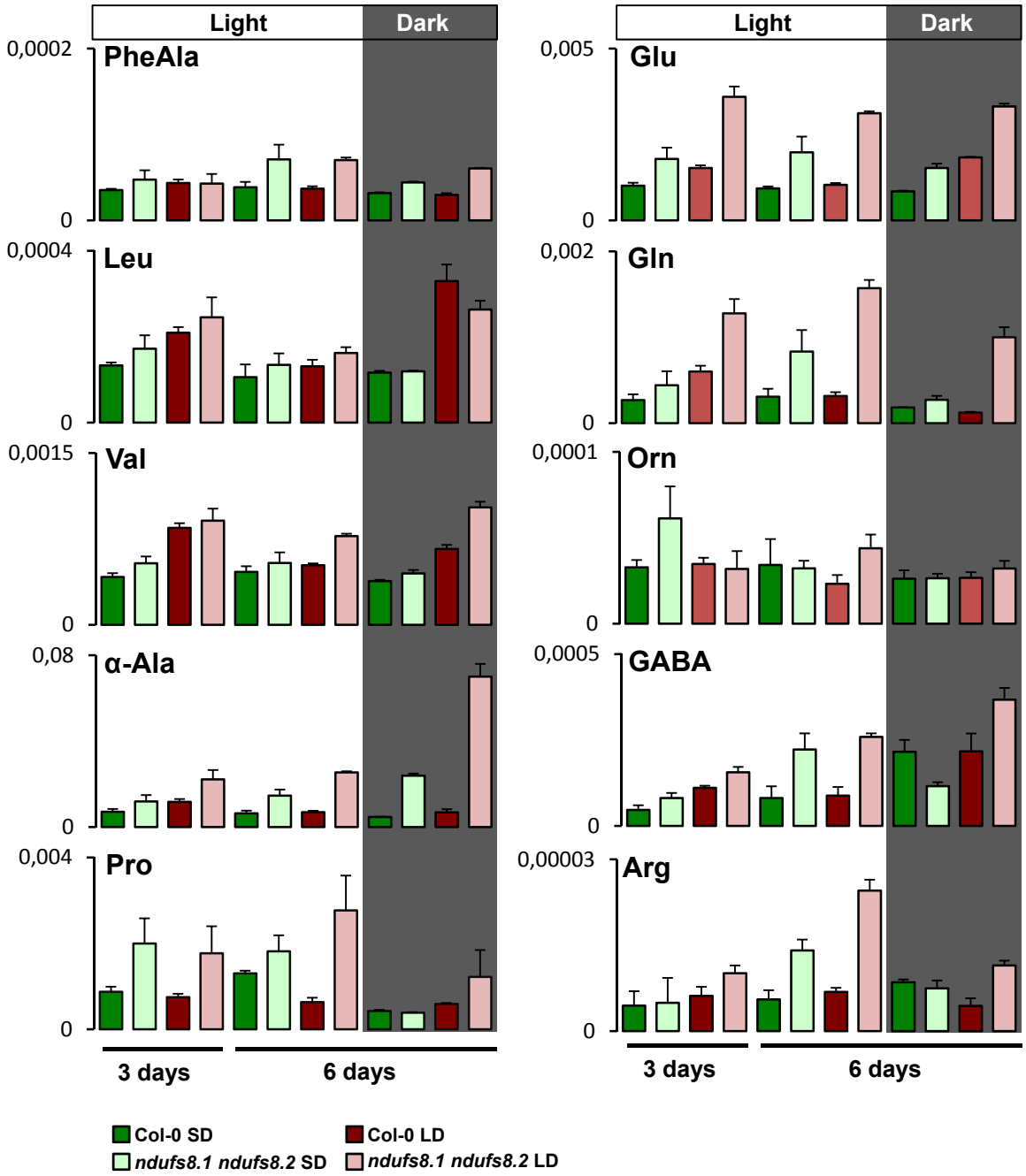

Figure S8. Changes in contents of amino acids in Col-0 and *ndufs8.1 ndufs8.2* plants during the day/night cycle analyzed by GC-MS (part 1). Leaves of SD and LD plants were sampled in the middle of the light period at day 3 (light, columns 1-4), and both in the light (columns 5-8) and at the end of the dark period (columns 9- 12) at day 6. Contents are expressed in relative units.

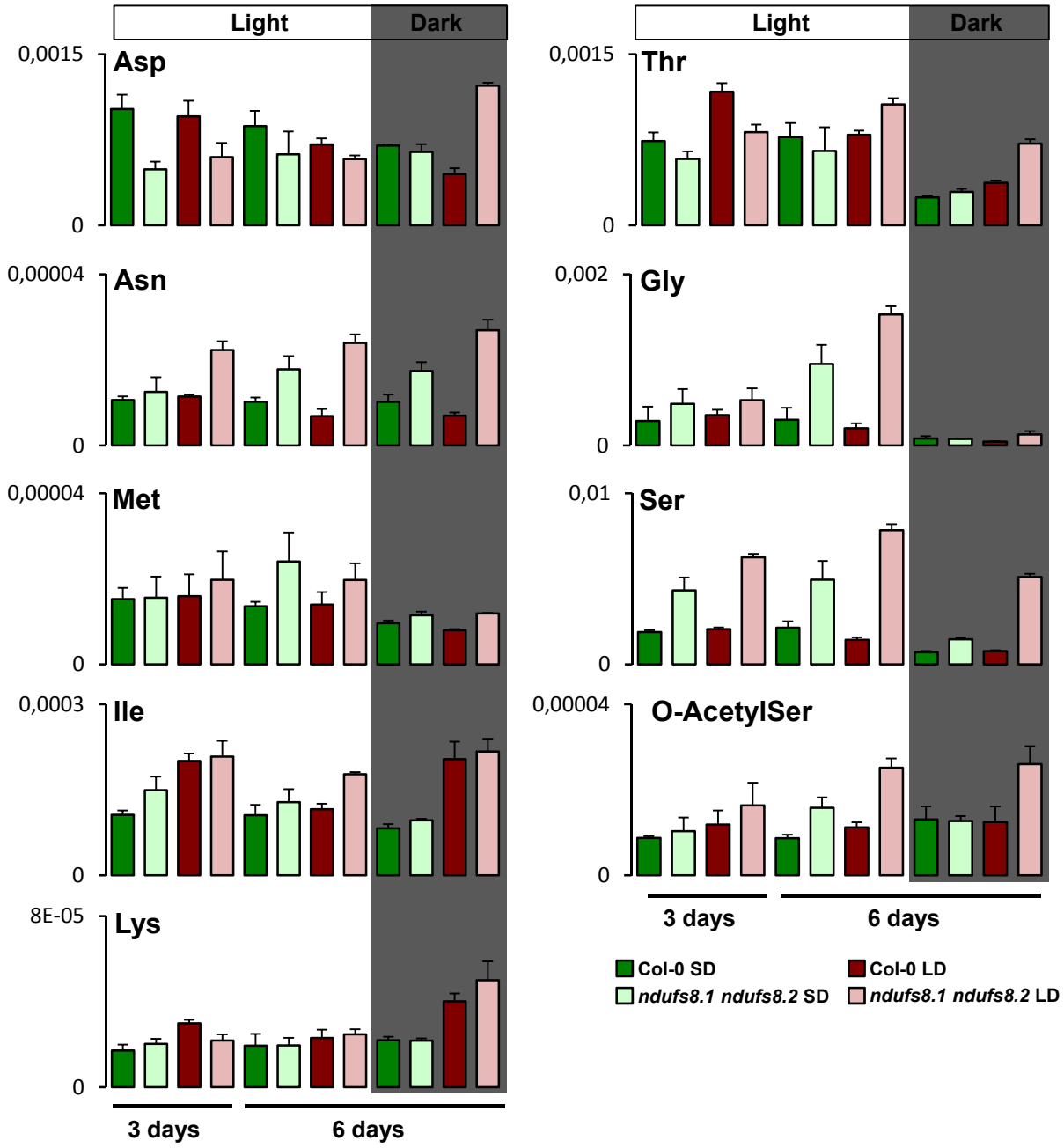

Figure S9. Figure S9. Changes in contents of amino acids in Col-0 and *ndufs8.1 ndufs8.2* plants during the day/night cycle analyzed by GC-MS (part 2). Leaves of SD and LD plants were sampled in the middle of the light period at day 3 (light, columns 1-4), and both in the light (columns 5-8) and at the end of the dark period (columns 9- 12) at day 6. Contents are expressed in relative units.

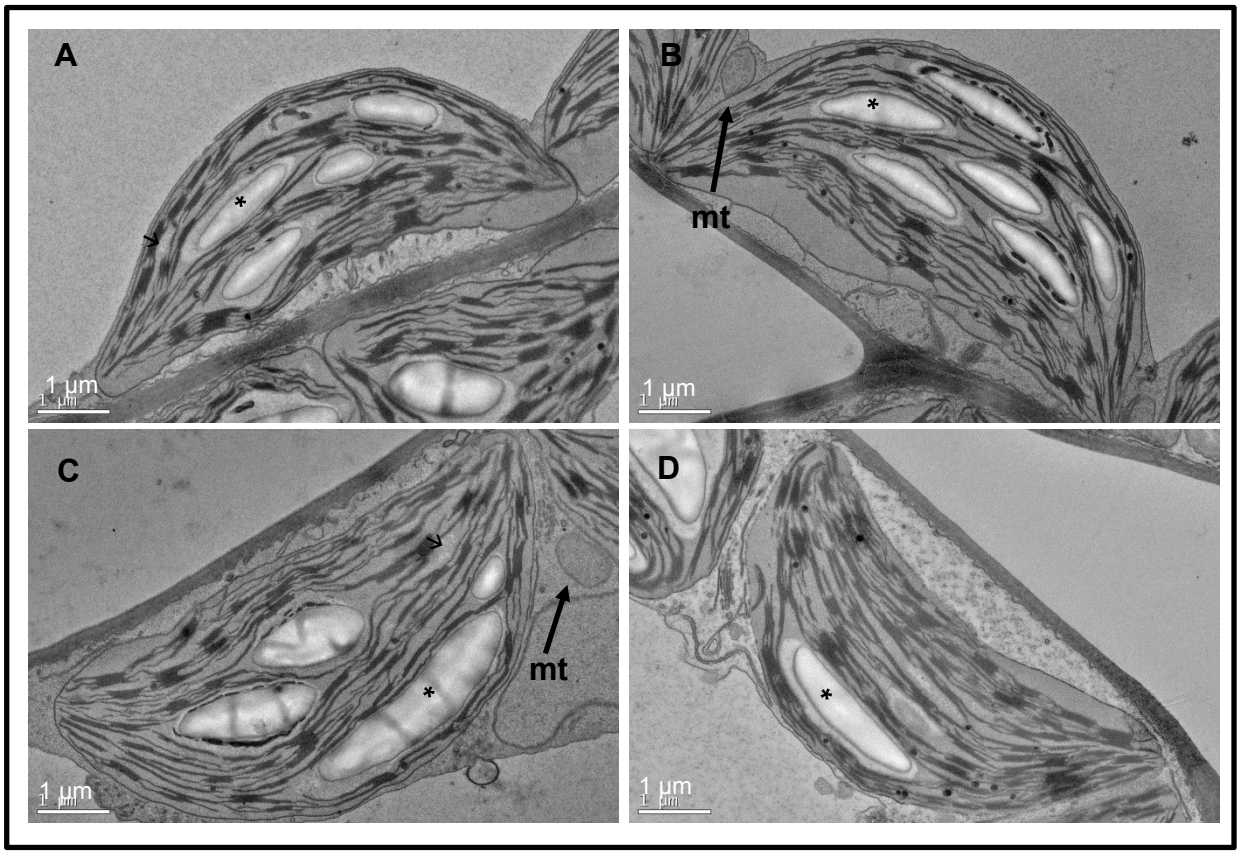

Figure S6. Micrographs of chloroplast ultrastructure in Col-0 and *ndufs8.1 ndufs8.2* plants

Leaves were sampled from SD12/LD12 plants.
A, Col-0 under SD condition
B, Col-0 under LD condition
C, *ndufs8.1 ndufs8.2* mutant under SD condition
D, *ndufs8.1 ndufs8.2* mutant under LD condition
In all cases, typical features of chloroplast and their associated thylakoids are shown. The asterisks indicates starch granules; mt: mitochondria. Bar = 1 µm in all micrographs.

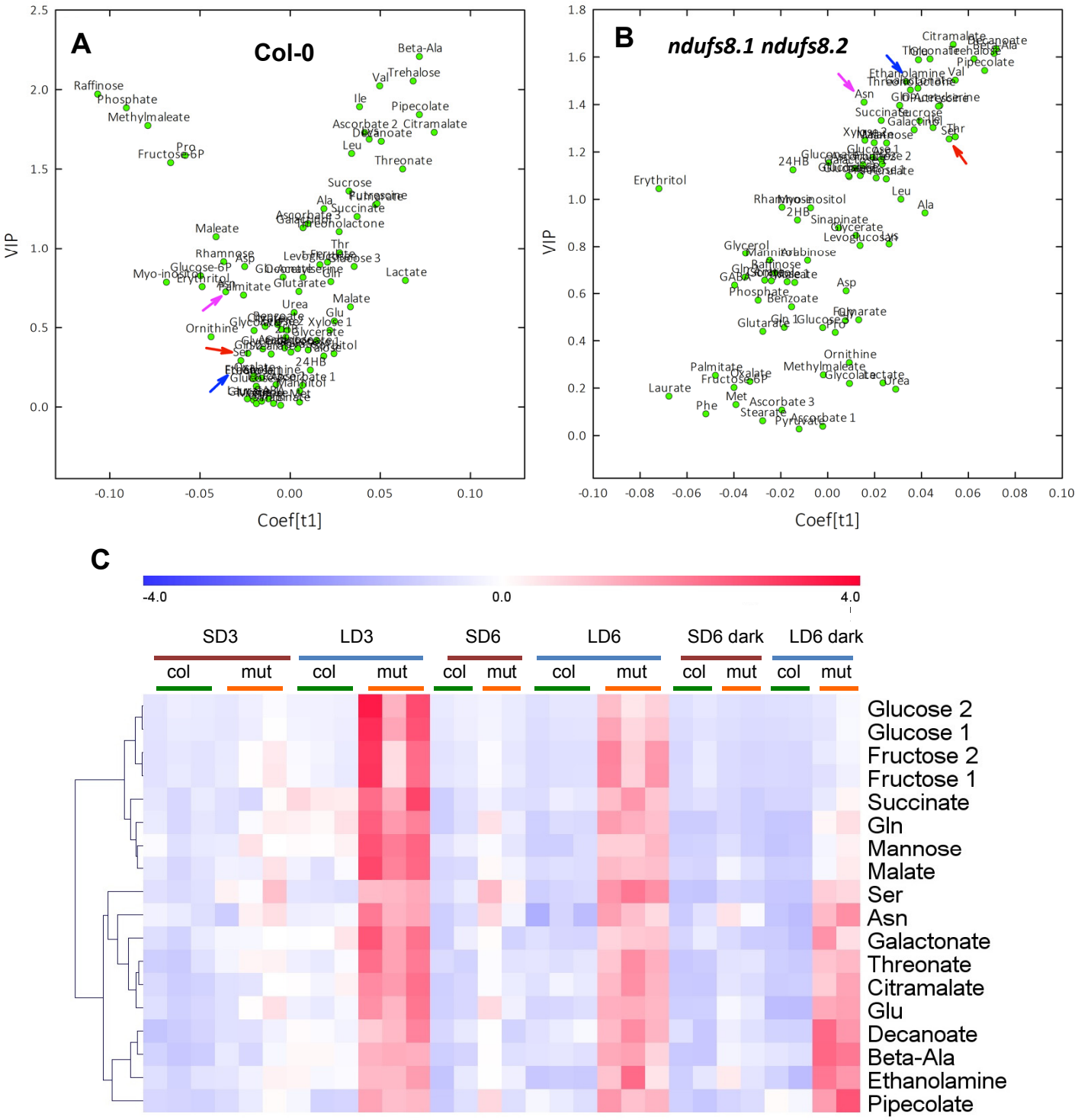

Figure S11. Metabolomic pattern in Col-0 and *ndufs8.1 ndufs8.2* plants and photoperiod × genotype interaction
Leaves were sampled from SD3/LD3 plants at the middle of the light period and from SD6/LD6 plants both at the middle of the light period and at the end of the night period (dark). Metabolomic analyses were carried out 3 times for each condition (*i.e.* 3 biological replicates).
A, Col-0 Volcano plot of the SD/LD multivariate discriminant analysis (OPLS-DA) showing the VIP (variable importance for projection) as a function of loading along axis 1.
B, *ndufs8.1 ndufs8.2* mutant Volcano plot of the SD/LD multivariate discriminant analysis (orthogonal partial least-squares-discriminant analysis ,OPLS-DA) showing the VIP (variable importance for projection) as a function of loading along axis 1.
C, Univariate analysis using 2-way ANOVA, here showing metabolites significant for photoperiod × genotype interaction (P<0.01); Col-0 and *ndufs8.1 ndufs8.2* are referred to as “col” and “mut”, and “obs” indicates sampling at the end of the night period; data are shown as a heat map (color scale on top) with a hierarchical clustering (cosine correlation) on the left.
Arrows point towards metabolites that have both very different positions in volcano plots (A-B) and significant P-value for interaction in the ANOVA: Ser (red), Asn (pink) and ethanolamine (blue).

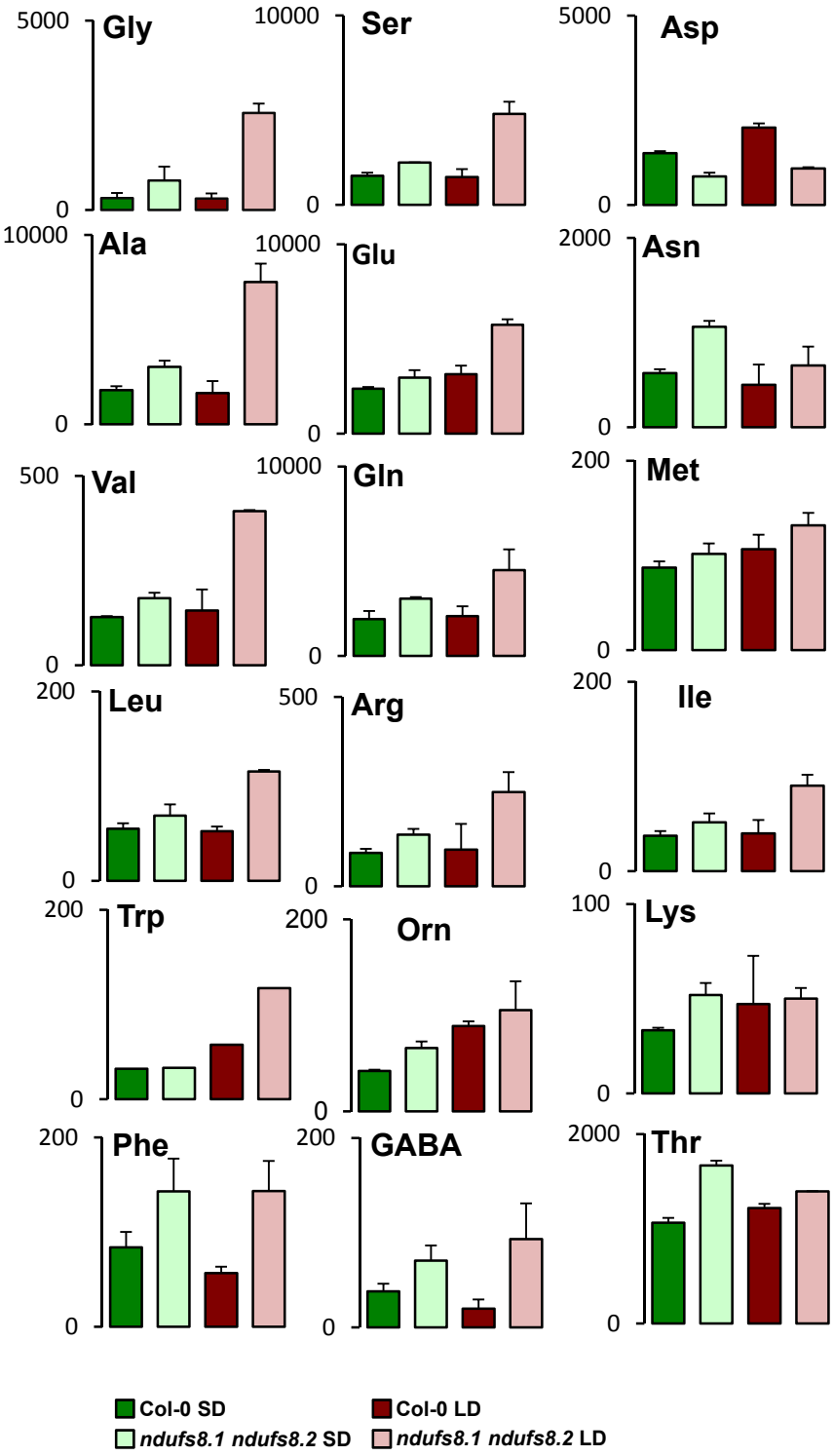

Figure S12. **HPLC quantitation of amino acids in Col-0 and *ndufs8.1 ndufs8.2* leaves**
Quantitation was performed on illuminated leaves of SD12 and LD12 plants. Data are means + SE of at least 3 independent measurements on different plants. Contents are expressed in nmol mg^{-1} FW.

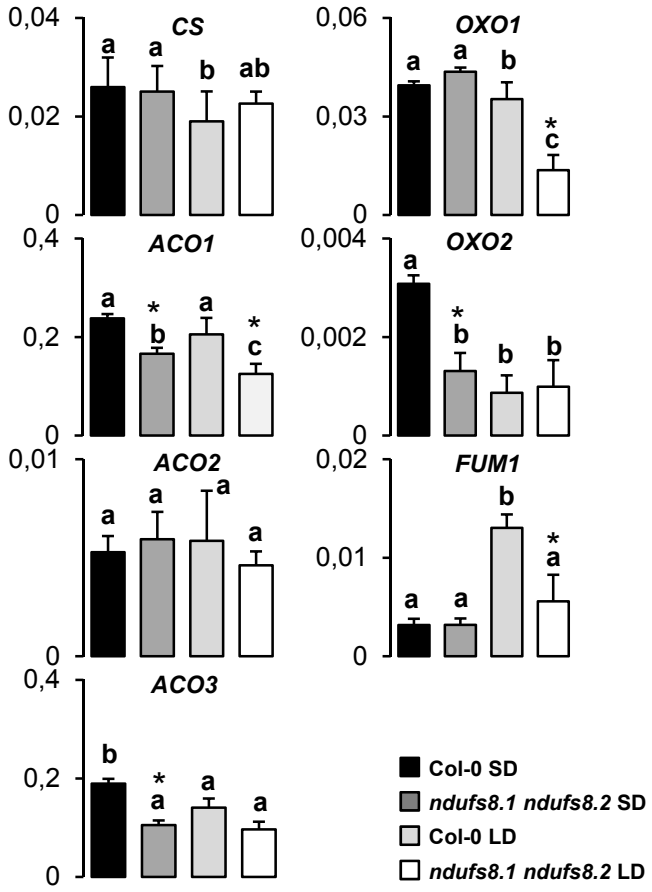

Figure S13. Transcriptional analysis of TCA-related enzymes in Col-0 and *ndufs8.1 ndufs8.2* leaves

RT-qPCR analyses of citrate synthase *(CS*), aconitase (*ACO 1, 2, 3*), 2-oxoglutarate dehydrogenase (*OXO 1, 2*) and fumarase (*FUM1*) were performed on extracts of SD6 and LD6 illuminated leaves, using *ACT2* as a reference. Data are means +SE of at least three independent analyses on different plants. * indicate significant differences between mutant and WT in the same photoperiod condition, according to Student *t* test.

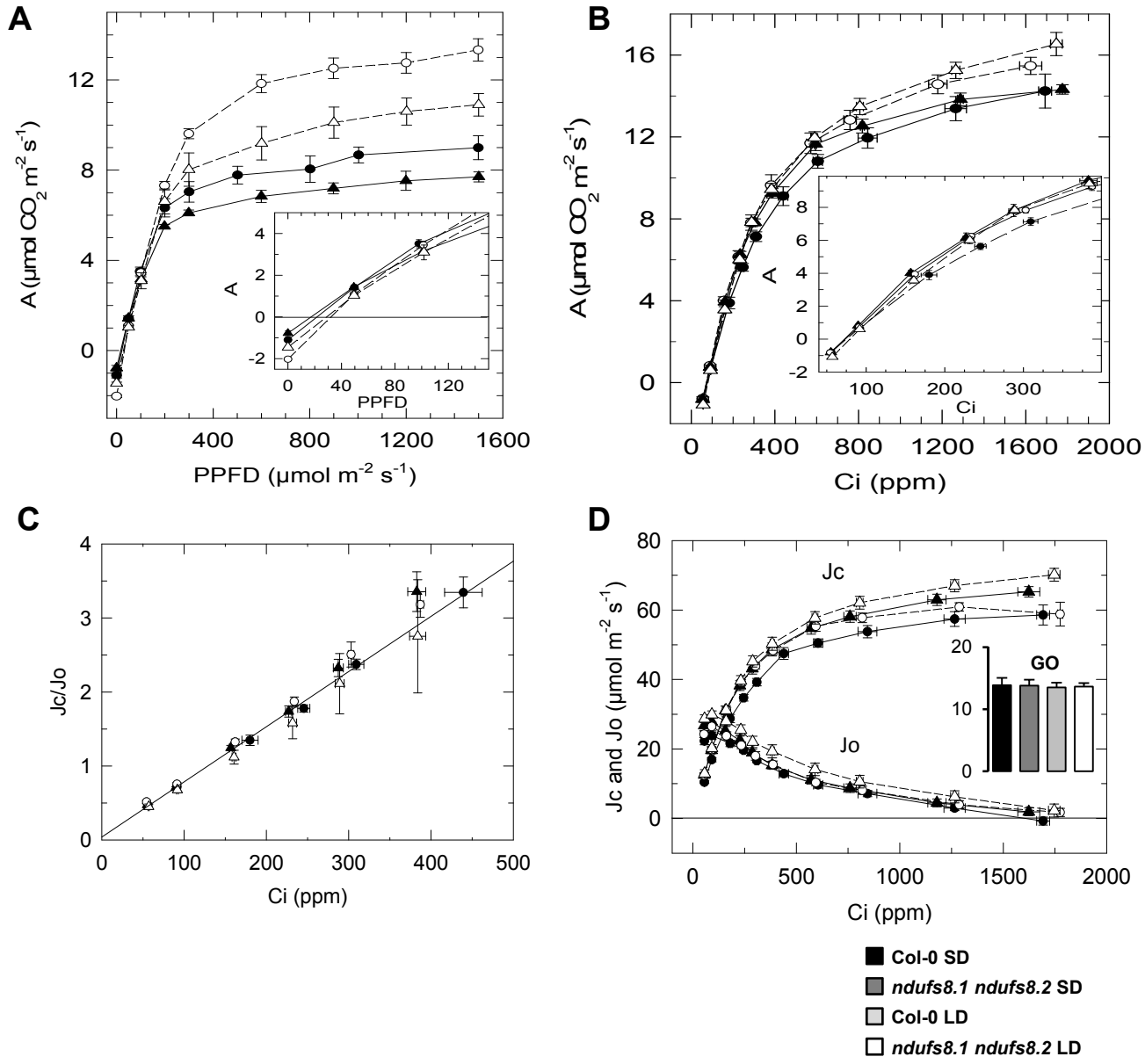

Figure S14. Gas exchange measurements of Col-0 and *ndufs8.1 ndufs8.2* plants maintained under SD and LD conditions

Measurements were performed on attached leaves of LD12 and SD12 plants. Closed symbols: SD; open symbols: LD conditions; circles: Col-0; triangles: *ndufs8.1 ndufs8.2* mutant.

(**A**) Carbon assimilation curves as a function of light, A (L) at ordinary CO_2 mole fraction (380 µmol mol^{-1}). Data are means +/- SE from at last 3 different plants. Inset: corresponding enlargement.

(**B**) Carbon assimilation curves in function of Ci, A(Ci), performed at 300 µmol m^{-2} s^{-1}. Data are means +/- SE from at last 6 different plants. Inset: corresponding enlargement.

(**C**) Relation of the J_c/J_o ratio (a relative estimation of chloroplastic CO_2 molar ratio, Cc) as a function of Ci. Data are means +/- SE calculated on at least 6 different plants.

(**D**) Carboxylation (J_C) and oxygenation (J_O) curves. Inset: glycolate oxidase activity (GO, in nkat g^{-1}FW).

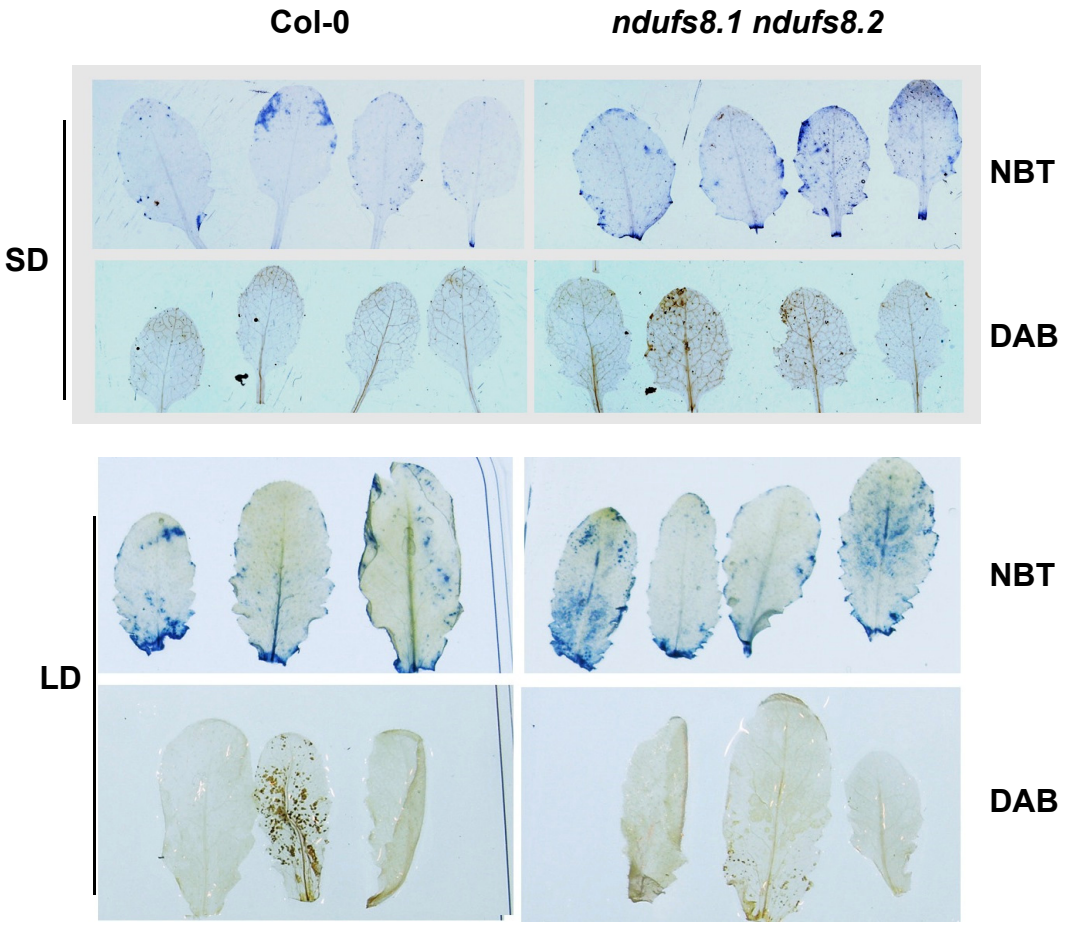

Figure S15. *In situ* detection of leaf superoxide and hydrogen peroxide in Col-0 and *ndufs8.1 ndufs8.2* plants grown under LD and SD conditions

Nitroblue tetrazolium (NBT) and diaminobenzidine (DAB) stains were used to detect superoxide and hydrogen peroxide, respectively, in consecutive adult leaves of the same rosette plant. The experiment was repeated at least 6 times on different plants with similar results.

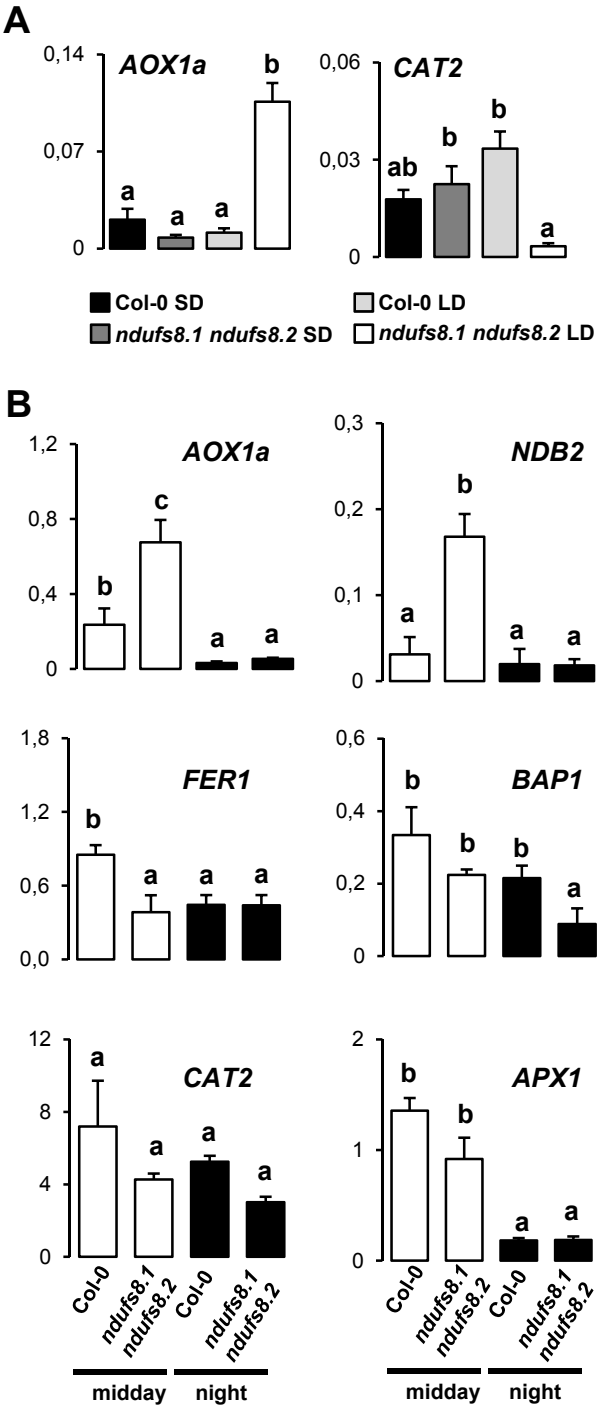

Figure S16. Transcriptional analysis of redox enzymes in Col-0 and *ndufs8.1 ndufs8.2* **plants under various illumination conditions**

mRNAs abundances of *AOX1*, *NDB2, FER1*, *APX1*, *CAT2* and *BAP1* are expressed relative to *ACT2*. Results are means +SE of at least three different plants. Different letters indicate statistically significant differences according to Student *t* test.

A, Transcriptional analysis of *AOX1a* and *CAT2* in plants grown under SD and LD conditions. Col-0 and *ndufs8.1 ndufs8.2* plants were maintained under 100 µmol photons m^{-2} s^{-1} PAR for one week, then transferred under 200 µmol photons m^{-2} s^{-1} for 3 days.

B, Comparison of leaf transcript abundance at midday and at the end of the night period. Col-0 and *ndufs8.1 ndufs8.2* plants were grown in the greenhouse with supplemental 16h-lighting. Open bars: middle of the light period; closed bars: end of the dark period.

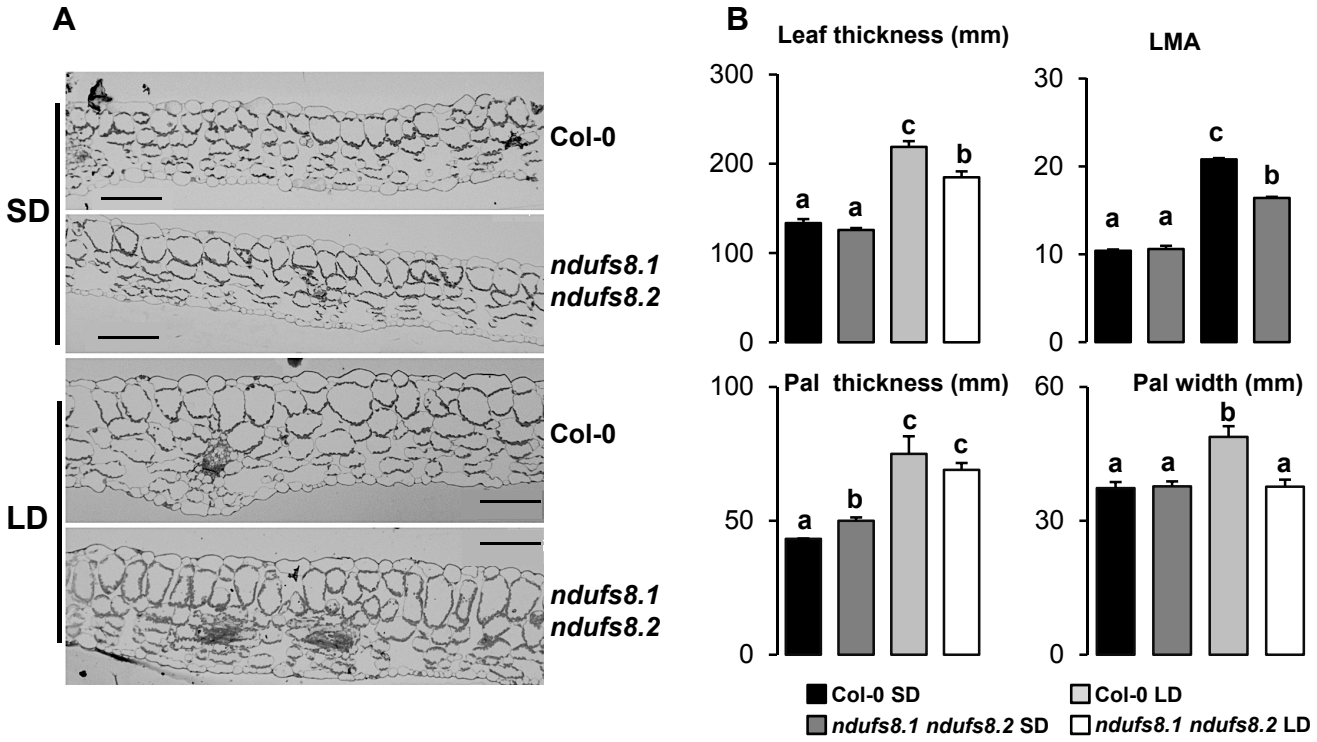

Figure S5. Dimensions of leaf cells of Col-0 and *ndufs8.1 ndufs8.2* plants in SD and LD condition

Leaves were sampled from SD12 / LD12 plants.
A, Photographs of semi-thin sections (300 nm) of leaves. In all figures, bar = 100 µm.
B, Quantitative comparisons of leaf mass area (LMA), of leaf thickness and of dimensions of palisade cells (Pal) measured on semi-thin sections, expressed in mm**.** Data are means +SE of measurements performed on 3 different plants. Different letters indicate significant differences according to Student *t* test; differences between SD12 and LD12 plants are significant in both genotypes for all parameters, except for Pal width, where they were significant in Col-0 only.

Supplemental methods

Metabolomic measurements

Gas chromatography coupled to time-of-flight mass spectrometry (GC-TOF-MS) profiling and quantitative analysis of amino acids by high performance liquid chromatography (HPLC), were performed as described in detail in Noctor et al. (2007b) and Tcherkez et al. (2010), using the isotopic facility structure of the Plateforme Metabolisme-Metabolome (Orsay, France). Metabolites considered to vary significantly between genotypes or photoperiodic conditions using GC-TOF-MS analyses were examined using a two-way ANOVA with P=0.01 as a significance threshold value. With this value, there was a very low false discovery rate (FDR), estimated as in Tan and Xu (2014) including the Hochberg-Benjamini correction (Hochberg and Benjamini, 1990): in all cases, it was less than 0.01. A discriminant analysis was conducted separately in each genotype so as to highlight discrimination of samples (photoperiodic effect) with metabolites. This was done using OPLS-DA carried out with Simca® (MKS Umetrics, Sweden). The effect of each feature in explaining the discrimination was quantified using the coefficient along axis 1 (loading score) and the variable importance for the projection (VIP). The accuracy of the model was estimated with the overall determination coefficient R^2 and its robustness with the cross-validation determination coefficient Q^2. Both R^2 and Q^2 had acceptable values (0.99 and 0.89, respectively) indicating that the OPLS-DA model was reliable.

Untargeted metabolomics by HILIC Mass Spectrometry

Polar metabolites were detected using a method adapted from Paglia et al. (2012). Hydrophobic Interaction Liquid Chromatography (HILIC) coupled to Time-of-Flight Mass Spectrometry (q-TOF-MS) was used to obtain metabolic fingerprints of methanolic extracts (methanol: water: formic acid, 10: 89.9: 0.1, v:v:v) from illuminated intact leaves (10 mg DW) of SD6 or LD6 plants (n = 3). The system consisted in an ACQUITY UPLC coupled to a SYNAPT G2 q-TOF mass spectrometer equipped with an electrospray ionization (ESI) source (Waters, UK). HILIC separation was performed on an ACQUITY UPLC amide column (2.1 × 150 mm, 1.7 µm, Waters) with a pre-column of same chemistry phase. The flow rate was 200 µL min^{-1} with solvent A (100% acetonitrile) and solvent B (100% water) both containing 0.1% formic acid (v:v), using the following gradient: 0.1 – 7 min 1 – 70 % B, 7 – 8 min 70 – 1 % B, 8 – 10 min, 1 % B. The column was maintained at 45 °C and the

injection volume was 10 µL. One blank (methanol: water, 50:50, v:v) was injected between each treatment condition, and two blanks between ESI^+ and ESI^- to facilitate stabilization of the ion modes.

Detection of cations (ESI^+) and anions (ESI^-) by SYNAPT G2 was operated in sensitivity mode with a scan time of 0.2 s over a mass range of 20 - 1200 Da using the MS full scan (no collision energy) and ramped in the transfer cell in elevated energy mode (5 to 45 eV, MS^E). The following parameters were used in ESI^+ and ESI^-: capillary voltage 2.5 kV, sampling cone voltage 20 V, extraction cone voltage 5 V, source temperature 120 °C, desolvation temperature 350 °C, desolvation gas flow 800 L h^{-1}, cone gas flow 50 L h^{-1}. The instrument was calibrated with a solution of sodium formate prior to the analyses with highly accurate detection (0.4 ppm). During each run we used accurate mass measurements by infusing the internal reference leucine encephalin as a lockmass. The system was piloted by MassLynx v 4.1 (Waters).

XCMS package in R (v 3.1.3) was used to integrate the metabolic signals (Smith et al., 2006) which were corrected for total ion current (TIC) and DW for each sample. Unsupervised principal component analyses (PCA) and supervised orthogonal partial least square discriminant analyses (OPLS-DA) were conducted in SIMCA v 13.0.3 (www.umetrics.com/products/simca) on Pareto-scaled and Log-transformed data. Multivariate projections were confirmed by satisfactory predictability and correlation parameters for both ESI^+ and ESI^- modes. Metabolic ions were filtered in MarVis v 1.9.4 (ANOVA $P < 0.01$ with an adjustment for multiple testing by Benjamini-Hochberg False Discovery Rate, FDR), corrected for adducts and/or isotopes, and clustered according to treatments as described before (marvis.gobics.de/; (Kaever et al., 2012; Pétriacq et al., 2016).

Putative identification of metabolite was assigned by screening with chemical databases (tolerance: m/z = 0.1 Da, RT = 10 s) using Kegg, AraCyc and MetaCyc databases as documented in several studies (Kaever et al., 2009; Kaever et al., 2012; Gamir et al., 2014; Pastor et al., 2014; Pétriacq et al., 2016). Accuracy and chemical formula were determined with METLIN (https://metlin.scripps.edu/) and pathways confirmed with PubChem (https://pubchem.ncbi.nlm.nih.gov/).

Rubisco radioisotopic assay

For each sample, the frozen leaf disc was ground to a fine powder in a mortar and pestle pre-cooled with liquid nitrogen and homogenized in extraction buffer (1 mL Tris-HCl 0.1 M pH8, $MgCl_2$ 10 mM, DTT 5 mM and PMSF 0.2 mM). After it had been ground, the sample extract

was quickly transferred to a 1.5 mL microcentrifuge tube and centrifuged at 4°C, 8000 *g* for 1 min. The supernatant was desalted on NAP5 column (GE-Healthcare). Total Rubisco activity was determined from the rate of $^{14}CO_2$ incorporation into acid-stable compounds and subsequent liquid scintillation counting of ^{14}C, according to Seemann and Sharkley (1986).

Detection of ROS content

In situ ROS determination was performed using nitroblue tetrazolium (NBT) and diaminobenzidine (DAB) stains, detecting superoxide and hydrogen peroxide respectively, as described in Dutilleul et al. (2003b).

Room-temperature spin-trapping EPR spectroscopy was carried out to measure apoplastic ROS, as described by Michelet and Krieger-Liszkay (2012). Briefly, leaf disks were vacuum-infiltrated with the buffer containing the spin trap reagents prior to the illumination and then floating on the same buffer during the illumination. Samples were illuminated with white light (1500 µmol quanta m^{-2} s^{-1}) in the presence of 50 mM 4-POBN, 4% ethanol, 50 µM FeEDTA, and buffer (25 mM HEPES, pH 7.5, 5 mM $MgCl_2$, 0.3 M sorbitol).

Luminol chemiluminescence was performed on leaves according to Veljovic-Jovanovic et al. (2002). Results were calibrated using H_2O_2 as the ROS source.

Nitrate determination

Nitrate ions contents were determined as described by Cataldo et al. (1975). Leaf samples were ground into powder in LN then extracted with 1 mL HCl 100 mM in the presence of insoluble PVP. Extracts were centrifuged for 5 min at 14000 *g* and 4 °C. Resulting supernatants were further used to determine nitrate ions content, using a method previously described by Cataldo et al. (1975). Briefly, 10 µL of sample were added to 40 µL of 5% (w/v) salicylic acid prepared in concentrated H_2SO_4 and incubated for 20 min at 37 °C. Reaction was stopped by adding 950 µL of 2 N NaOH, and after total cooling, OD (410 nm) was measured. Nitrate ions were determined as referred to a calibration curve using KNO_3.

Electron Microscopy

Leaf samples were processed as described in Hawes and Satiat-Jeunemaitre (2001). Ultrathin sections (80 nm) were cut with a ultramicrotome EM UC6 (Leica Microsystems) and collected on formvar carbon-coated copper grids. Ultrathin sections were stained with uranyl acetate (Merck) and lead citrate (Agar) before observation with a JEOL JEM-1400

transmission electron microscope operating at 120 kV. Images were acquired using a post-column high-resolution (11 megapixels) high-speed camera (SC1000 Orius; Gatan) and processed with Digital Micrograph (Gatan).

Supplemental Table 1. DNA primers used

Primer sequences used for analysis of genomic DNA (rows 1 to 6), RT-PCR products (rows 7 to 10) and quantitative PCR (rows 11 to 54)

N°	Oligonucleotide	Sequence 5' 3'	Agi code
1	gRP23A	CTTCCCCAGTTGGATACCTTC	At1g16700
2	gLP23A	CAGGCACATCGAAGAAGAGAG	At1g16700
3	LB-Sail	TAGCATCTGAATTTCATAACCAATCTCGATACAC	
4	gRP23B	TGAGGAACAGGGTGTTTATGC	At1g79010
5	gLP23B	AATTTTCCATCACCAATGGTG	At1g79010
6	LBb1-Salk	GCGTGGACCGCTTGCTGCAACT	
7	23A-R	CTCCGAACCGAAAACACCTAAT	At1g79010
8	23AD1	CCATTCTACAACAGTCTCTGC	At1g79010
9	23BR4	CTCAATGGACCCTTCTCAAAAG	At1g16700
10	23BD8	TCAGGGCAAGGTTTACAGG	At1g16700
11	Actin2-F	CTGTACGGTAACATTGTGCTCAG	At3g48780
12	Actin2-R	CCGATCCAGACACTGTACTTCC	At3g48780
13	23aQ-5	TGGCTTCGATTTTGGCTC	At1g79010
14	23aQ-3	TTGCTGCCATAAGATATACCAC	At1g79010
15	23bQ-5	TACTAGCTCGCAGGTCGTTCAG	At1g16700
16	23bQ-3	GATATAGCACGGGACTGTAGCC	At1g16700
17	Lst8.2F	AGATGGCACAGTTAAGATCTG	At3g18140
18	Lst8.2R	GGCTCAAACTCTGTCATTGTC	At3g18140
19	FER-3	CTAGAGACAGAGCCAACTCC	At5g01600
20	FER-5	CAAGTGAGGAAGAGAGAGGG	At5g01600
21	NR2-RP	CGGTAAGCAAACTCG	At1g37130
22	NR2-LP	TCACAGGGAAACATCCCTTC	At1g37130
23	NR1-RP	TCACCTCAACCCTCGTTACC	At1g77760
24	NR1-LP	CTCTCGTTGATGCTGAGCTG	At1g77760
25	NiR-RP	TGGAAGAACGTCATCAGCAG	At2g15620
26	NiR-LP	CGGTTTGGATTCAATTTGCT	At2g15620
27	CAT2-F	TGCTGGAAACTACCCTGAATGG	At4g35090
28	CAT2-R	TCAACACCATACGTCCAACAGG	At4g35090
29	AO-F	GATCGT TCACGCTGCTGATA	At5g14760
30	AO-R	TGTGTTCAAGCCATCCTGAG	At5g14760
31	QS-F	AAGCTTTGCTCAAGCTCAGG	At5g50210
32	QS-R	TCAAGACCCCTTGCACTTCT	At5g50210
33	QPT-R	ATCTACCAACCGCAAACCAG	At2g01350
34	QPT-L	GGAATTGCAACCCTTACCAA	At2g01350
35	NaMNAT-F	ATGTC CGTTACCAGTCGAG	At5g55810
36	NaMNAT-R	GGAGGATTGAAACTCCCAGT	At5g55810
37	NADS-F	AGGAATTTCAGCTCCCCATT	At1g55090
38	NADS-R	GCCGTGTCGATAAACTGGAT	At1g55090

39	NaPT2-F	GTGGAAGTGCAGATGAAGCA	At2g23420
40	NaPT2-R	TGATCAGGTCGCATGTTTTC	At2g23420
41	NaPT4-F	ATGCATTTGGAATTGGAACC	At4g36940
42	NaPT4-R	AAAGTTTGATCCGAGGCTGA	At4g36940
43	PARP2-F	AAGAAAAATCCGGTGGGTCT	At2g31320
44	PARP2-R	TTGGTCGAGTGTTTCCCTCT	At2g31320
45	TOR2-F	CGTGATTTTTCTTCGTCT	At1g50030
46	TOR2-R	GGCTTGATTGATTAGTTTT	At1g50030
47	NDB2-F	TACGCCAGTAAGCAAGTGAG	At4g05020
48	NDB2-R	AGAAAGCAACAAGTGAG	At4g05020
49	AOX1a-F	TGTGTATT GAGCCTTGG	At3g22370
50	AOX1a-R	TCGTCGGAGCTCTAGTCCAT	At3g22370
51	APX1-F	GCACTATTGGACGACCCTGT	At1g07890
52	APX1-R	GCAAACCCAAGCTCAGAAAG	At1g07890
53	BAP1-F	CGAATCGAGAAGCAATC	At3g61190
54	BAP1-R	TTCCCATGAAATCATTCGTTG	At3g61190
55	FUM1-S	CTCACACTCAAGATGCTACACG	At2g47510
56	FUM1-R	GCACGCCTAAATTCAGAGCCGC	At2g47510
57	ACO1-S	TTGATGGAACGAGGTGTGG	At4g35830
58	ACO1-R	GACCAACTTCTCCTTTCAAGTG	At4g35830
59	ACO2-S	GTAACAACAGACCACATCTCTC	At4g26970
60	ACO2-R	TACCACGAGCCATAACCTC	At4g26970
61	ACO3-S	CCATGCTACAGGGTGTTAAAG	At2g05710
62	ACO3-R	GTCAATCCAAGAGTATCTGCG	At2g05710
63	CS-S	TGAAGTCAGAACATGGGAAGG	At2g44350
64	CS-R	TCGACAATCCCCTAAAGCG	At2g44350
65	CCA1-S	GGGGTGTGAATGATGGAAAAGA	At2g46830
66	CCA1-R	CGATCTTCATTGGCCATCTCAG	At2g46830
67	LHY-S	GACAACGCGGTTCAAGATGTTC	At1g01060
68	LHY-R	CCAAGGGTAGTTTTGCATGCTG	At1g01060